AFRL-AFOSR-VA-TR-2016-0162

General and Robust Strategies for Multifunctional Oragnic-Inorganic Nanocomposites via Direct Growth of Monodisperse Nanocrystals Intimately and Permanently Connected with Polymers

Zhiqun Lin
GEORGIA TECH RESEARCH CORPORATION

04/21/2016
Final Report

Air Force Research Laboratory
AF Office Of Scientific Research (AFOSR)/ RTB2
Arlington, Virginia 22203
Air Force Materiel Command

REPORT DOCUMENTATION PAGE

Form Approved
OMB No. 0704-0188

PLEASE DO NOT RETURN YOUR FORM TO THE ABOVE ORGANIZATION.

1. REPORT DATE *(DD-MM-YYYY)*	2. REPORT TYPE	3. DATES COVERED *(From - To)*
04-17-2016	Final Performance Report	03/01/2013-05/31/2016

4. TITLE AND SUBTITLE
General and Robust Strategies for Multifunctional Organic-Inorganic Nanocomposites via Direct Growth of Monodisperse Nanocrystals Intimately and Permanently Connected with Polymers

5a. CONTRACT NUMBER

5b. GRANT NUMBER
FA9550-13-1-0101

5c. PROGRAM ELEMENT NUMBER

6. AUTHOR(S)
Lin, Zhiqun

5d. PROJECT NUMBER

5e. TASK NUMBER

5f. WORK UNIT NUMBER

7. PERFORMING ORGANIZATION NAME(S) AND ADDRESS(ES)
Georgia Institute of Technology
School of Materials Science and Engineering
771 Ferst Dr., NW
Atlanta, GA 30332

8. PERFORMING ORGANIZATION REPORT NUMBER

9. SPONSORING/MONITORING AGENCY NAME(S) AND ADDRESS(ES)
AFOSR/RSA

875 North Randolph Street
Suite 325, Room 3112
Arlington, VA 22203

10. SPONSOR/MONITOR'S ACRONYM(S)
AFOSR

11. SPONSOR/MONITOR'S REPORT NUMBER(S)

12. DISTRIBUTION/AVAILABILITY STATEMENT
Distribution A, public disclosure

13. SUPPLEMENTARY NOTES

14. ABSTRACT
The objectives of this proposal are to: (1) Synthesize a series of novel amphiphilic block copolymers with well-defined molecular architectures (i.e., star-like block copolymers, bottlebrush-like block copolymers, and Janus star-like block copolymers) and block ratios based on β-cyclodextrin (β-CD) by living polymerization techniques; (2) Craft a large variety of monodisperse plain and core/shell NPs and NRs as well as Janus NPs of different dimension, chemistry, and properties, which are intimately and permanently capped by polymers on their surface (i.e., forming organic-inorganic nanocomposites), by capitalizing on amphiphilic star-like, bottlebrush-like, and Janus star-like block copolymers as nanoreactors; and (3) Characterize and explore these multifunctional organic-inorganic nanocomposites by measuring their physical properties (e.g., dielectric, magnetic, magnetoelectric, and optical properties) for potential use in spintronic devices, capacitors, actuators, transducers, sensors, photocatalysis, and photonic devices that are anticipated to fill a critical need in future military.

15. SUBJECT TERMS
Multifunctional Organic-Inorganic Nanocomposites

16. SECURITY CLASSIFICATION OF:			17. LIMITATION OF ABSTRACT	18. NUMBER OF PAGES	19a. NAME OF RESPONSIBLE PERSON
a. REPORT	b. ABSTRACT	c. THIS PAGE			19b. TELEPHONE NUMBER *(Include area code)*

Reset

INSTRUCTIONS FOR COMPLETING SF 298

1. REPORT DATE. Full publication date, including day, month, if available. Must cite at least the year and be Year 2000 compliant, e.g. 30-06-1998; xx-06-1998; xx-xx-1998.

2. REPORT TYPE. State the type of report, such as final, technical, interim, memorandum, master's thesis, progress, quarterly, research, special, group study, etc.

3. DATES COVERED. Indicate the time during which the work was performed and the report was written, e.g., Jun 1997 - Jun 1998; 1-10 Jun 1996; May - Nov 1998; Nov 1998.

4. TITLE. Enter title and subtitle with volume number and part number, if applicable. On classified documents, enter the title classification in parentheses.

5a. CONTRACT NUMBER. Enter all contract numbers as they appear in the report, e.g. F33615-86-C-5169.

5b. GRANT NUMBER. Enter all grant numbers as they appear in the report, e.g. AFOSR-82-1234.

5c. PROGRAM ELEMENT NUMBER. Enter all program element numbers as they appear in the report, e.g. 61101A.

5d. PROJECT NUMBER. Enter all project numbers as they appear in the report, e.g. 1F665702D1257; ILIR.

5e. TASK NUMBER. Enter all task numbers as they appear in the report, e.g. 05; RF0330201; T4112.

5f. WORK UNIT NUMBER. Enter all work unit numbers as they appear in the report, e.g. 001; AFAPL30480105.

6. AUTHOR(S). Enter name(s) of person(s) responsible for writing the report, performing the research, or credited with the content of the report. The form of entry is the last name, first name, middle initial, and additional qualifiers separated by commas, e.g. Smith, Richard, J, Jr.

7. PERFORMING ORGANIZATION NAME(S) AND ADDRESS(ES). Self-explanatory.

8. PERFORMING ORGANIZATION REPORT NUMBER. Enter all unique alphanumeric report numbers assigned by the performing organization, e.g. BRL-1234; AFWL-TR-85-4017-Vol-21-PT-2.

9. SPONSORING/MONITORING AGENCY NAME(S) AND ADDRESS(ES). Enter the name and address of the organization(s) financially responsible for and monitoring the work.

10. SPONSOR/MONITOR'S ACRONYM(S). Enter, if available, e.g. BRL, ARDEC, NADC.

11. SPONSOR/MONITOR'S REPORT NUMBER(S). Enter report number as assigned by the sponsoring/ monitoring agency, if available, e.g. BRL-TR-829; -215.

12. DISTRIBUTION/AVAILABILITY STATEMENT. Use agency-mandated availability statements to indicate the public availability or distribution limitations of the report. If additional limitations/ restrictions or special markings are indicated, follow agency authorization procedures, e.g. RD/FRD, PROPIN, ITAR, etc. Include copyright information.

13. SUPPLEMENTARY NOTES. Enter information not included elsewhere such as: prepared in cooperation with; translation of; report supersedes; old edition number, etc.

14. ABSTRACT. A brief (approximately 200 words) factual summary of the most significant information.

15. SUBJECT TERMS. Key words or phrases identifying major concepts in the report.

16. SECURITY CLASSIFICATION. Enter security classification in accordance with security classification regulations, e.g. U, C, S, etc. If this form contains classified information, stamp classification level on the top and bottom of this page.

17. LIMITATION OF ABSTRACT. This block must be completed to assign a distribution limitation to the abstract. Enter UU (Unclassified Unlimited) or SAR (Same as Report). An entry in this block is necessary if the abstract is to be limited.

General and Robust Strategies for Multifunctional Oragnic-Inorganic Nanocomposites via Direct Growth of Monodisperse Nanocrystals *Intimately* and *Permanently* Connected with Polymers

Zhiqun Lin; Professor
School of Materials Science and Engineering, Georgia Institute of Technology,
Atlanta, GA 30332

Final Report on the AFOSR project: FA9550-13-1-0101 **(03/2013-05/2016)**

Over the past three years, we have made very good progress on the project. The key results are summarized as follows.

Recent research has witnessed tremendous advances in isotropic nanomaterials synthesis, which has provided access to a large array of nanoparticles with controlled size, shape and functionality. Going beyond simple zero-dimensional nanoparticles,(*1, 2*) one-dimensional nanocrystals such as nanorods,(*3*) nanotubes,(*4*) nanowires,(*5*) and shish-kebab-like heterostructures(*6, 7*) exhibit a broad range of unique properties (e.g., optical,(*8*) electrical,(*9*) magnetic,(*10*) and catalytic properties(*11*)) that are dependent sensitively on their size and shape. Such nanocrystals of both fundamental and practical interest.(*12, 13*) Current emerging synthesis approaches, including template-assisted synthesis,(*14-16*) chemical vapor deposition,(*17*) and colloidal synthesis,(*18*) render the preparation of intriguing 1D nanocrystals with controlled dimensions. However, some of these procedures involve tedious multistep reactions and purification, require rigorous experimental conditions, and more importantly are difficult to be generalized. Clearly, it remains a grand challenge to identify a viable approach that applies to the synthesis of any desirable and uniform 1D nanocrystals.

In this context, our strategy capitalizes on a set of rationally designed bottlebrush-like block copolymers, with well-defined molecular architecture and molecular weight (MW), as nanoreactors to effectively produce a myriad of 1D nanocrystals with unprecedented control over their dimension, composition, and architecture. These bottlebrush-like block copolymers (BBCPs) are unimolecular cylindrical polymer brushes possessing a cellulose backbone with densely grafted diblock or triblock copolymers as side chains (i.e., arms). Cellulose forms a rigid backbone because of intramolecular hydrogen bridges between the secondary hydroxyl groups at the C3 position of an anhydroglucose unit (AGU) and the oxygen of the pyrane ring in the adjacent AGU.(*19*) As a result, the free rotation around the glycosidic bond is hindered. In addition, the three substitutable hydroxyl groups on each AGU offer easy access to graft dense polymer side chains from the cellulose backbone. Thus, we utilize these advantages peculiar to cellulose for the synthesis of straight cylindrical BBCPs carrying densely grafted functional block copolymer side chains (see **Supplementary Information Sections I-III**). A family of BBCPs synthesized by either sequential atom transfer radical polymerization (ATRP) or ATRP(s) followed by a click reaction include cellulose-*graft*-[poly(acrylic acid)-*block*-polystyrene] (denoted cellulose-*g*-[PAA-*b*-PS]) and cellulose-*graft*-[poly(acrylic acid)-*block*-poly(ethylene glycol)] (cellulose-*g*-[PAA-*b*-PEG]) with linear amphiphlic PAA-*b*-PS and all hydrophilic PAA-*b*-PEG diblock copolymers as side chains, respectively, and cellulose-*graft*-[poly(4-vinylpyridine)-*block*-poly(*tert*-butyl acrylate)-*block*-polystyrene] (cellulose-*g*-[P4VP-*b*-P*t*BA-*b*-PS]),

cellulose-*graft*-[poly(4-vinylpyridine)-*block*-poly(*tert*-butyl acrylate)-*block*-poly(ethylene glycol)] (cellulose-*g*-[P4VP-*b*-P*t*BA-*b*-PEG]), cellulose-*graft*-[polystyrene-*block*-poly(acrylic acid)-*block*-polystyrene] (cellulose-*g*-[PS-*b*-PAA-*b*-PS]) and cellulose-*graft*-[polystyrene-*block*-poly(acrylic acid)-*block*-poly(ethylene glycol)] (cellulose-*g*-[PS-*b*-PAA-*b*-PEG]) with linear amphiphlic P4VP-*b*-P*t*BA-*b*-PS, P4VP-*b*-P*t*BA-*b*-PEG, PS-*b*-PAA-*b*-PS and PS-*b*-PAA-*b*-PEG triblock copolymers as side chains, respectively.

Starting with the simplest architecture, plain nanorods and nanowires of varied diameters and chemical compositions were first synthesized by exploiting amphiphilic cellulose-*g*-[PAA-*b*-PS] BBCP as a nanoreactor (**Figure 1a**, **Table S2**, and **Supplementary Information Sections III-IV**). As each AGU in the celloulose backbone enables the growth of three P*t*BA-*b*-PS diblocks by ATRP due to the presence of three hydroxyl groups per AGU (upper left panel in **Figure 1a**; **Supplementary Information Sections II-III**), the heavily grafted P*t*BA-*b*-PS diblock brushes in conjuction with the inherent rigidity of the cellulose backbone forces the cellulose-*g*-[P*t*BA-*b*-PS] BBCP to adopt a well-defined, straight, cylindrical conformation that exhibits exceptionally high chain stiffness (upper right panel in **Figure 1a**). The subsequent hydrolysis of the P*t*BA blocks yields amphiphilic cellulose-*g*-[PAA-*b*-PS] composed of inner hydrophilic PAA blocks and outer hydrophobic PS blocks (lower right panel in **Figure 1a**). Upon addition of inorganic precursors, they are preferentially segregated in the interior cylindrical region occupied by densely grown PAA blocks via strong cooridination reaction between the carboxylic acid groups of PAA and the metal moieties of precursors.(*20*) This leads to the formation of nanorods (or nanowires) by refluxing in dimethylformamide (DMF) at the elevated temperature (see **Supplementary Information Section V** for the proposed formation mechanisms). The direct tethering of PS chains on the surface of nanorods (and nanowires) facilitates their dispersion and solubility in various organic solvents (lower left panel in **Figure 1a**).

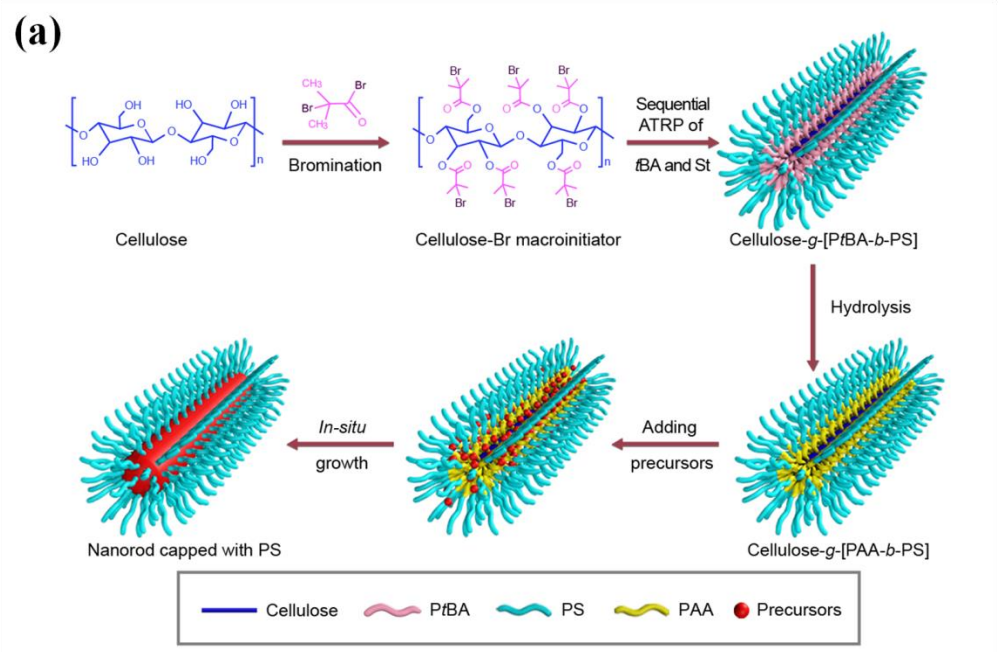

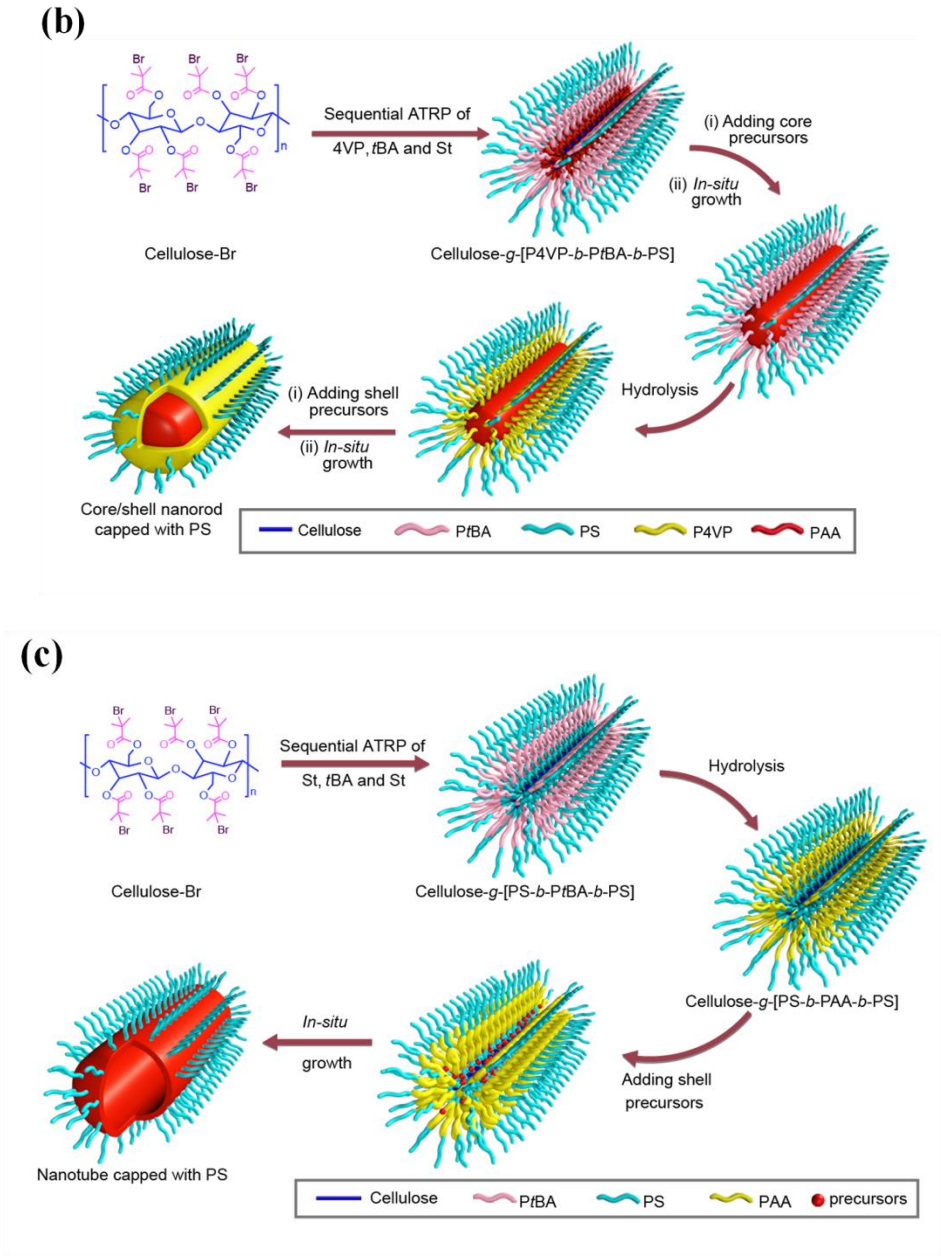

Figure 1. Stepwise representation of synthetic strategies for 1D nanocrystals with precisely controlled dimension, composition, surface chemistry and architecture by capitalizing on amphiphilic cylindrical bottlebrush-like block copolymers (BBCPs) as nanoreactors. (a) Synthesis of plain nanrods and nanowires; (b) Synthesis of core/shell nanorods; and (c) Synthesis of nanotubes.

As proof of concept, we synthesized upconversion $NaYF_4$:Yb/Er nanorods as an illustrative example of our nanoreactor strategy for producing high-quality 1D plain nanorods. Representative TEM images at different magnifications in **Figure 2a** clearly demonstrate the formation of uniform $NaYF_4$:Yb/Er nanorods with an average diameter of 9.8±0.5 nm and length of 97±9 nm. These nanorods are highly crystalline and possess a hexagonal phase as revealed by high-resolution TEM (HRTEM; **Figure 2a**) and X-ray

powder diffraction (XRD) measurements (**Figure S80**), respectively. Energy dispersive X-ray spectroscopy (EDS) microanalysis also confirmed the composition of $NaYF_4$:Yb/Er nanorods (**Figure S92**). Thermogravimetric analysis (TGA) measurements showed that the volume fraction of PAA blocks encapsulated in $NaYF_4$:Yb/Er nanorods was approximately ~11.2% (**Figure S64**).

It is worth noting that ATRP, a living free radical polymerization technique, affords a superior controllability over molecular weight (MW), and thus enables the precise design of unimolecular architecture and functionality of BBCPs with a tunable MW and narrow MW distribution of each constituent block. Consequently, the diameter (core diameter and shell thickness, or shell thickness) of 1D plain nanorods (core/shell nanorods, or hollow nanotubes) is dictated by the chain length of hydrophilic inner block (hydrophilic inner and intermediate blocks, or hydrophilic intermediate block) in a BBCP brush, which can be readily regulated by tuning the polymerization time of the different blocks during ATRP. Moreover, the solubilty of 1D nanocrystals, either organic solvent-soluble or water-soluble, is rendered by the type of outer blocks of the BBCP brushes, which are originally covalently bonded to the inner (or intermediate) blocks. Finally, the length of 1D nanocrystals can be easily adjusted by varying the length of the cellulose-based macroinitiator (denoted cellulose-Br; **Supplementary Information Section II**), that is, essentially the backbone of BBCP nanoreactor. To obtain a specific length of cellulose-Br macroinitiator, natural cellulose after being modified with 2-bromoisobutyryl bromide in a mixed solvent of ionic liquid 1-allyl-3-methylimidazolium chloride (AMIMCl), anhydrous 1-methyl-2-pyrrolidione (NMP) and DMF was purified by fractional precipitation (see **Supplementary Information Section II)**. Taking noble metal Au nanorods as an exmple, **Figure 2b** depicts such facile control over the length and diameter of nanorods by deliberately tuning the length of the cellulose-Br macroinitiator and the molecular weight of the PAA blocks, respectively, in cellulose-*g*-[PAA-*b*-PS]. Obviously, as the molecular weight of cellulose-Br increased from $11.2x10^3$ g/mol to $23.5x10^3$ g/mol to $41.8x10^3$ g/mol to $79.6x10^3$ g/mol, the length *L* of the Au nanorods synthesized by employing cellulose-*g*-[PAA-*b*-PS] increased from 51±4 nm to 98±8 nm to 206±19 nm to 414±39 nm (upper panel; the corresponding diameters are *D* = 10.4±0.6 nm for *L* = 51±4 nm and *L* = 98±8 nm long Au nanorods; and *D* = 21.2±1.5 nm for *L* = 206±19 nm and *L* = 414±39 nm long Au nanorods). With the increase of molecular weight of PAA block from $5.2x10^3$ g/mol to $11.2x10^3$ g/mol, the diameter *D* of Au nanorods increased from 10.4±0.6 nm to 21.2±1.5 nm (lower panel; the corresponding lengths are *L* = 98±8 nm for *D* = 10.4±0.6 nm, and *L* = 206±19 nm for *D* = 21.2±1.5 nm Au nanorods).

Conceptually, as appropriate precursors that are amenable to the cylindrical unimolecular nanoreactor strategy are quite diverse, a rich variety of plain nanorods and nanowires with high uniformilty can thus be created. **Figure 3** shows noble metal Au and Pt, ferroelectric $BaTiO_3$, upconversion $NaYF_4$:Yb/Er, semiconducting CdSe, and thermoelectric PbTe nanorods, as well as magnetic Fe_3O_4 nanowires synthesized by subjecting the appropriate precursors to selectively react with the PAA blocks in cylindrical cellulose-*g*-[PAA-*b*-PS] nanoreactors. It is noteworthy that they represent just a few examples of the kind of plain nanorods and nanowires that can be crafted using this technique. Conversely, such good control over the size and shape of nanorods and nanowires signifies that cylindrical unimolecular nanoreactors are structurally stable under various experimental conditions. Moreover, it is interesting to note that our strategy enabled the synthesis of some nanorods (e.g., $BaTiO_3$ and Fe_3O_4 described above) with uniform diameter and length which have not yet been demonstrated via wet-chemistry approaches in literature. The possible mechanisms for the growth of these plain nanorods and nanowires are discussed in

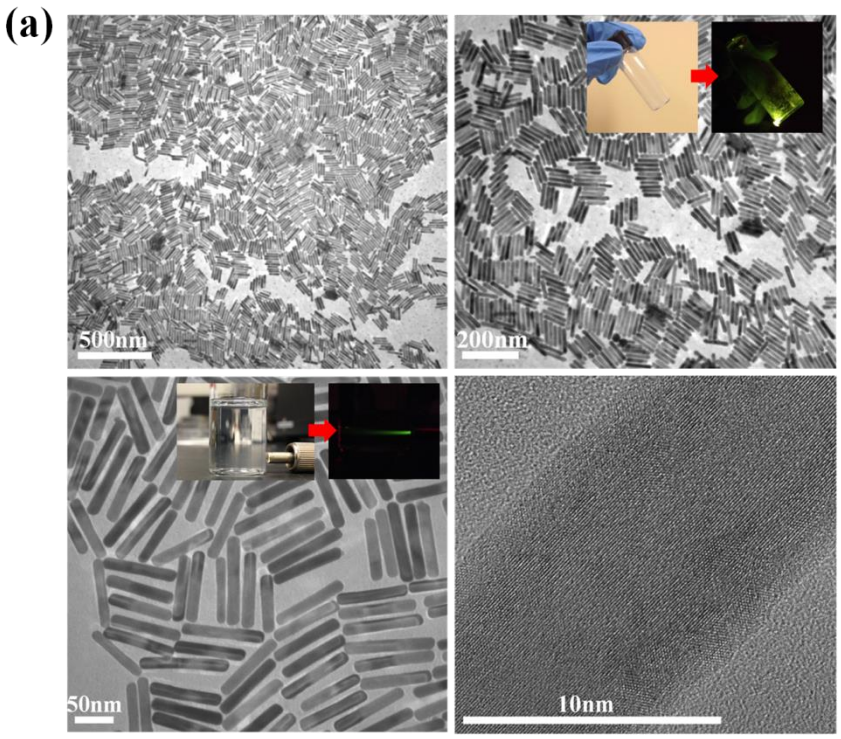
(a)
500nm
200nm
50nm
10nm

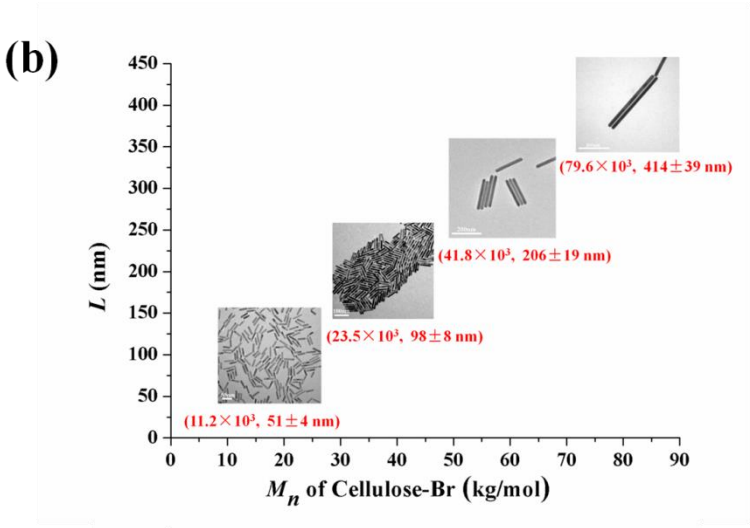
(b)
L (nm)
M_n of Cellulose-Br (kg/mol)
(11.2×10³, 51±4 nm)
(23.5×10³, 98±8 nm)
(41.8×10³, 206±19 nm)
(79.6×10³, 414±39 nm)

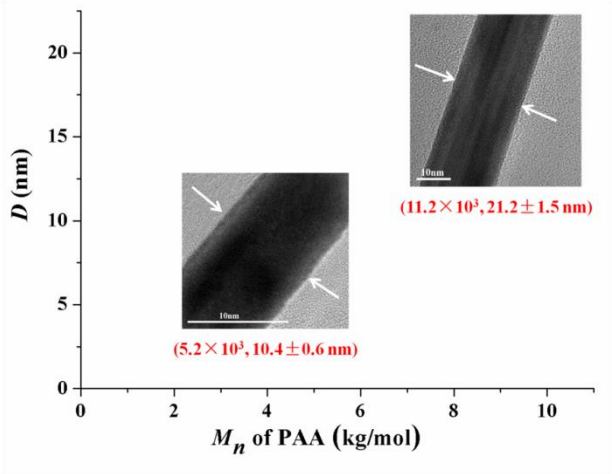
D (nm)
M_n of PAA (kg/mol)
(5.2×10³, 10.4±0.6 nm)
(11.2×10³, 21.2±1.5 nm)

Figure 2. Formation of plain nanrods and nanowires. (a) Representative TEM images of upconversion $NaYF_4$:Yb/Er nanorods at different magnifications (length, L = 97±9 nm, D = 9.8±0.5 nm) synthesized by empolying cylindrical cellulose-*g*-[PAA-*b*-PS] BBCP as a nanoreactor (i.e., Sample-2A in Table S2). An HRTEM image of an $NaYF_4$:Yb/Er nanorod with clear crystalline lattices is shown on the lower right panel. Insets: digital images of $NaYF_4$:Yb/Er nanorods in toluene (lower left panel) and dry state (upper right panel) before (left) and after (right) exposure to a 2W 980-nm near-infrared laser, respectively. (b) The dimension tunability of 1D nanocrystals illustrated by utilizing metallic Au nanorods as an example. The upper panel depicts the dependence of the length of Au nanorods (i.e., 51±4 nm, 98±8 nm, 206±19 nm and 414±39 nm) on the molecular weight of cellulose-Br macroinitiator (Sample-1, Sample-2, Sample-3 and Sample-4 as nanoreactors, respectively, in Table S1). The lower panel displays the dependence of the diameter of Au nanorods (i.e., 10.4±0.6 nm and 21.2±1.5 nm) on the molecular weight of PAA blocks in BBCP nanoreactor (Sample-2A, and Sample-3B as nanoreactors, respectively, in Table S2).

Supplementary Information Section V. Their crystalline lattices are shown as insets in **Figure 3** and **Fig. S61**. Their crystal structures and compositions were further substantiated by XRD measurements and EDS microanalysis (**Supplementary Information Section X**). As the surface of nanorods and nanowires is directly and permanently tethered with PS chains that prevent their aggregation, they are readily sobluble in a wide range of organic solvents (e.g, toluene), forming a homogeneous solution as clearly evidenced in **Figure S62**. It is notable that the excess precursors that are present outside the cylindrical BBCP nanoreactor can easily form large, irregular, inorganic materials due to the lack of surface capping by PS chains, and thus readily precipitated from organic solvents. Clearly, our nanoreactor strategy is very convenient and effective in producing relatively pure 1D nanocrystals (**Supplementary Information Section VI**).

Quite intriguingly, by simply employing double-hydrophilic cylindrical cellulose-*g*-[PAA-*b*-PEG] BBCP as a nanoreactor synthesized by a combination of ATRP and a click reaction (**Figure S14**, **Table S3**, and **Supplementary Information Section III**), a series of water-soluble PEG-tethered plain nanorods and nanowires, such as Au (**Figure S30**-**S31**), $NaYF_4$:Yb/Er (**Figure S32**), and Fe_3O_4 (**Figure S33**), are also successfully created (**Supplementary Information Section IV**). These water-soluble 1D nanocrystals are pertinent to a number of scientific areas including self-assembly, bioimaging and biosensors.(*13*)

Strikingly, our cylindrical BBCP nanoreactor strategy also affords a unique platform to synthesize high-quality core/shell nanorods composed of two substantially disparate materials with large lattice mismatches between them. For synthesis of high-quality core/shell nanoparticles, it often relies on moderate lattice mismatch (<2%) between two dissilamar materials in order to entail an expitaxial growth.(*21*) This greatly limits the core and shell material choices due to such conditioned material combination (i.e., crystal structure, bonding, and epitaxial growth sequence)(*22*) for epitaxial linkage. More importantly, in comparison to core/shell nanoparticles, the effective methods to produce core/shell nanorods are comparatively few and limited in scope.(*23*)

The creation of core/shell nanorods with controlled dimensions (i.e., core diameter,

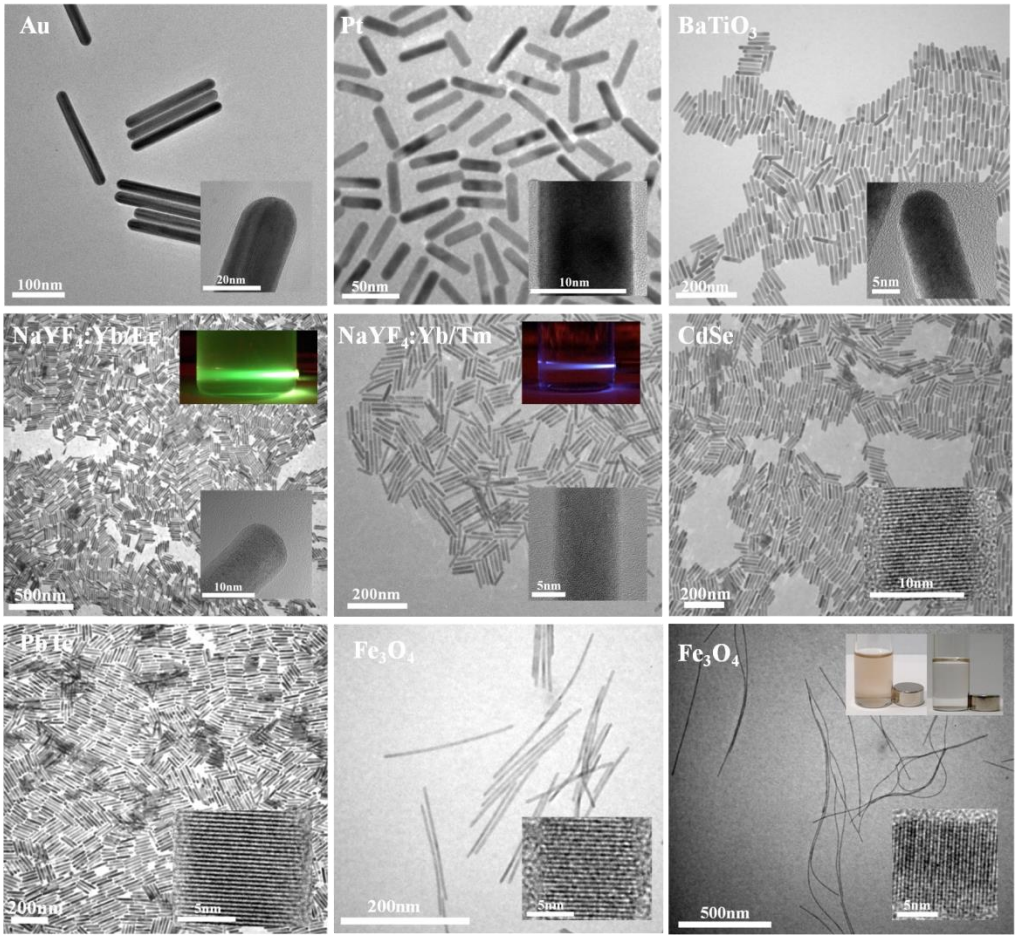

Figure 3. Representative TEM images of a rich variety of plain nanorods and nanowires crafted by using cellulose-*g*-[PAA-*b*-PS] as a nanoreactor (i.e., Sample-1A, Sample-2A, Sample-3A, Sample-3B and Sample-5A in Table S2). They include noble metal (Au and Pt), ferroelectric ($BaTiO_3$), upconversion ($NaYF_4$:Yb/Er; green emitting; $NaYF_4$:Yb/Tm, blue emitting), semiconducting (CdSe), and thermoelectric (PbTe) nanorods, as well as magnetic (Fe_3O_4) nanowires. The dimensions of these 1D nanocrystals are as follows: Au nanorods (L = 206±19 nm, D = 21.2±1.5 nm; Sample-3B as nanoreactor); Pt nanorods (L = 48±5 nm, D = 10.2±0.6 nm; Sample-1A as nanoreactor); $BaTiO_3$ nanorods (L = 101±8 nm, D = 10.6±0.8 nm; Sample-2A as nanoreactor); $NaYF_4$:Yb/Er nanorods (green emitting, L = 99±10 nm, D = 9.6±0.4 nm; Sample-2A as nanoreactor); $NaYF_4$:Yb/Tm nanorods (blue emitting, L = 103±7 nm, D = 10.4±0.5 nm; Sample-2A as nanoreactor); CdSe nanorods (L = 98±9 nm, D = 10.1±0.7 nm; Sample-2A as nanoreactor); PbTe nanorods (L = 102±10 nm, D = 9.9±0.6 nm; Sample-2A as nanoreactor); Fe_3O_4 nanowires (L = 203±16 nm, D = 10.2±0.8 nm, Sample-3A as nanoreactor; and L = 916±87 nm, D = 10.3±0.5 nm, Sample-5A as nanoreactor). The crystalline lattices of each sample are clearly evident in the HRTEM images shown as insets. Corresponding digital images of these nanorods and nanowires are included in Figure S62. Insets: digital images of upconversion nanorods under near-infrared laser illumination (980 nm at 2W) displaying green ($NaYF_4$:Yb/Er) and blue ($NaYF_4$:Yb/Tm) fluorescence. Likewise, digital images of Fe_3O_4 nanowires toluene solution demonstrating their magnetic properties are shown in inset. Fe_3O_4 nanowires were deposited on the wall of vials (right) by placing a magnetic bar next to the vial.

shell thickness, and length) and compositions, including organic solvent-soluble and water-soluble core/shell nanorods, is enabled by employing a new class of cylindrical BBCPs comprising densely grafted amphiphilic triblock copolymer as side chains, that is, cellulose-*g*-[P4VP-*b*-P*t*BA-*b*-PS] and cellulose-*g*-[P4VP-*b*-P*t*BA-*b*-PEG], respectively, as nanoreactors (**Supplementary Information Section IV**) through coordination reactions between functional blocks in the triblock copolymer-containing BBCP and the respective precursors.

We utilize the synthesis of noble metal/magnetic Au/Fe_3O_4 core/shell nanorods as an example to demonstrate the effectiveness of cylindrical cellulose-*g*-[P4VP-*b*-P*t*BA-*b*-PS] BBCPs (upper right panel in **Figure 1b)** as nanoreactors in producing organic solvent-soluble core/shell nanorods (**Supplementary Information Section III**). The Au core nanorod with L = 103±7 nm and D = 10.5±0.6 nm (**Figure 4b**) was first synthesized through the preferential incorporation of its precursors in the space occupied by the inner P4VP blocks via the selective coordination interaction between the pyridyl functional group of P4VP blocks and the metal moieties of precursors (central panel in **Figure 1b**). The possible formation mechanism is illustrated in **Figure S53**. Subsequently, the P*t*BA blocks of P*t*BA-*b*-PS tethered on the surface of Au core nanorod were hydrolyzed into PAA blocks (**Supplementary Information Section IV**), thus templating the formation of Fe_3O_4 shell (**Figure S54**). The resulting Au/Fe_3O_4 core/shell nanorods tethered by PS chains exhibited uniform dimensions. The HRTEM image in **Figure 4b** clearly shows that the highly crystalline Au core appeared dark and was surrounded by a shell of relatively lighter Fe_3O_4 (4.6 ± 0.4 nm thick). The XRD and EDS measurements further verified the crystal structures and compositions of Fe_3O_4 and Au, respectively (**Figure S85** and **Figure S97**). It is important to note that in spite of a more than 50% lattice mismatch between Fe_3O_4 and Au,(*24*) Au/Fe_3O_4 core/shell nanorods were successfully created by capitalizing on the cylindrical cellulose-*g*-[P4VP-*b*-P*t*BA-*b*-PS] BBCP nanoreactor. More importantly, organic solvent-soluble core/shell nanorods with many other material combinations can also be readilly prepared by choosing appropriate precursors (e.g., magnetic/metallic Fe_3O_4/Au in **Figure S35**, and metallic/semiconducting Au/TiO_2 in **Figure S37**).

Similarly, the use of cylindrical cellulose-*g*-[P4VP-*b*-P*t*BA-*b*-PEG] BBCP containing two independent template compartments (i.e., inner P4VP for core, and PAA hydrolyzed from P*t*BA for shell) (**Supplementary Information Section III**; upper right panel in **Figure S16**) as a nanoreactor yielded water-soluble core/shell nanorods (lower left panel in **Figure S16**); such as metallic/semiconducting Au/TiO_2 (**Figure S39**), metallic/upconversion Au/$NaYF_4$:Yb/Er (**Figure S40**) directly connected with hydrophilic PEG blocks (**Table S5** and **Supplementary Information Section IV**). Likewsie, the crystal structures and compositions of these nanorods were comfirmed by XRD and EDS measurements (**Supplementary Information Section X**).

We note that the core diameter and shell thickness of nanorods can be precisely tuned by varying the molecular weight of the inner P4VP block and the intermediate P*t*BA block (subsequently hydrolyzed into PAA). These are readily controlled by mediating the polymerization time during the ATRP of 4-vinylpyridine and *tert*-butyl acrylate, respectively. Moreover, the uniform length of nanorods is also attainable by controlling the length of cellulose-Br macroinitiator through fractional precipitation. More importantly, as the core and shell materials can be grown independently in the respective templates, this cylindrical cellulose-*g*-[P4VP-*b*-P*t*BA-*b*-PEG] BBCP nanoreactor strategy virtually eliminates the restriction of lattice matching requirements.(*21*) Thus, our cylindrical BBCP composed of

amphiphilic triblock copolymer arms has the potential to underpin the creation of an exotic set of core/shell nanorods which would otherwise be challenging to obtain. These multifunctional core/shell nanorods render the tailoring and exploration of their unique size and shape-dependent material properties.

Remarkably, the amphiphilic cylindrical BBCP nanoreactor strategy is quite versatile as it also enables the synthesis of uniform nanotubes (i.e., hollow nanorods) by selectively restricting the appropriate precursors in the intermediate *B* block to grow into nanotubes, where their inside and outside surfaces are tethered by inner and outer *A* blocks, when cylindrical BBCP comprising A-*b*-B-*b*-A triblock copolymers as arms is exploited as nanoreactor. As an example, organic solvent-soluble Au nanotubes (**Table S6**; **Supplementary Information Section IV**) were synthesized by using amphiphilic cellulose-*g*-[PS-*b*-PAA-*b*-PS] as a nanoreactor (upper right panel in **Figure 1c**). The Au precursors were sequestered in the intermediate PAA compartment, and ultimately formed PS-tethered Au nanotubes (lower left panel in **Figure 1c**). **Figure 4c** clearly shows that the center of nanotubes appears brighter and signifies that they were hollow. The HRTEM image (lower right panel in **Figure 4c**) and XRD pattern (**Figure S87**) suggested that the nanotubes are highly crystalline. Moreover, the composition analysis by EDS measurements further corroborated the successful formation of Au nanotubes (**Figure S99**). The diameter of the hollow interior and the thickness of the nanotube can be accurately controlled by tailoring the molecular weights of the inner PS block and intermediate P*t*BA block during the ATRP of styrene and *tert*-butyl acrylate, respectively. Thus, an assortment of nanotubes with different sizes and compositions can be produced, including upconversion $NaYF_4$:Yb/Er nanotubes (**Figure S42**) and semiconducting TiO_2 nanotubes (**Figure S44**). Despite the uniform diameter and thickness, there was a distribution of Au nanotube length (**Figure 4c**) due to the presence of different lengths of individual cellulose-Br macroinitiators used to prepare cellulose-*g*-[PS-*b*-PAA-*b*-PS] nanoreactors. However, cellulose-Br macroinitiators with uniform length can be realized by fractional precipitation as demonstrated in the production of plain and core/shell nanorods. Likewise, by using cellulose-*g*-[PS-*b*-PAA-*b*-PEG] as a nanoreactor (**Figure S18**), water-soluble nantubes (e.g., Au, TiO_2 and $NaYF_4$:Yb/Er in **Figure S45, S46** and **S47**, respecitively) intimately linked with hydrophilic PEG blocks can also be synthesized (**Table S7**; **Supplementary Information Section IV**).

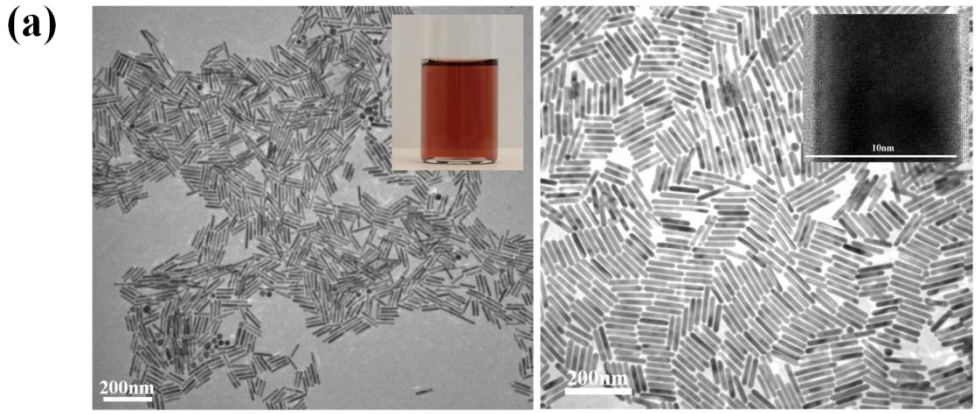

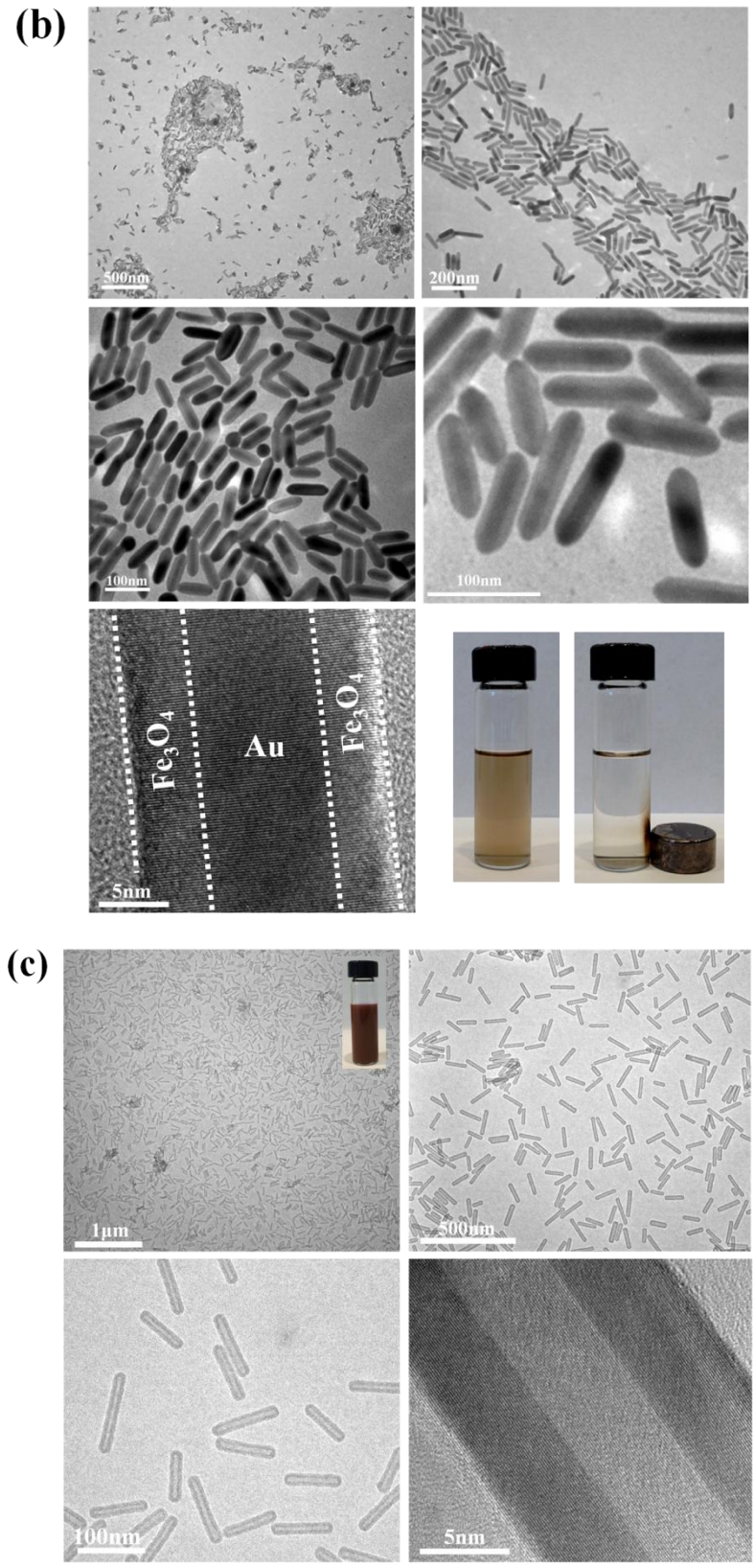

Figure 4. TEM and digital images of metallic/magnetic Au/Fe_3O_4 core/shell nanorods and metallic Au nanotubes formed by exploiting cellulose-*g*-[P4VP-*b*-P*t*BA-*b*-PS] (Sample-2B in Table S4) and cellulose-*g*-[PS-*b*-PAA-*b*-PS] (Sample-2A in Table S6) as nanoreactors,

respectively. (A) TEM images of Au nanorods as core (L = 103±7 nm, D = 10.5±0.6 nm) at two different magnifications. Digital image of the Au core nanorods toluene solution and HRTEM image of a Au nanorod are shown as insets. (B) TEM images of Au/Fe_3O_4 core/shell nanorods (Fe_3O_4 shell thickness, t = 4.6±0.4 nm) at varied magnifications. The representative HRTEM image clearly shows the crystalline lattices of the Au core and Fe_3O_4 shell (relatively dark Au core surrounded by light Fe_3O_4 shell; white dashed lines for guidance). The magnetic properties of Au/Fe_3O_4 nanorods are evident in the digital image of Au/Fe_3O_4 nanorods toluene solution in response to an external magnet, during which the solution became clear and nanorods were deposited on the wall of the vial. (C) TEM images of Au nanotubes at different magnifications (L = 103±12 nm, t = 5.1±0.5 nm; the diameter of hollow interior = 5.3±0.4 nm). Interestingly, the representative HRTEM image of Au nanotubes revealed that the Au shell was highly crystalline, and the appearance of crystalline lattice in the center was due to the presence of the crystalline Au shell below and above the hollow interior during imaging.

For all 1D nanocrystals produced (**Figures 2-4**), the two ends of each nanocrystal were round. This is not surprising as each cellulose backbone was heavily grafted with diblock or triblock copolymers as arms, these densely populated arms can stretch out at the two ends of cylindrical BBCP due to the free space available at the ends. Moreover, the two ends of a cellulose backbone had two hydroxyl groups which allowed for the growth of a diblock or triblock copolymer arm at each end by ATRP. Taken together, the brushes on the ends of the cylindrical BBCP possessed a hemi-spherical chain conformation. This lead to the formation of hemisphere-shaped nanocrystals situated at both ends of the 1D nanocrystals. It is also noteworthy that the formation of highly crystalline nanorods (HRTEM images in **Figure 2a-2b** and **Figure 3**), core/shell nanorods (HRTEM images in **Figure 4a-4b**), and nanotubes (HRTEM image in **Figure 4b**) is of special interest in their own right. They merit a detailed *in-situ* TEM study and will be the subject of future investigation.

In summary, over the past three years we developed a general and roubust strategy for the synthesis of a spectacular variety of 1D nanocrystals with high-level control over dimension, anisotropy, composition, surface chemistry (i.e., tethered with either hydrophobic polymers for organic solvent-soluble nanocrystals or hydrophilic polymers for water-soluble nanocrystals), architecure (i.e., plain nanorods and nanowires, core/shell nanorods, and nanotubes). Central to this effective strategy is the rational design and synthesis of functional BBCPs as nanoreactors. Theses cylindrical BBCPs are composed of a cellulose backbone densely grafted with diblock or triblock copolymers of precisely tunable arm lengths. In particular, this cylindrical BBCP nanoreactor strategy provides exciting opportunities for crafting intriguing size-tailorable core/shell nanorods composed of two dissimilar materials. They possess unique properties due to the close proximity between disparate constituent materials and offer an opportunity for exploring many fundamental nanoscale physics. All these 1D nanocrystals can serve as building blocks for the bottom-up assembly for nanostructured materials and devices with desirable characteristics enabled by the properties of individual nanocrystals and their proper spatial arrangement for use in optics, electronics, photonics, optoelctronics, magnetic technologies, sensory materials and devices, lightweight structural materials, catalysis, drug delivery, biotechnology. They can also serve as model systems for fundamental research in self-assembly, phase behavior and crystallization kinetics of nanocrystals.(*25*) Looking to the future, more compositionally-different and morphologically-complex multifunctional 1D nanocrystals (for example, core/shell 1/shell 2

nanorods) may also be created by conveniently implementing cylindrical BBCP templates possessing tetrablocks, pentablocks, and more block copolymers as arms, thus rendering investigation of their peculiar properties (e.g., synergistic functionality) for versatile applications. Moreover, this preparative strategy may also enable the production of a wealth of polymeric 1D nanostructures(*26*) reached through selectively crosslinking the target block of grafted copolymer arms in cylindrical BBCPs, for example, 1D nanocapsules for potential applications in selective ion transport, biosensor, controlled release of drugs, etc.(*27*) Finally, we note that the future of 1D nanocrystal synthesis capitalizing on cylindrical BBCPs as nanoreactors is to scale up production for a myriad of technological applications. This will be the focus of future work.

References

1. X. Pang, L. Zhao, W. Han, X. Xin, Z. Lin, A general and robust strategy for the synthesis of nearly monodisperse colloidal nanocrystals. *Nat. Nanotechnol.* **8**, 426-431 (2013).
2. Y. Yin, A. P. Alivisatos, Colloidal nanocrystal synthesis and the organic-inorganic interface. *Nature* **437**, 664-670 (2005).
3. A. Gole, C. J. Murphy, Seed-mediated synthesis of gold nanorods: role of the size and nature of the seed. *Chem. Mater.* **16**, 3633-3640 (2004).
4. R. H. Baughman, A. A. Zakhidov, W. A. de Heer, Carbon nanotubes--the route toward applications. *Science* **297**, 787-792 (2002).
5. Y. Huang, X. Duan, Q. Wei, C. M. Lieber, Directed assembly of one-dimensional nanostructures into functional networks. *Science* **291**, 630-633 (2001).
6. H. Xu, Y. Xu, X. Pang, Y. He, J. Jung, H. Xia, Z. Lin, A general route to nanocrystal kebabs periodically assembled on stretched flexible polymer shish. *Sci. Adv.* **1**, e1500025 (2015).
7. J. Hu, A. Liu, H. Jin, D. Ma, D. Yin, P. Ling, S. Wang, Z. Lin, J. Wang, A versatile strategy for shish-kebab-like multi-heterostructured chalcogenides and enhanced photocatalytic hydrogen evolution. *J. Am. Chem. Soc.* **137**, 11004-11010 (2015).
8. B. Piccione, C.-H. Cho, L. K. van Vugt, R. Agarwal, All-optical active switching in individual semiconductor nanowires. *Nat. Nanotechnol.* **7**, 640-645 (2012).
9. J. Hu, T. W. Odom, C. M. Lieber, Chemistry and physics in one dimension: synthesis and properties of nanowires and nanotubes. *Acc. Chem. Res.* **32**, 435-445 (1999).
10. K.-B. Lee, S. Park, C. A. Mirkin, Multicomponent magnetic nanorods for biomolecular separations. *Angew. Chem. Int. Ed.* **116**, 3110-3112 (2004).
11. J. Wang, Z. Lin, Freestanding TiO2 nanotube arrays with ultrahigh aspect ratio via electrochemical anodization. *Chem. Mater.* **20**, 1257 (2008).
12. M. Law, L. E. Greene, J. C. Johnson, R. Saykally, P. Yang, Nanowire dye-sensitized solar cells. *Nat. Mater.* **4**, 455-459 (2005).
13. L. Vigderman, B. P. Khanal, E. R. Zubarev, Functional gold nanorods: functional gold nanorods: synthesis, self-assembly, and sensing applications. *Adv. Mater.* **24**, 5016-5016 (2012).
14. J. Yuan, Y. Xu, A. Walther, S. Bolisetty, M. Schumacher, H. Schmalz, M. Ballauff, A. H. E. Muller, Water-soluble organo-silica hybrid nanowires. *Nat. Mater.* **7**, 718-722 (2008).
15. K. T. Nam, D.-W. Kim, P. J. Yoo, C.-Y. Chiang, N. Meethong, P. T. Hammond, Y.-M. Chiang, A. M. Belcher, Virus-enabled synthesis and assembly of nanowires for lithium ion battery electrodes. *Science* **312**, 885-888 (2006).
16. M. R. Jones, K. D. Osberg, R. J. Macfarlane, M. R. Langille, C. A. Mirkin, Templated techniques for the synthesis and assembly of plasmonic nanostructures. *Chem. Rev.* **111**, 3736-3827 (2011).
17. C. Ma, Z. L. Wang, Road map for the controlled synthesis of CdSe nanowires, nanobelts, and nanosaws—a step towards nanomanufacturing. *Adv. Mater.* **17**, 2635-2639 (2005).
18. D. J. Milliron, S. M. Hughes, Y. Cui, L. Manna, J. Li, L.-W. Wang, A. Paul Alivisatos, Colloidal nanocrystal heterostructures with linear and branched topology. *Nature* **430**, 190-195 (2004).
19. D. Roy, M. Semsarilar, J. T. Guthrie, S. Perrier, Cellulose modification by polymer grafting: a review. *Chem. Soc. Rev.* **38**, 2046-2064 (2009).
20. S. Kidambi, J. Dai, J. Li, M. L. Bruening, Selective hydrogenation by Pd nanoparticles embedded in polyelectrolyte multilayers. *J. Am. Chem. Soc.* **126**,

2658-2659 (2004).
21. J. Zhang, Y. Tang, K. Lee, M. Ouyang, Nonepitaxial growth of hybrid core-shell nanostructures with large lattice mismatches. *Science* **327**, 1634-1638 (2010).
22. C. J. Palmstrom, Epitaxy of dissimilar materials. *Annu. Rev. Mater. Sci.* **25**, 389-415 (1995).
23. J. Tang, Z. Huo, S. Brittman, H. Gao, P. Yang, Solution-processed core-shell nanowires for efficient photovoltaic cells. *Nat. Nanotechnol.* **6**, 568-572 (2011).
24. H. Yu, M. Chen, P. M. Rice, S. X. Wang, R. L. White, S. Sun, Dumbbell-like bifunctional Au−Fe3O4 nanoparticles. *Nano Lett.* **5**, 379-382 (2005).
25. C. Burda, X. Chen, R. Narayanan, M. A. El-Sayed, Chemistry and properties of nanocrystals of different shapes. *Chem. Rev.* **105**, 1025-1102 (2005).
26. J. Qian, X. Li, D. J. Lunn, J. Gwyther, Z. M. Hudson, E. Kynaston, P. A. Rupar, M. A. Winnik, I. Manners, Uniform, high aspect ratio fiber-like micelles and block co-micelles with a crystalline π-conjugated polythiophene core by self-seeding. *J. Am. Chem. Soc.* **136**, 4121-4124 (2014).
27. K. Huang, J. Rzayev, Charge and size selective molecular transport by amphiphilic organic nanotubes. *J. Am. Chem. Soc.* **133**, 16726-16729 (2011).

Publications from 2013 to 2016 on this AFOSR project:

13. X. Pang, Y, He, J. Jung, and **Z. Lin***, "An Enticing and General Strategy for Crafting One-Dimensional Nanocrystals with Unprecedented Control over Dimension, Composition and Architecture", ***Science*** (revision submitted).

12. M. He, X. Pang, X. Liu, B. Jiang, Y. He, H. Snaith, and **Z. Lin***, "Monodisperse Dual-Functional Upconversion Nanoparticles-Enabled Near-Infrared Organolead Halide Perovskite Solar Cells", ***Angewandte Chemie International Edition***, **55**, 4280 (2016). (featured on the **Cover** of Angewandte Chemie International Edition)

11. H. Xu, Y. Xu, X. Pang, Y. He, J. Jung, H. Xia, and **Z. Lin***, "A general route to nanocrystal kebabs periodically assembled on stretched flexible polymer shish", Science Advances. **1**, e1500025 (2015). (Highlighted by: [**Science**]; [**Georgia Institute of Technology**]; [**PhysOrg**]; [**ScienceDaily**]; [**Nanowerk**]; [**World of Chemicals**]; [**Nanotechnology Now**]; [**Pinterest**]; [**Fnews**]; [**Nano Daily**]; [**TrendsSoul**]; and [more])

10. B. Jiang, X. Pang, B. Li, and **Z. Lin***, "Organic-inorganic nanocomposites via placing monodisperse ferroelectric nanocrystals in direct and permanent connect with ferroelectric polymers", ***Journal of the American Chemical Society***, **137**, 11760 (2015).

9. D. Yang, X. Pang, Y. He, Y. Wang, G. Chen, W. Wang, and **Z. Lin***, "Precisely Size-Tunable Magnetic/Plasmonic Core/Shell Nanoparticles with Controlled Optical Properties", ***Angewandte Chemie International Edition***, **127**, 12259 (2015).

8. D. Zheng, X. Pang, M. Wang, Y. He, C. Lin, and **Z. Lin***, "Unconventional Route to Hairy Plasmonic/Semiconductor Core/Shell Nanoparticles with Precisely Controlled Dimensions and Their Use in Solar Energy Conversion", ***Chemistry of Materials***, **27**, 5271 (2015).

7. H. Xu, X. Pang, Y. He, M. He, J. Jung, H. Xia, and **Z. Lin***, "An Unconventional Route to Monodisperse and Intimate Semiconducting Organic-Inorganic Nanocomposites", ***Angewandte Chemie International Edition***, **54**, 4636 (2015). (featured on the **Cover** of Angewandte Chemie International Edition).

6. Y. Xu, C. Wang, S. Zhong, W. Li, and **Z. Lin***, "Self-assembly of Miktoarm Star-Like ABn Block Copolymers: From Wet to Dry Brushes", ***Langmuir***, **31**, 2905 (2015).

5. X. Pang, C. Wan, M. Wang, and **Z. Lin***, "Strictly biphasic soft and hard Janus structures: synthesis, properties and applications", ***Angewandte Chemie International Edition***, **53**, 5524 (2014).

4. M. He, M. Wang, C. Lin, and **Z. Lin***, "Optimization of molecular organization and nanoscale morphology for high performance low bandgap polymer solar cells", ***Nanoscale***, **6**, 3984 (2014). (featured on **Inside Front Cover** of Nanoscale).

3. M. He, D. Zheng, M. Wang, C. Lin, and **Z. Lin***, "High efficiency perovskite solar cells: from complex nanostructure to planar heterojunction", ***Journal of Materials Chemistry A***, **2**, 5994 (2014). (featured on **Cover** of Journal of Materials Chemistry A).

2. X. Pang, C. Feng, H. Xu, W. Han, X. Xin, H. Xia, and **Z. Lin***, "Unimolecular micelles composed of inner coil-like blocks and outer rod-like blocks crafted by combination of living polymerization with click chemistry", ***Polymer Chemistry,* 5**, 2747 (2014).

1. C. Feng, X. Pang, Y. He, B. Li, and **Z. Lin***, "Robust Route to Unimolecular Core–Shell and Hollow Polymer Nanoparticles", ***Chemistry of Materials,* 26**, 6058 (2014). (Highlighted by **ACS Noteworthy Chemistry**.

Supplementary Information

General and Robust Strategies for Multifunctional Oragnic-Inorganic Nanocomposites via Direct Growth of Monodisperse Nanocrystals *Intimately* and *Permanently* Connected with Polymers

Zhiqun Lin; Professor
School of Materials Science and Engineering, Georgia Institute of Technology, Atlanta, GA 30332

Final Report on the AFOSR project: FA9550-13-1-0101 **(03/2013-05/2016)**

Content

Section I

Materials and Characterizations

1. Materials

Cellulose powder (microcrystalline, MP Biomedicals *LLC*), 1-methylimidazole (99%, Alfa Aesar) and allyl chloride (> 98.0%, TCI) were used as starting materials without further purification. 2-Bromoisobutyryl bromide (98%), *N*,*N*,*N'*,*N''*,*N''*-pentamethyldiethylene triamine (PMDETA, 99%), tris[2-(dimethylamino)ethyl]amine (Me_6-TREN, 97%), 1-methyl-2-pyrrolidinone (NMP, anhydrous, 99.5%) and propargyl bromide solution (80 wt.% in toluene) were purchased from Sigma-Aldrich, and used as received. CuBr (98%, Sigma-Aldrich) was stirred for 24 h in acetic acid, filtered, washed with ethanol and diethyl ether successively, and dried in vacuum. Two samples of poly(ethylene glycol) methyl ether (mPEG, M_n =5,000 and M_n =10,000, respectively; Sigma-Aldrich) was used as received. *tert*-Butyl acrylate (*t*BA, Sigma-Aldrich, 98%), 4-vinylpyridine (4VP, ≥ 95%, Sigma-Aldrich), methyl ethyl ketone (99.9%, Fisher Scientific) and *N*,*N*-dimethylformamide (DMF, Fisher Scientific, 99.9%) were dried by CaH_2 and distilled under reduced pressure prior to use. Styrene (St, Sigma-Aldrich ≥99%) was purified with 10% NaOH aqueous solution and water successively, dried by adding anhydrous $MgSO_4$ and CaH_2 sequentially, and then distilled under reduced pressure. Diphenylmethyl sodium (DPMNa) (c = 0.56 M) was prepared according to the literature.[1] Tetrahydrofuran (THF, 99%, BDH) was dried by refluxing with sodium, and then distilled from sodium naphthalenide solution. Trifluoroacetic acid (TFA, 99%), Yttrium(III) oxide (Y_2O_3, 99.99%), Ytterbium(III) oxide (Yb_2O_3, 99.9%), Erbium(III) oxide (Er2O3, ≥99.99%) and Thulium(III) oxide (Tm_2O_3, 99.9%) were purchased from Sigma-Aldrich and used as received. Gold(III) chloride trihydrate ($HAuCl_4 \cdot 3H_2O$, ≥99.9%), *tert*-butylamine borane (TBAB, 97%), chloroplatinic acid hexahydrate ($H_2PtCl_6.6H_2O$, ACS reagent, ≥ 37.50% Pt basis), ethylene glycol (EG**,** anhydrous, 99.8%), sodium hydroxide (NaOH, ≥ 98%), barium chloride dihydrate ($BaCl_2.2H_2O$, ≥ 99%), titanium(IV) chloride ($TiCl_4$, ≥ 99%), iron(II) chloride tetrahydrate ($FeCl_2.4H_2O$, ≥ 99%), iron(III) chloride hexahydrate ($FeCl_3 \cdot 6H_2O$, ≥

98%), ammonium hydroxide solution ($NH_3.H_2O$, ACS reagent, 28.0-30.0% NH_3 basis), cadmium acetylacetonate ($Cd(acac)_2$, ≥ 99.9%), selenium powder (Se, 99.99%), lead(II) carbonate ($PbCO_3$, ≥ 99.99%), sodium borohydride ($NaBH_4$, ≥ 99%), tellurium powder (Te, 99.99%), and titanium(IV) isopropoxide (TTIP, ≥ 97.0%) were purchased from Sigma-Aldrich and used as starting materials without further purification. All other reagents were purified by common purification procedures.

2. Methods

Synthesis of 1D nanocrystals using cylindrical bottlebrush-like block copolymers as nanoreactors. For the synthesis of plain nanorods and nanowires, for example, $NaYF_4$:Yb/Er nanorods, 10 mg of cellulose-*g*-[PAA-*b*-PS] template was dissolved in a 10 mL DMF at room temperature, followed by the addition of an appropriate amount of precursors (i.e., $Na(CF_3COO)$, $Y(CF_3COO)_3$, $Yb(CF_3COO)_3$ and $Er(CF_3COO)_3$) that were preferentially encapsulated within the compartment occupied by inner PAA blocks. To maximize the incorporation of precursors into the PAA domains, the molar ratio of acrylic acid (AA) units in PAA block to precursors was set at 1:10. The mixture was then stirred for 1h under argon to ensure that all precursors were well dissolved in DMF. The reaction system was then slowly heated to the boiling point of DMF and refluxed for a period of time (i.e., 2 h for $NaYF_4$:Yb/Er nanorods). In order to to yield a highly crystalline hexagonal phase of $NaYF_4$:Yb/Er nanorods, the resulting solution and additional quantitative CF_3COONa were then transferred to a 20 mL Teflon-lined autoclave, stirred and heated at 200^oC for 2h. For the preparation of core/shell nanorods, for example, Au/Fe_3O_4 core/shell nanorods, 10 mg cellulose-*g*-[P4VP-*b*-P*t*BA-*b*-PS] template was dissolved in 10 mL of DMF at room temperature. First, the core material was produced via the incorporation of its precursors (i.e., $HAuCl_4.3H_2O$ with tert-butylamine-borane complex (TBAB) as reducer) in the space occupied by the inner P4VP blocks followed by reaction at a certain temperature for a period of time (i.e., at 60^oC for 2 h for Au). Likewise, the molar ratio of 4-vinylpyridine (4VP) unit in P4VP block to precursors was also set to

be 1:10. Subsequently, the P*t*BA blocks of P*t*BA-*b*-PS situated on the surface of Au nanorod were hydrolyzed into PAA by trifluoroacetic acid (TFA). The shell material (Fe_3O_4, $FeCl_2 \cdot 4H_2O$ + $FeCl_3 \cdot 6H_2O$ + $NH_3.H_2O$ used as precursors) was then formed by performing the reaction at 50^{o}C for 30 min in DMF, with PAA blocks functioning as the template. Subsequently, the black mixture was aged at 80°C for 1 h to improve the Fe_3O_4 crystallization of the resulting Au/Fe_3O_4 core/shell nanorods. For the creation of nanotubes, for example Au nanotubes, 10 mg cellulose-*g*-[PS-*b*-PAA-*b*-PS] template was dissolved in 10 mL of DMF at room temperature. Similarly, the precursor (i.e., $HAuCl_4.3H_2O$ with TBAB as reducer) was added into the template solution. The reaction solution was then slowly heated to a certain temperature for a period of time (i.e., at 60^{o}C for 2 h for Au nanotubes). For the synthesis of water-soluble 1D nanocrystals tethered with hydrophilic PEG blocks as ligands, see **Supplementary Information IV**.

Synthesis of 1D nanocrystals using linear block copolymers as templates. Linear block copolymers (i.e., PAA-*b*-PS, P4VP-*b*-P*t*BA-*b*-PS, and PS-*b*-PAA-*b*-PS) with similar molecular weights and block ratios to those of BBCPs were also synthesized by sequential ATRP. They were used as controls to assess the ability of these linear block copolymers to form 1D nanocrystals under the same experimental conditions. Instead of 1D nanocrystals, large aggregates with irregular size and shape were obtained when these linear block copolymers were utilized as templates (see **Supplementary Information Section XI** for detailed comparisons).

3. Characterizations

(1) Molecular weights of all synthesized polymers that can be well-dissolved in THF were characterized by gel permeation chromatography (GPC, Shimadzu) equipped with an LC-20 AD HPLC pump and a refractive index detector (RID-10A, 120 V). THF was used as the mobile phase at a flow rate of 1.0 ml/min at 35°C. One Phenogel

5 mm linear column and one Phenogel 5 mm 10E4A mixed bed column were calibrated with 10 monodisperse PS standard samples with molecular weights ranging from 500 to 1.2×10^6 g/mole.

(2) GPC analysis of P4VP-based polymers was performed in DMF containing 0.1% LiBr additive at 1 mL/min flow rate (LC-20AD pump) on a Shimadzu GPC setup equipped with two Phenomenex Phenogel 10 μm linear columns (300×7.8mm), autosampler (SIL-20A) and column oven (CTO-20A) set at 40°C. The detection was achieved using a RI detector (RID-10A). The instrument was calibrated with EasiVial poly(methyl methacrylate) standards (Agilent).

(2) All ^{1}H-NMR spectra were acquired using a Bruker 400 MHz spectrometer.

(3) FTIR spectra were recorded on the Shimadzu IRAffinity-1 spectrometer equipped with a Miracle Single Reflection Horizontal ATR Accessory (Pike Technologies).

(4) Morphologies of 1D nanocrystals were characterized by TEM (JEOL TEM 100CX; operated at 100 kV), and HRTEM (FEI Tecnai F30; operated at 300kV).

(5) Energy-dispersive x-ray spectroscopy (EDS) analysis of samples was carried out with scanning electron microscopy (SEM, LEO 1530, Zeiss).

(6) Crystal structures of all samples were examined by XRD (X'Pert PRO, Netherlands).

(7) UV-vis absorption spectra were obtained using a Shimadzu UV-2600 UV-vis spectrophotometer.

(8) Photoluminescence spectra were acquired using a Shimadzu RF-5301 spectrofluorometer (equipped with a 150 W xenon lamp light source and a R928 photomultiplier).

(9) Emission spectra of 1D upconversion nanocrystals were recorded on a LS-55 luminescence spectrometer (Perkin-Elmer) with an external tunable 2-W 980-nm

diode laser as the excitation source in the spectrometer.

(10) Weight fractions of polymers in 1D nanocrystals were measured by thermogravimetric analysis (TGA; TA Instrument TGA Q 50).

Section II

Synthesis, purification and characterization of cellulose-based macroinitiators (cellulose-Br) with different lengths (molecular weights) for ATRP

Because of chain stiffness and close packing via numerous intermolecular and intramolecular hydrogen bonds, it is extremely difficult to dissolve cellulose in water and most common organic solvents. Recently, ionic liquids as polar solvents exhibiting a negligible vapor pressure have garnered considerable attention for the processing of cellulose.[2-5] Interestingly, cellulose in high concentrations without derivatization was found to be dissolved using 1-allyl-3-methylimidazolium chloride (AMIMCl) as the solvent for homogeneous esterification of cellulose.[6] Considering the volatility, toxicity, difficulty for solvent recovery, and stability in application, we chose AMIMCl as the ionic liquid to dissolve cellulose in order to prepare cellulose-based macroinitiators (i.e., cellulose-Br).

1. **Preparation of 1-allyl-3-methylimidazolium chloride (AMIMCl) as ionic liquid (Figure S1)[7]**

1-Methylimidazole (50 mL) and allyl chloride (100 mL) were added to a round-bottomed flask. The solution was then refluxed under stirring at 55 °C for 8 h. The unreacted and excess chemical reagents were removed by vacuum distillation, and the resulting viscous product, AMIMCl, is slightly yellowish.

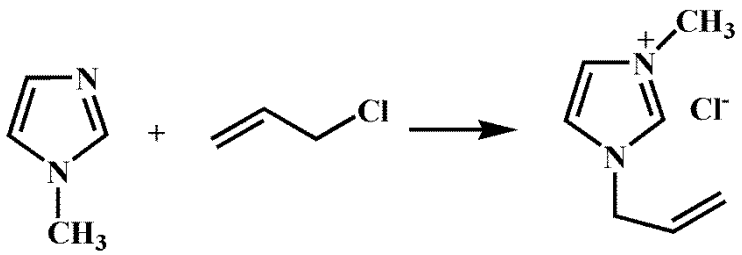

Figure S1. Synthesis of 1-allyl-3-methylimidazolium chloride (AMIMCl).

2. **Synthesis of linear cellulose-based macroinitiator (i.e., cellulose-Br) by a two-step esterification process for subsequent atom transfer radical polymerization (ATRP)**

(1) First esterification

Synthesis of cellulose-Br macroinitiator was carried out according to the procedure shown in **Figure S2**. Prior to dispersing in 50g of AMIMCl (**Figure S1**), a total of 5.0 g of cellulose was vacuum-dried at 80^{o}C for 24 h, and a trace amount of water was removed by the azeotropic distillation with 50 mL of dry toluene. The mixture was heated to 80 ^{o}C under stirring until the cellulose powder was completely dissolved, forming a viscous transparent solution. Subsequently, 30 mL anhydrous NMP and 30 mL anhydrous DMF were added in the reaction solution as the absorbents for HBr generated in the reaction and the diluting agents. 2-Bromoisobutyryl bromide (23mL, the molar ratio of 2-bromoisobutyryl bromide to hydroxyl groups of cellulose = 2:1) was added dropwise to the cellulose solution under magnetic stirring at 0 ^{o}C. After this process was complete, the reaction temperature was maintained at 0 ^{o}C for 1 h and then slowly increased to room temperature, at which the esterification reaction was allowed to continue for 24 h. The resulting brownish solution was poured into 500 mL DI water, yielding white precipitate. After filtration, the final product was purified by dissolution-precipitation twice with acetone and DI water, and dried at 60 ^{o}C in vacuum for 1 day. After the first esterification, the conversion (i.e., esterification) efficiency of hydroxyl groups of cellulose was approximately 82% as calculated from the ^{1}H-NMR spectrum based on the ratio of the integral areas of methyl groups of cellulose-Br to that of protons of cellulose.

(2) Second esterification

In order to convert all hydroxyl groups of cellulose by reacting with 2-bromoisobutyryl bromide, the second esterification process was performed. 20g of dry cellulose-Br was dissolved in a 100 mL of anhydrous NMP and kept in ice-water bath. 20 mL of 2-bromoisobutyryl bromide was then added dropwise into the reaction system. The reaction solution was first maintained in ice water bath for 2 h, and then slowly increased to room temperature. The reaction was kept at room temperature for 24 h. The resulting crude solution was poured into 500 mL of DI water, yielding

white precipitate. After filtration, the final product was purified by dissolution-precipitation twice with acetone and DI water, and dried at 60 ^{o}C in vacuum for 1 day. After the two-step esterification noted above, the esterification efficiency of hydroxyl groups of cellulose was nearly 100%, suggesting that all hydroxyl groups of cellulose were completely converted to bromoisobutyryl units as revealed by ^{1}H-NMR measurement (**Figure S3**).

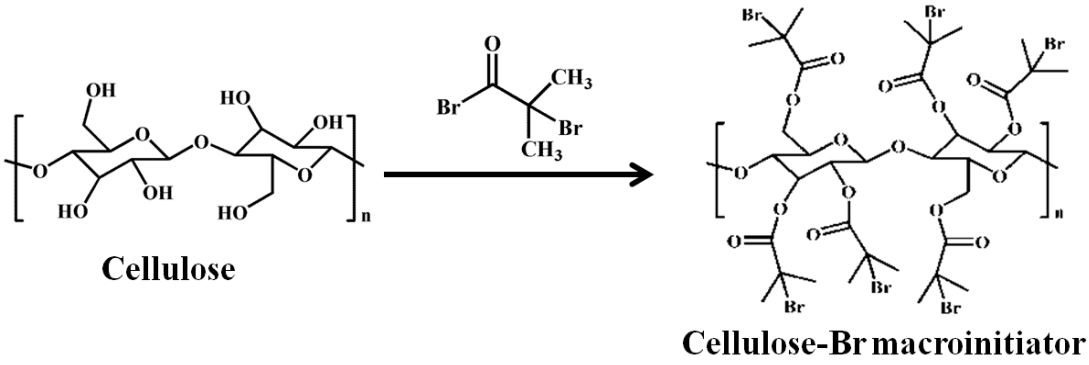

Figure S2. Synthesis of linear cellulose-based macroinitiator (i.e., cellulose-Br) for subsequent ATRP.

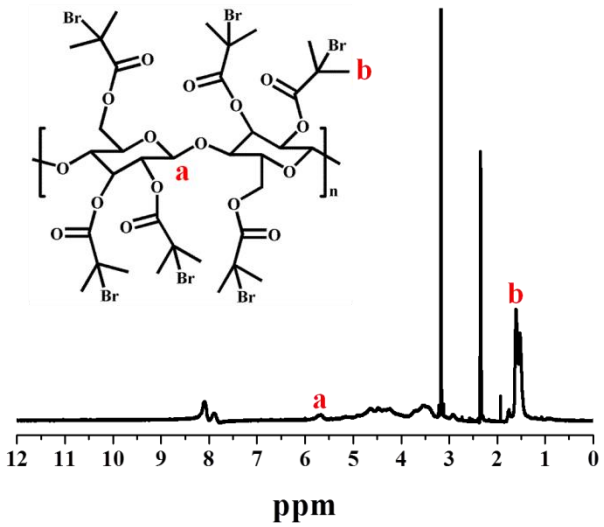

Figure S3. ^{1}H-NMR spectrum of cellulose-Br (DMSO-d_6 as solvent).

The efficiency of esterification of hydroxyl groups of cellulose can be calculated based on the following equation:

$$E_T = \frac{A_b}{18A_a} \quad \text{(S1)}$$

where E_T is the esterification efficiency of hydroxyl groups of cellulose; and A_b and A_a are the integral areas of the methyl protons of cellulose-Br and protons of cellulose, respectively.

3. Preparation of a series of cellulose-Br macroinitiators with different molecular weights and low polydispersity index (PDI) by fractional precipitation

In order to synthesize high-quality 1D nanocrystals possessing uniform length using cylindrical bottlebrush-like block copolymers containing cellulose as the nanoreactor, it is of key importance to prepare monodisperse cellulose chains with narrow molecular weight distribution (i.e., low polydispersity index (PDI); for example, PDI <1.2). This is because the length of 1D nanocrystals is governed by the length of cellulose.

As noted above, due to chain stiffness and close packing induced by numerous intermolecular and intramolecular hydrogen bonds, natural cellulose cannot be dissolved in water and most common organic solvents. Therefore, it is almost impossible to directly separate and purify natural cellulose by fractional precipitation.

It is noteworthy that after esterification as described above, the resulting cellulose-Br macroinitiators can be easily dissolved in a large variety of organic solvents (e.g., acetone, THF, DMF, etc.) (**Figure S4**) as the intramolecular and intermolecular hydrogen bridges in cellulose no longer exist. Under this condition, crude cellulose-Br macroinitiators can be readily separated and purified. Thus, crude cellulose-Br was separated into a series of pure linear macroinitiators with very low PDI (below 1.2) by fractional precipitation with acetone as solvent and DI water as precipitator. Five samples with different molecular weights were thus yielded by fractional precipitation technique (**Figure S6** and **Table S1**).

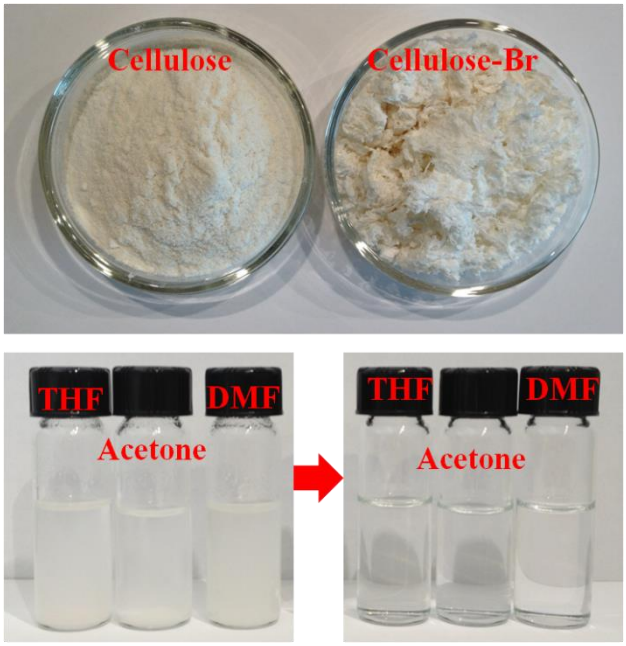

Figure S4. Comparison of solubility of natural cellulose and cellulose-Br in different solvents (THF, acetone and DMF) before (left) and after (right) the esterification process.

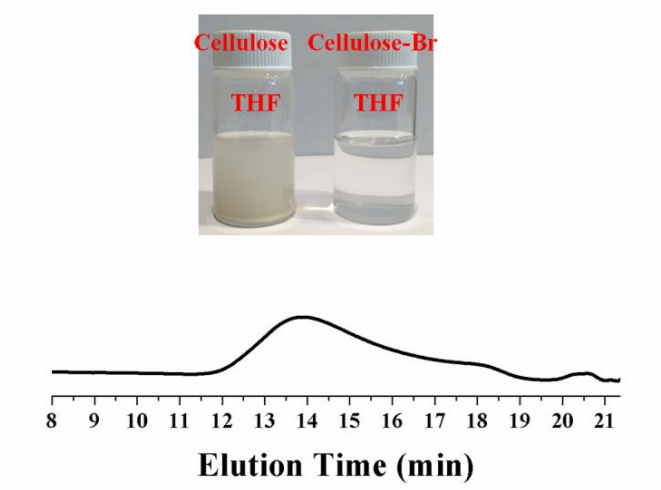

Figure S5. GPC trace of crude macroinitiator (i.e., cellulose-Br) using THF as solvent before the fractional precipitation process.

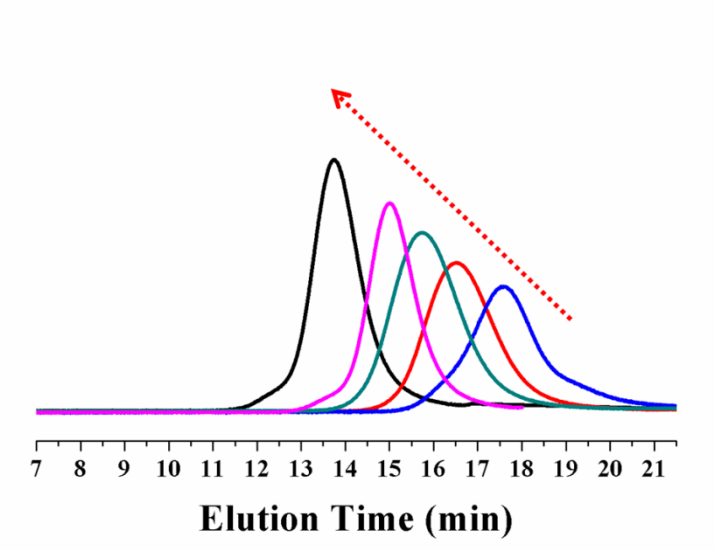

Figure S6. GPC traces of purified cellulose-Br macroinitiators with different molecular weights after fractional precipitation process.

Table S1. Molecular weights of purified cellulose-Br macroinitiators after fractional precipitation process (i.e., samples in **Figure S6**).

Entry	M_n [(a)] (g/mol)	PDI[(b)]	Length (nm) [(c)]
Sample-1	11.2K	1.19	~51
Sample-2	23.5K	1.16	~98
Sample-3	41.8K	1.12	~206
Sample-4	79.6K	1.09	~414
Sample-5	169.0K	1.18	~916

[(a)] Number-average molecular weight determined by GPC, calibrated with PS standards. [(b)] Polydispersity index (PDI) determined by GPC. [(c)] Length (L) of corresponding inorganic nanorods or nanowires.

Section III

Synthesis and characterization of a new class of BBCPs by either sequential atom transfer radical polymerization (ATRP) or a combination of ATRP[8, 9] with click reaction,[10, 11] including cellulose-*graft*-[poly(acrylic acid)-*block*-polystyrene] (denoted cellulose-*g*-[PAA-*b*-PS]) and cellulose-*graft*-[poly(acrylic acid)-*block*-poly(ethylene glycol)] (cellulose-*g*-[PAA-*b*-PEG]) with linear amphiphilic PAA-*b*-PS and double hydrophilic PAA-*b*-PEG diblock copolymers as side chains, respectively, and cellulose-*graft*-[poly(4-vinylpyridine)-*block*-poly(*tert*-butyl acrylate)-*block*-polystyrene] (cellulose-*g*-[P4VP-*b*-P*t*BA-*b*-PS]), cellulose-*graft*-[poly(4-vinylpyridine)-*block*-poly(*tert*-butyl acrylate)-*block*-poly(ethylene glycol)] (cellulose-*g*-[P4VP-*b*-P*t*BA-*b*-PEG]), cellulose-*graft*-[polystyrene-*block*-poly(acrylic acid)-*block*-polystyrene] (cellulose-*g*-[PS-*b*-PAA-*b*-PS]) and cellulose-*graft*-[polystyrene-*block*-poly(acrylic acid)-*block*-poly(ethylene glycol)] (cellulose-*g*-[PS-*b*-PAA-*b*-PEG]) with linear amphiphilic P4VP-*b*-P*t*BA-*b*-PS, P4VP-*b*-P*t*BA-*b*-PEG, PS-*b*-PAA-*b*-PS and PS-*b*-PAA-*b*-PEG triblock copolymers as side chains, respectively.

The synthetic schemes for the BBCPs used as nanoreactors for 1D nanocrystals are shown in **Figure 1** and **Figures S7, S14-S18**.

1. Synthesis of amphiphilic cellulose-*g*-[PAA-*b*-PS] BBCP (Figure 1a and Figure S7; steps a-c) and double hydrophilic cellulose-*g*-[PAA-*b*-PEG] BBCP (Figure S14; steps d-h)

(a) Synthesis of cellulose-*g*-P*t*BA bottlebrush-like polymer utilizing cellulose-Br as a macroinitiator

Cellulose-*g*-P*t*BA bottlebrush-like polymer containing P*t*BA as side chains was first prepared by ATRP with the purified cellulose-Br of different molecular weights as macroinitiators. The polymerization of *tert*-butyl acrylate (*t*BA) monomers was

carried out in an ampoule. In a typical process, an ampoule was loaded with CuBr, PMDETA, cellulose-Br, *t*BA, and methyl ethyl ketone (as solvent) (the molar ratio of *t*BA : Br of cellulose-Br macroinitiator: copper bromide: PMDETA = 1000 : 1 : 2 : 2; the volume ratio of monomer : solvent = 1:1), and was then degassed by three freeze-pump-thaw cycles in liquid nitrogen. The ampoule was immersed into an oil bath at 60°C. The polymerization was stopped by removing the ampoule from the oil bath and dipping into the ice/water bath at the different desired times. The copper salt in the crude solution was removed by diluting the crude solution with acetone and then passing through a neutral alumina column. The solution was concentrated by the rotary evaporator, and then precipitated in the mixture of methanol/water (v/v=1:1). The final product cellulose-*g*-P*t*BA bottlebrush-like polymer was obtained by dissolution-precipitation twice with acetone and the mixture of methanol/water. The final product was dried at 50^{o}C under vacuum for 1 day.

(b) Synthesis of cellulose-*g*-[P*t*BA-*b*-PS] BBCP comprising linear P*t*BA-*b*-PS as side chains by ATRP using cellulose-*g*-P*t*BA in (a) as cylindrical macroinitiator

Cellulose-*g*-[P*t*BA-*b*-PS] BBCP comprising linear P*t*BA-*b*-PS as side chains was prepared by the sequential ATRP process. In an ampoule, the reaction mixture containing macroinitiator, monomer and catalyst (the molar ratio of styrene monomer : Br in cellulose-*g*-P*t*BA BBCP macroinitiator : copper bromide: PMDETA = 1000 : 1 : 2 : 2) in anisole (as solvent; the volume ratio of monomer : solvent = 1:2) was degassed by three freeze-pump-thaw cycles in liquid nitrogen, and then placed in an oil bath maintained at 90°C for polymerization. The ampoule was taken out from the oil bath and dipped into the ice/water bath at the desired time interval to terminate the polymerization. The crude solution was diluted with THF, and then passed through a neutral alumina column to remove the catalyst. Cellulose-*g*-[P*t*BA-*b*-PS] BBCP was precipitated in an excess of cold methanol, and then filtered and dried under vacuum to yield pure cellulose-*g*-[P*t*BA-*b*-PS] BBCP containing linear P*t*BA-*b*-PS as side chains (i.e., brushes).

(c) Synthesis of amphiphilic cellulose-*g*-[PAA-*b*-PS] BBCP via the hydrolysis of

the *tert*-butyl ester groups of P*t*BA blocks in cellulose-*g*-[P*t*BA-*b*-PS] BBCP

In a typical process, cellulose-*g*-[P*t*BA-*b*-PS] BBCP was dissolved in CH_2Cl_2, and then a 10-fold molar excess of trifluoroacetic acid (CF_3COOH, TFA) with respect to the amount of *t*-butyl groups in P*t*BA blocks was added. The reaction solution was stirred at room temperature for 24 h. During the hydrolysis process, the resulting amphiphilic cellulose-*g*-[PAA-*b*-PS] BBCP (**Figure 1a**, **Figure S7** and **Table S2**) was gradually precipitated from solution. The crude product was separated by filtration, washed with CH_2Cl_2, and then thoroughly dried under vacuum at 60 °C for 24 h.

Table S2. Summary of amphiphilic cellulose-*g*-[PAA-*b*-PS] BBCPs.

Macroinitiators in **Table S1**	BBCPs[(a)]	Length (nm) [(b)]	$M_{n,PAA}$ [(c)] (g/mol)	$M_{n,PS}$ [(d)] (g/mol)	PDI[(e)]	Diameter (nm) [(f)]
Sample-1	Sample-1A	~51	5.2K	5.6K	1.13	~10
Sample-2	Sample-2A	~98	5.4K	5.9K	1.10	~10
Sample-3	Sample-3A	~206	5.3K	5.2K	1.16	~10
	Sample-3B	~206	11.2K	12.3K	1.18	~21
Sample-4	Sample-4A	~414	11.8K	12.6K	1.14	~21
Sample-5	Sample-5A	~916	5.8K	6.1K	1.12	~10

[(a)]Six samples were produced via the hydrolysis of inner P*t*BA blocks of cellulose-*g*-[P*t*BA-*b*-PS] BBCPs that were synthesized by using different cellulose-Br macroinitiators as shown in **Table S1.** [(b)] Length (L) of corresponding inorganic nanorods or nanowires. [(c)]Number-average molecular weight (M_n) of each PAA block calculated from the molecular weight difference between P*t*BA block (before hydrolysis) and PAA block (after hydrolysis). [(d)]M_n of each PS block calculated from ^{1}H NMR data. [(e)]Polydispersity index (PDI) determined by GPC. [(f)] Diameter (D) of

corresponding inorganic nanorods or nanowires. For M_n of each P*t*BA block, it can be obtained from the calculation of ^{1}H-NMR spectrum based on the ratio of the integral area of the methyl protons in *tert*-butyl group of P*t*BA to that of protons at the α-end of grafted P*t*BA in BBCP.

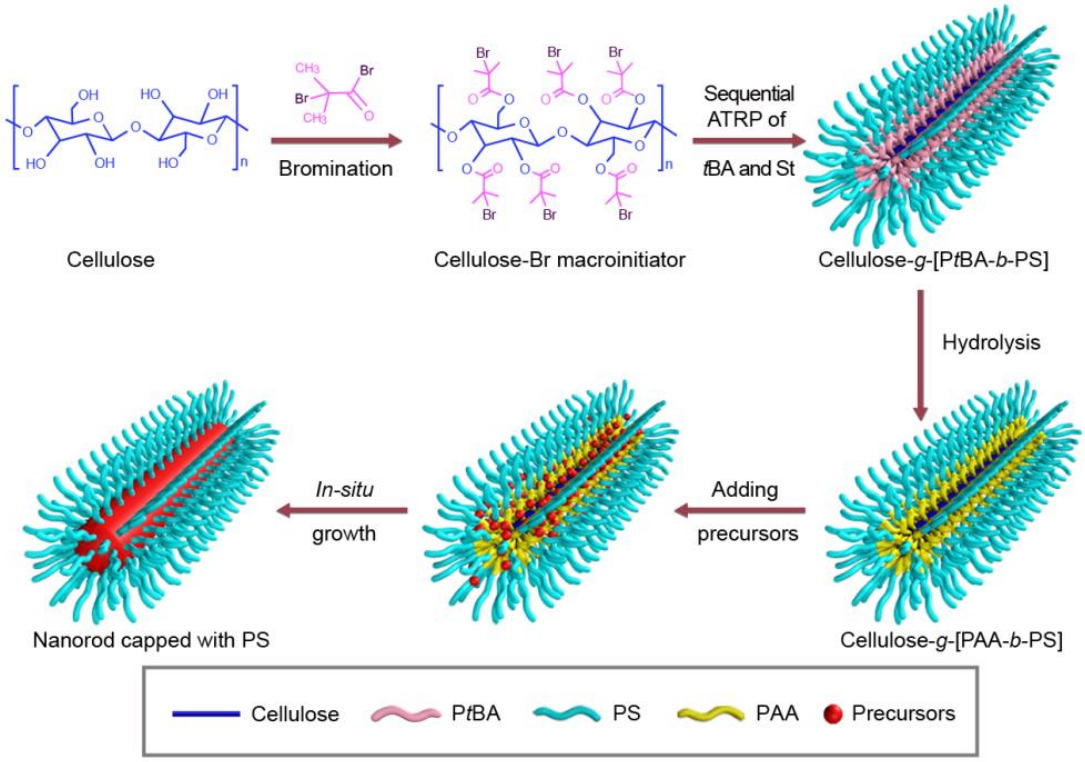

Figure S7. Schematic representation of synthesis of cellulose-*g*-[PAA-*b*-PS] BBCP and its use as cylindrical nanoreactor for the preparation of PS-tethered (i.e., organic solvent-soluble) plain 1D nanocrystals (nanorods and nanowires).

To demonstrate the success in preparing amphiphilic cellulose-*g*-[PAA-*b*-PS] BBCP, a series of characterizations by taking Sample-2A in **Table S2** as an example were shown as follows:

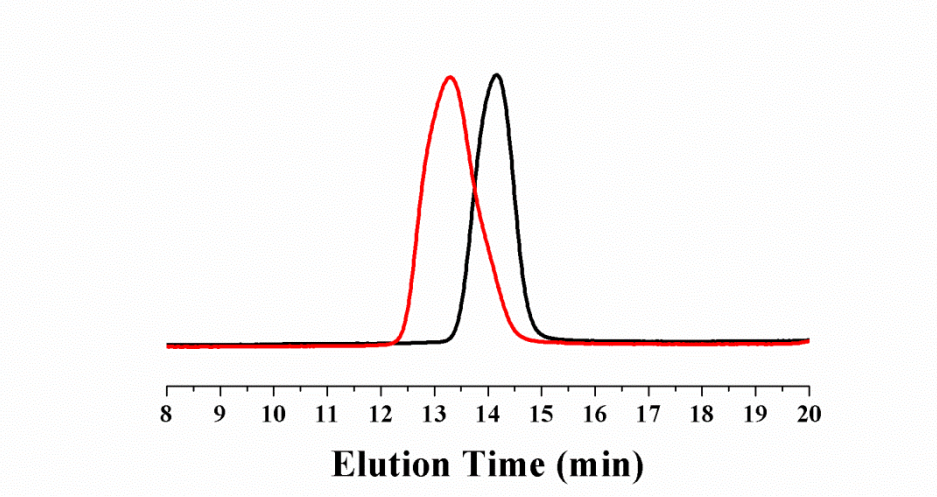

Figure S8. GPC traces of cellulose-*g*-P*t*BA bottlebrush-like polymer (right black curve) and cellulose-*g*-[P*t*BA-*b*-PS] BBCP (left red curve; its hydrolysis yielded cellulose-*g*-[PAA-*b*-PS] (i.e., Sample-2A in **Table S2)**).

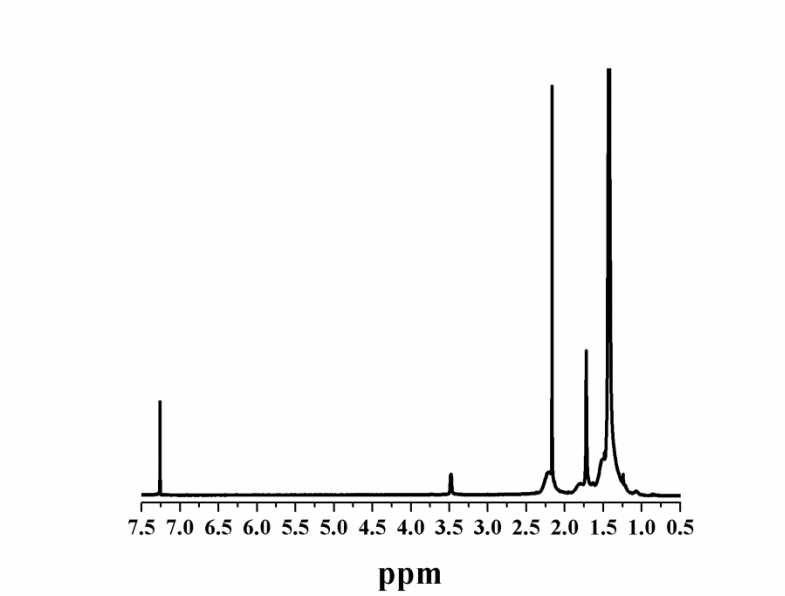

Figure S9. ^{1}H-NMR spectrum of cellulose-*g*-P*t*BA bottlebrush-like polymer. It was subsequently used as a macroinitiator for synthesis of cellulose-*g*-[P*t*BA-*b*-PS] BBCP. $CDCl_3$ was used as solvent in the ^{1}H-NMR measurement. An intense characteristic peak at δ = 1.45 ppm corresponded to the methyl protons in *tert*-butyl group of P*t*BA block. The chemical shift at δ = 1.21 ppm represented the methyl protons at the α-end of P*t*BA side chains arms in cellulose-*g*-P*t*BA bottlebrush-like polymer. We note that the hydrolysis of cellulose-*g*-[P*t*BA-*b*-PS] yielded cellulose-*g*-[PAA-*b*-PS] (i.e., Sample-2A in **Table S2**).

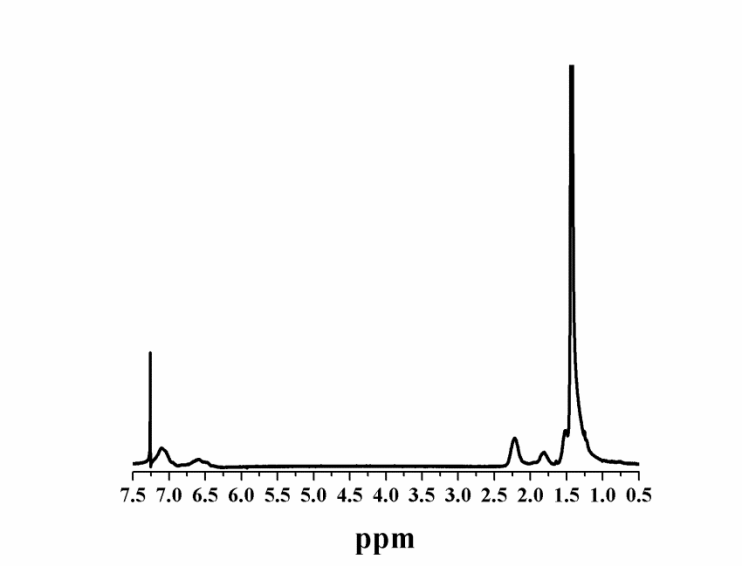

Figure S10. ^{1}H-NMR spectrum of cellulose-*g*-[P*t*BA-*b*-PS] BBCP. $CDCl_3$ was used as solvent in the ^{1}H-NMR measurement. The chemical shift at δ = 6.33-7.31 ppm can be assigned to the protons on the phenyl ring of the outer PS blocks. Its hydrolysis yielded cellulose-*g*-[PAA-*b*-PS] (i.e., Sample-2A in **Table S2)**.

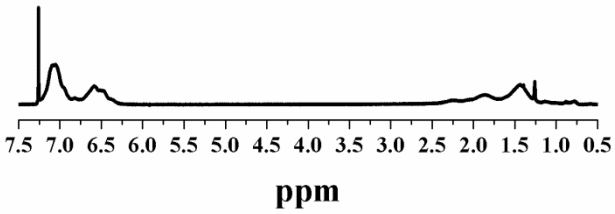

Figure S11. ^{1}H-NMR spectrum of cellulose-*g*-[PAA-*b*-PS] BBCP (Sample-2A in **Table S2**). DMF-d_7 was used as solvent in the ^{1}H-NMR measurement. The complete disappearance of the intense characteristic peak at δ =1.45 ppm, corresponding to the methyl protons of the *tert*-butyl group, suggested that P*t*BA blocks were successfully hydrolyzed into PAA.

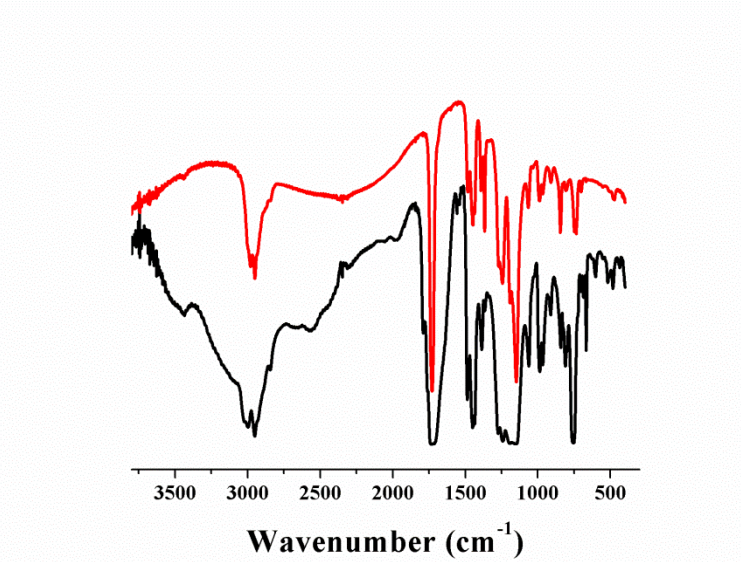

Figure S12. FTIR spectra of cellulose-*g*-[P*t*BA-*b*-PS] BBCP (upper red curve) and the resulting amphiphilic cellulose-*g*-[PAA-*b*-PS] BBCP (lower black curve, Sample-2A in **Table S2**). A broad absorbance was seen at 2500-3600 cm^{-1}, indicating the formation of carboxylic acid group after the hydrolysis of P*t*BA blocks.

(d) Synthesis of cellulose-*g*-(P*t*BA-N_3) BBCP with azide-functionalized P*t*BA as side chains

Cellulose-*g*-(P*t*BA-Br) BBCP (1.0 g) was dissolved in 20 mL of anhydrous DMF, and then sodium azide (the molar ratio of Br in cellulose-*g*-(P*t*BA-Br): sodium azide = 1:10) was added to the reaction system. The reaction solution was stirred for 24 h at room temperature. 50 mL of CH_2Cl_2 was added to the mixture, and then passed through the alumina column to remove the sodium salt. After that, the mixture was washed with DI water for three times. The CH_2Cl_2 layer was dried with anhydrous $MgSO_4$, and the solution was concentrated under vacuum. The product was precipitated in the cold mixture of methanol/water (1:1, volume ratio). The final product was collected and dried in vacuum oven at 40°C for 6 h.

(e) Synthesis of diphenylmethyl sodium (DPMNa)[1]

100mL of dry THF and 7.7 g (0.06 mol) of naphthalene were added to a 250 mL three-necked flask, and 1.38 g sodium with a fresh surface was at 40°C added under

argon atmosphere. After stirring at room temperature for 4 h, 11.1g (0.066 mol) of diphenylmethane was introduced into the reaction system with a syringe, and the reaction solution was then refluxed at 80 ^{o}C for 24 h. The concentration of DPMNa THF solution was 0.56 M by titrating with 0.1 M HCl.

(f) Synthesis of alkyne-terminated mPEG (mPEG-propargyl)

Alkyne-terminated mPEG (i.e., mPEG-propargyl) was prepared by the nucleophilic substitution of terminal hydroxyl group of mPEG (M_n =5,000 and M_n =10,000, respectively; Sigma-Aldrich; see **Materials** in **Section I**) with an alkyne group. In a typical process, a 250 mL three-necked round bottom flask was loaded by dry mPEG-OH (10.0 g, 2.0 mmol) and dry THF (150 mL). The reaction solution was then purged with argon. The DPMNa solution prepared in **(e)** was then added dropwise until the reaction system turned reddish-brown. The reaction flask was immersed in ice bath, during which propargyl bromide (10.0 mmol) was added dropwise into the reaction solution. The nucleophilic substitution reaction was allowed to proceed for 24 h at room temperature. The crude solution was diluted by adding 100 mL of CH_2Cl_2, and then passed through the alumina column to remove the sodium salt. The product solution was concentrated under vacuum, and the resulting mPEG-alkyne was then precipitated in cold diethyl ether. After being dried under vacuum at 50 ^{o}C, white powder was obtained. Another sample, mPEG-propargyl with M_n of 10,000 g/mol, was prepared by the same synthetic procedure.

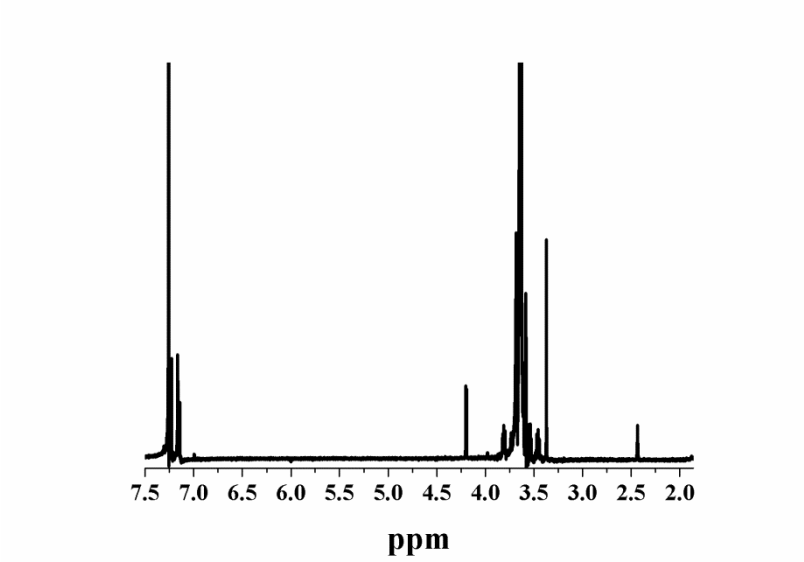

Figure S13. ^{1}H-NMR spectrum of mPEG-propargyl (M_n = 5,000 g/mol). $CDCl_3$ was used as solvent in the ^{1}H-NMR measurement. ^{1}H-NMR δ ppm: 2.44 (t, 1H, -OCH$_2$C≡C***H***), 4.20 (d, 2H, -OC***H***$_2$C≡CH), 3.38 (s, 3H, C***H***$_3$-O-PEG), and 3.60-3.70 (m, -C***H***$_2$C***H***$_2$O- of PEG main chain).

(g) Synthesis of cellulose-*g*-[P*t*BA-*b*-PEG] BBCP via click reaction

A series of cellulose-*g*-[P*t*BA-*b*-PEG] BBCPs were synthesized by click reaction between cellulose-*g*-(P*t*BA-N_3) prepared in **(d)** and mPEG-alkyne prepared in **(f)**. In a typical process, click reaction was carried out in a dry ampoule loaded by cellulose-*g*-(P*t*BA-N_3), mPEG-alkyne, CuBr, PMDETA and DMF (solvent). The molar ratio of –N_3 of cellulose-*g*-(P*t*BA-N_3), mPEG-alkyne, CuBr and PMDETA is 1 : 2 : 10 : 10. The reaction solution was degassed by three freeze-pump-thaw cycles in liquid nitrogen. The click reaction was conducted at 90^{o}C for 24 h. The crude product solution was diluted with CH_2Cl_2, and then passed through the alumina column to remove catalyst. The final product was precipitated in cold methanol and dried under vacuum condition at 60^{o}C for 12h.

(h) Synthesis of cellulose-*g*-[PAA-*b*-PEO] BBCP via the hydrolysis of *tert*-butyl ester groups of P*t*BA blocks

The hydrolysis of P*t*BA blocks was completed in a mixed solution containing CH_2Cl_2 and TFA. Briefly, 0.5g of cellulose-*g*-[P*t*BA-*b*-PEG] was dissolved into 50 mL of CH_2Cl_2, and 10 mL of TFA was then introduced. The hydrolysis reaction

continued at room temperature for 24 h. During the hydrolysis, the resulting final product was gradually precipitated from the CH_2Cl_2 solution. The final purified product, cellulose-*g*-[PAA-*b*-PEG] BBCP (**Figure S14** and **Table S3**), was obtained by washing with CH_2Cl_2 and drying under vacuum at 60 ^oC for 12 h.

Table S3. Summary of double hydrophilic cellulose-*g*-[PAA-*b*-PEG] BBCPs.

Macroinitiators in **Table S1**	BBCPs[(a)]	Length (nm) [(b)]	$M_{n,PAA}$[(c)] (g/mol)	$M_{n,PEG}$ (g/mol) [(d)]	PDI[(e)]	Diameter (nm) [(f)]
Sample-1	Sample-1A	~51	5.2K	5K	1.16	~10
Sample-2	Sample-2A	~98	5.4K	5K	1.14	~10
Sample-3	Sample-3A	~206	5.3K	5K	1.18	~10
	Sample-3B	~206	11.2K	10K	1.13	~21
Sample-4	Sample-4A	~414	11.8K	10K	1.19	~21
Sample-5	Sample-5A	~916	5.8K	5K	1.15	~10

[(a)]Six samples were synthesized via the hydrolysis of the inner P*t*BA blocks of cellulose-*g*-[P*t*BA-*b*-PEG] BBCPs that were synthesized by using different cellulose-Br macroinitiators as shown in **Table S1.** [(b)] Length (L) of corresponding inorganic nanorods or nanowires. [(c)]Number-average molecular weight (M_n) of each PAA block calculated from the molecular weight difference between P*t*BA block (before hydrolysis) and PAA block (after hydrolysis). [(d)]M_n of each PEG block. [(e)] PDI determined by GPC. [(f)]Diameter (D) of corresponding inorganic nanorods or nanowires.

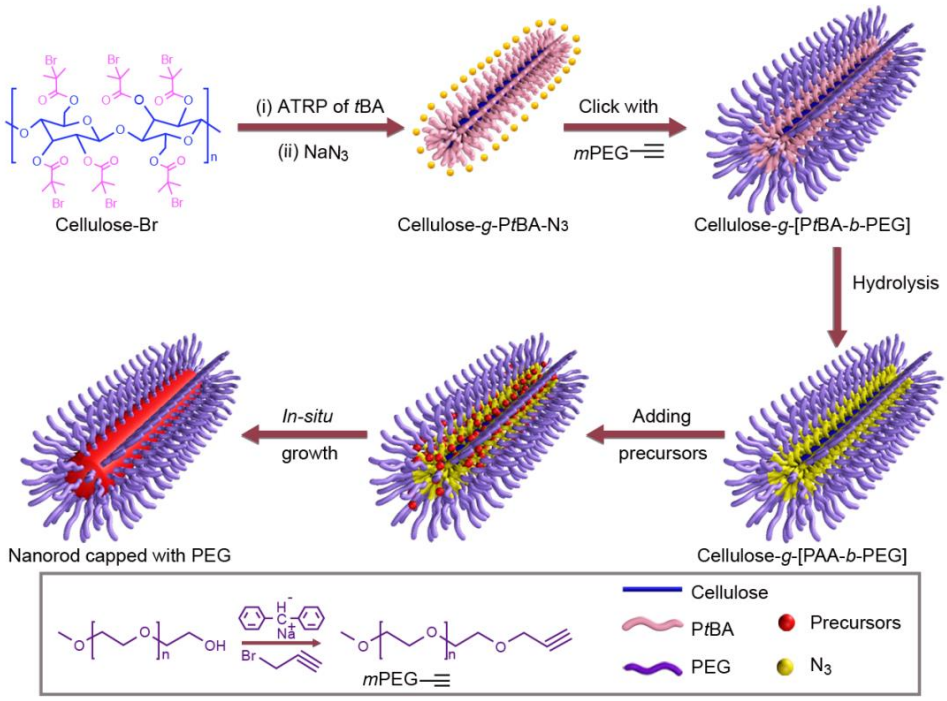

Figure S14. Schematic representation of synthesis of cellulose-*g*-[PAA-*b*-PEG] BBCP and its use as a cylindrical nanoreactor for the preparation of PEG-tethered (i.e., water-soluble) plain 1D nanocrystals (nanorods and nanowires).

2. Synthesis of cellulose-*g*-[P4VP-*b*-P*t*BA-*b*-PS] BBCP (Figure S15; steps a-c) and cellulose-*g*-[P4VP-*b*-P*t*BA-*b*-PEG] BBCP (Figure S16; step d) with linear amphiphilic P4VP-*b*-P*t*BA-*b*-PS and P4VP-*b*-P*t*BA-*b*-PEG triblock copolymers as side chains, respectively

Synthesis of amphiphilic cellulose-*g*-[P4VP-*b*-P*t*BA-*b*-PS] and cellulose-*g*-[P4VP-*b*-P*t*BA-*b*-PEG] BBCPs with linear P4VP-*b*-P*t*BA-*b*-PS and P4VP-*b*-P*t*BA-*b*-PEG triblock copolymers as grafted side chains, respectively, was carried out using the same cellulose-Br macroinitiators and the same preparation procedures as cellulose-*g*-[PAA-*b*-PS] and cellulose-*g*-[PAA-*b*-PEG]. That is, sequential ATRP (for cellulose-*g*-[P4VP-*b*-P*t*BA-*b*-PS]) and a combination of sequential ATRP with click reaction (for cellulose-*g*-[P4VP-*b*-P*t*BA-*b*-PEG]) were employed.

(a) Synthesis of cellulose-*g*-P4VP bottlebrush-like polymer by ATRP using cellulose-Br macroinitiator

Cellulose-Br was used as a macroinitiator for ATRP of 4VP monomers. Briefly, an ampoule was loaded with cellulose-Br, CuBr, Me_6-TREN, 4VP and 2-propanol (solvent). It was then degassed by three freeze-pump-thaw cycles in liquid nitrogen and immersed into an oil bath at 50°C. The molar ratio of –Br in cellulose-Br, CuBr, Me_6-TREN and 4VP was 1: 2: 2: 1000. The volume of 2-propanol was twice that of the 4VP monomer. The polymerization reaction was stopped by dipping the reaction system into ice/water bath at a desired time. The crude solution was diluted with 2-propanol and passed through a neutral alumina column to remove the catalyst. The final solution was concentrated under vacuum and precipitated in cold hexane. The final product was purified by dissolution/precipitation twice with 2-propanol and cold hexane, and then dried in a vacuum oven at 60°C for 2 days.

(b) Synthesis of cellulose-*g*-[P4VP-*b*-P*t*BA] BBCP utilizing cellulose-*g*-P4VP bottlebrush-like polymer as an ATRP macroinitiator

Similar to the synthesis of cellulose-*g*-[P*t*BA-*b*-PS] by sequential ATRP, the polymerization of the second monomer *t*BA was carried out in an ampoule. The polymerization solution (the molar ratio of *t*BA : Br of cellulose-*g*-P4VP : CuBr : Me_6-TREN = 1000 : 1 : 2 : 2) in methyl ethyl ketone (1 ml *t*BA in 2 ml solvent) were degassed by three freeze-pump-thaw cycles in liquid nitrogen. The polymerization was conducted at 60 ^{o}C for a desired time. The crude mixture was diluted with THF, and then passed through a neutral alumina column to remove the catalyst. The final cellulose-*g*-[P4VP-*b*-P*t*BA] BBCP was precipitated in an excess of cold methanol, and then dried under vacuum at 60 ^{o}C for 12 h.

(c) Synthesis of cellulose-*g*-[P4VP-*b*-P*t*BA-*b*-PS] BBCP by ATRP using

cellulose-*g*-[P4VP-*b*-P*t*BA] as macroinitiator

In a typical process, cellulose-*g*-[P4VP-*b*-P*t*BA] macroinitiator, styrene monomer, CuBr, Me_6-TREN, and anisole as solvent were added to an ampoule and then degassed by three freeze-pump-thaw cycles. The molar ratio of styrene, bromoisobutyryl groups on cellulose-*g*-[P4VP-*b*-P*t*BA], CuBr, Me_6-TREN was 1000: 1: 2: 2, and the concentration of styrene monomers in anisole was 1 g St monomer per 2 mL anisole. The sealed ampoule was then immersed in an oil bath at 90 °C. After a certain time, the ampoule was dipped into ice/water bath to stop the polymerization. The mixture solution was then diluted with THF and passed through a column of neutral alumina to remove the catalyst. The final polymers (cellulose-*g*-[P4VP-*b*-P*t*BA-*b*-PS] BBCP; **Figure 1b**, **Figure S15** and **Table S4**) were precipitated with an excess of cold methanol, filtered, and dried under vacuum at 60 ^{o}C for 1 day.

Table S4. Summary of cellulose-*g*-[P4VP-*b*-P*t*BA-*b*-PS] BBCPs.

Cellulose-Br[(a)] in **Table S1**	BBCPs	Length (nm) [(b)]	$M_{n,P4VP}$ (g/mol) [(c)]	Diameter of core (nm) [(d)]	$M_{n,PtBA}$ (g/mol) [(e)]	Thickness of shell (nm) [(f)]	$M_{n,PS}$(g/mol) [(g)]	PDI[(h)]
Sample-2	Sample-2A	~98	7.8K	~10	8.4K	~3	8K	1.15
	Sample-2B	~98	7.8K	~10	11.6K	~5	13.2K	1.18
Sample-3	Sample-3A	~206	8.2K	~10	11.9K	~6	12.5K	1.12
Sample-4	Sample-4A	~414	21.5K	~22	49.5K	~23	32.2K	1.09

[(a)]Different cellulose-Br macroinitiators (see **Table S1**). [(b)]Length (L) of corresponding inorganic nanorods or nanowires. [(c)]Number-average molecular weight of each inner P4VP block in calculated from ^{1}H NMR data. [(d)]Diameter (D) of corresponding inorganic nanorods or nanowires. [(e)]Number-average molecular weight of each intermediate P*t*BA block calculated from ^{1}H NMR data. [(f)]Thickness (t) of shell of corresponding inorganic core/shell nanorods or nanowires. [(g)]M_n of each outer PS block calculated from ^{1}H NMR data. [(h)] PDI determined by GPC.

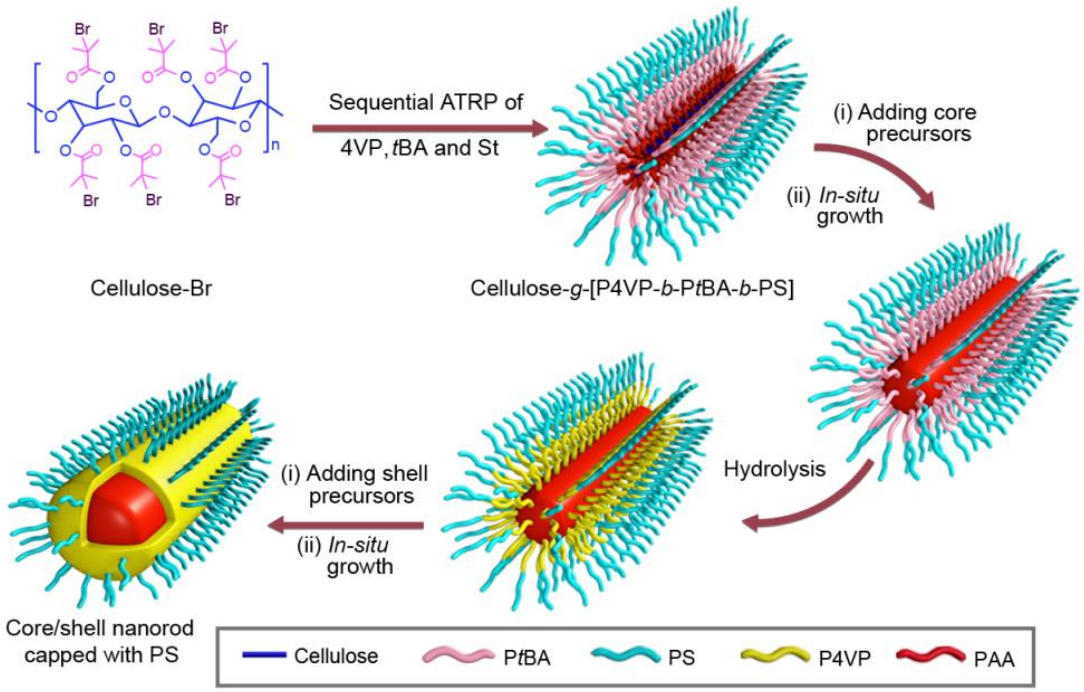

Figure S15. Schematic representation of the synthesis of cellulose-*g*-[P4VP-*b*-P*t*BA-*b*-PS] BBCP and its use as a cylindrical nanoreactor for the preparation of PS-tethered (i.e., organic solvent-soluble) core/shell nanorods.

(d) Synthesis of cellulose-*g*-[P4VP-*b*-P*t*BA-*b*-PEG] BBCP via a combination of sequential ATRP with click reaction

Similar to the synthesis of cellulose-*g*-[P*t*BA-*b*-PEG] BBCP, a series of cellulose-*g*-[P4VP-*b*-P*t*BA-*b*-PEG] BBCPs (**Figure S16** and **Table S5**) with different molecular weights were also synthesized via a combination of sequential ATRP and click reaction.

Table S5. Summary of cellulose-*g*-[P4VP-*b*-P*t*BA-*b*-PEG] BBCPs.

Cellulose-Br[(a)] in **Table S1**	BBCPs	Length (nm) [(b)]	$M_{n,P4VP}$ (g/mol) [(c)]	Diameter of core (nm) [(d)]	$M_{n,PtBA}$ (g/mol) [(e)]	Thickness of shell (nm) [(f)]	$M_{n,PEG}$ (g/mol)	PDI[(g)]
Sample-2	Sample-2A	~98	7.8K	~10	8.4K	~3	5K	1.19
	Sample-2B	~98	7.8K	~10	11.6K	~5	10K	1.14
Sample-3	Sample-3A	~206	8.2K	~10	11.9K	~6	10K	1.16
Sample-4	Sample-4A	~414	21.5K	~22	49.5K	~23	10K	1.15

[(a)]Different cellulose-Br macroinitiators (see **Table S1**). [(b)]Length (L) of corresponding inorganic nanorods or nanowires. [(c)]Number-average molecular weight of each inner P4VP block in calculated from ^{1}H NMR data. [(d)]Diameter (D) of corresponding inorganic nanorods or nanowires. [(e)]Number-average molecular weight of each intermediate P*t*BA block calculated from ^{1}H NMR data. [(f)]Thickness (t) of shell of corresponding inorganic core/shell nanorods or nanowires. [(g)] PDI determined by GPC.

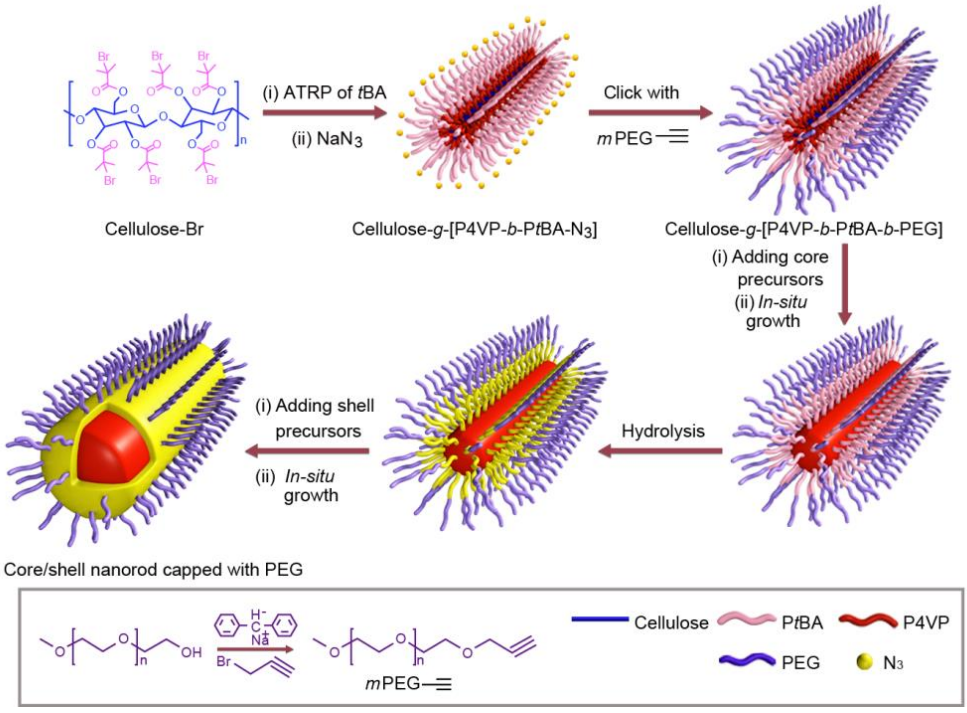

Figure S16. Schematic representation of the synthesis of cellulose-*g*-[P4VP-*b*-P*t*BA-*b*-PEG] BBCP and its use as a cylindrical nanoreactor for the preparation of PEG-tethered (water-soluble) core/shell 1D nanorods.

3. Synthesis of amphiphilic cellulose-*g*-[PS-*b*-PAA-*b*-PS] BBCP (Figure S17, steps a-d) and cellulose-*g*-[PS-*b*-PAA-*b*-PEG] BBCP (Figure S18, step e)

Similar to the synthesis of cellulose-*g*-[PAA-*b*-PS], cellulose-*g*-[PAA-*b*-PEG], cellulose-*g*-[P4VP-*b*-P*t*BA-*b*-PS] and cellulose-*g*-[P4VP-*b*-P*t*BA-*b*-PEG] BBCPs, amphiphilic cellulose-*g*-[PS-*b*-PAA-*b*-PS] and cellulose-*g*-[PS-*b*-PAA-*b*-PEG] BBCPs were also prepared by sequential ATRP and a combination of sequential ATRP with click reaction, respectively.

(a) Synthesis of cellulose-*g*-PS bottlebrush-like polymer with PS as side chains

A series of cellulose-Br with different molecular weights were used as macroinitiators. An ampoule filled with CuBr, PMDETA, cellulose-Br, and St monomer was degassed by three freeze-thaw-cycles in liquid nitrogen, then sealed and placed in an oil bath at 90°C. The polymerization was terminated by placing the reaction ampoule into an ice/water bath after different desired reaction times. The solution was diluted with CH_2Cl_2 and then passed through a neutral alumina column to remove the catalyst, and precipitated in an excess of cold methanol. After filtration, the final product was purified by dissolution-precipitation twice with CH_2Cl_2 and cold methanol, and then dried in vacuum at 60°C for 1 day.

(b) Synthesis of cellulose-*g*-[PS-*b*-P*t*BA] BBCP with PS-*b*-P*t*BA diblock copolymers as side chains

Cellulose-*g*-PS synthesized in **(a)** was used as a macroinitiator. The reaction mixture containing cellulose-*g*-PS macroinitiator, *t*BA monomer, CuBr, PMDETA and methyl ethyl ketone (solvent) was introduced into an ampoule. Then it was degassed by three freeze-pump-thaw cycles in liquid nitrogen. The molar ratio of bromoisobutyryl groups in cellulose-*g*-PS : *t*BA : CuBr : PMDETA was 1 : 1000 : 2: 2. The volume ratio of methyl ethyl ketone to *t*BA was 2 : 1. The polymerization reaction was carried out at 60 ^{o}C for a desired reaction time, and then the product was dipped into an ice/water bath to stop the reaction. The final solution was then diluted with acetone, and passed through a neutral alumina column to remove the catalyst. Cellulose-*g*-[PS-*b*-P*t*BA] was precipitated in a mixture of methanol/water (v/v=1/1), filtered, and then dried in a vacuum oven at 60 ^{o}C for 12 h.

(c) Synthesis of cellulose-*g*-[PS-*b*-P*t*BA-*b*-PS] BBCP with PS-*b*-P*t*BA-*b*-PS triblock copolymers as side chains

The polymerization reaction was carried out in an ampoule. The reaction mixture with the molar ratio of St monomer : bromoisobutyryl groups in cellulose-*g*-[PS-*b*-P*t*BA] BBCP : CuBr : PMDETA at 1000 : 1 : 2 : 2 in anisole (1g St in 2ml anisole) was degassed by three freeze-pump-thaw cycles in liquid nitrogen, and then placed in an oil bath previously maintained at 90°C. After a desired time, the polymerization was terminated by immersing the ampoule in ice/water bath. The product solution was then diluted with CH_2Cl_2, and passed through a neutral alumina column to remove the catalyst. The final product was precipitated in an excess of cold methanol, filtered, and dried under vacuum t at 60 ^{o}C for 12 h.

(d) Synthesis of amphiphilic cellulose-*g*-[PS-*b*-PAA-*b*-PS] BBCP via the hydrolysis of the *tert*-butyl ester groups of the P*t*BA blocks in cellulose-*g*-[PS-*b* P*t*BA-*b*-PS] BBCP

In a typical process, cellulose-*g*-[PS-*b*-P*t*BA-*b*-PS] BBCP (0.5 g) was dissolved in 50 mL of CH_2Cl_2 (solvent), and then 10 ml TFA was added. The reaction solution was stirred at room temperature for 24 h. During the hydrolysis process, the resulting cellulose-*g*-[PS-*b*-PAA-*b*-PS] BBCP (**Figure 1c**, **Figure S17** and **Table S6**) was gradually precipitated from the solution. The final product was purified by washing with CH_2Cl_2, and then dried under vacuum at 60°C for 12 h.

Table S6. Summary of cellulose-*g*-[PS-*b*-PAA-*b*-PS] BBCPs.

Cellulose-Br[a] in **Table S1**	BBCPs	Length (nm) [b]	$M_{n,PS}$ (g/mol) [c]	Diameter of hollow core (nm) [d]	$M_{n,PAA}$ [e] (g/mol)	Thickness of shell(nm) [f]	$M_{n,PS}$ [g] (g/mol)	PDI[h]
Sample-2	Sapmle-2A	~98	4.8K	~5	5.9K	~5	8K	1.18
Sample-3	Sapmle-3A	~206	11.2K	~11	6.5K	~6	9K	1.16

[a]Different cellulose-Br macroinitiators (**Table S1**). [b]Length (L) of corresponding inorganic nanotubes. [c]Number-average molecular weight of each inner PS block calculated from ^{1}H NMR data. [d]Diameter (D) of hollow interior of corresponding inorganic nanotubes. [e]Number-average molecular weight of each intermediate PAA block calculated from the molecular weight difference between P*t*BA blocks (before hydrolysis) and PAA blocks (after hydrolysis). [f]Thickness (t) of shell of corresponding inorganic nanotubes. [g]Number-average molecular weight of each outer PS block calculated from ^{1}H NMR data. [h]PDI determined by GPC.

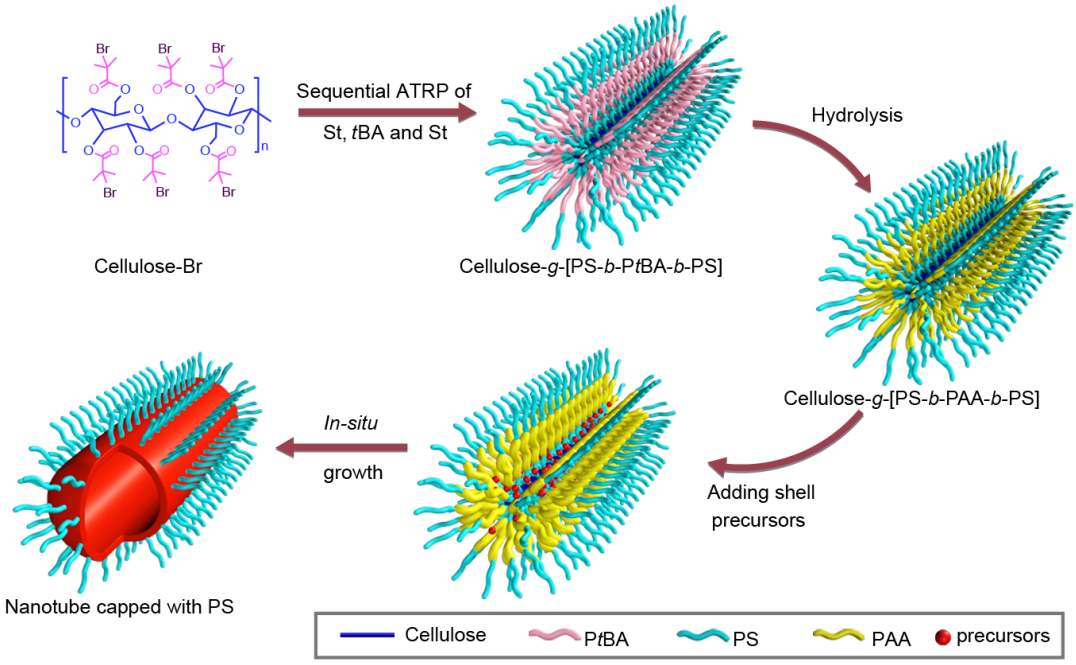

Figure S17. Schematic representation of synthesis of cellulose-*g*-[PS-*b*-PAA-*b*-PS] BBCP and its use as cylindrical nanoreactor for the preparation of PS-tethered (i.e., organic solvent-soluble) nanotubes.

(e) Synthesis of cellulose-*g*-[PS-*b*-PAA-*b*-PEG] BBCP

Similar to the synthesis of cellulose-*g*-[PAA-*b*-PEG], cellulose-*g*-[PS-*b*-P*t*BA-*b*-PEG] BBCP was also synthesized by a combination of sequential ATRP and click reaction. After the hydrolysis of the P*t*BA blocks in TFA, cellulose-*g*-[PS-*b*-PAA-*b*-PEG] BBCP (**Figure S18** and **Table S7**) was obtained.

Table S7. Summary of cellulose-*g*-[PS-*b*-PAA-*b*-PEG] BBCP.

Cellulose-Br[(a)] in **Table S1**	BBCPs	Length (nm) [(b)]	$M_{n,PS}$ (g/mol) [(c)]	Diameter of hollow core (nm) [(d)]	$M_{n,PAA}$ [(e)] (g/mol)	Thickness of shell(nm) [(f)]	$M_{n,PEG}$ (g/mol)	PDI[(g)]
Sample-2	Sapmle-2A	~98	4.8K	~5	5.9K	~5	5K	1.14
Sample-3	Sapmle-3A	~206	11.2K	~11	6.5K	~6	10K	1.19

[(a)]Different cellulose-Br macroinitiators (**Table S1**). [(b)]Length (L) of corresponding inorganic nanotubes. [(c)]Number-average molecular weight of each inner PS block calculated from ^{1}H NMR data. [(d)]Diameter (D) of hollow interior of corresponding inorganic nanotubes. [(e)]Number-average molecular weight of each intermediate PAA block calculated from the molecular weight difference between P*t*BA blocks (before hydrolysis) and PAA blocks (after hydrolysis). [(f)]Thickness (t) of shell of corresponding inorganic nanotubes. [(g)]PDI determined by GPC.

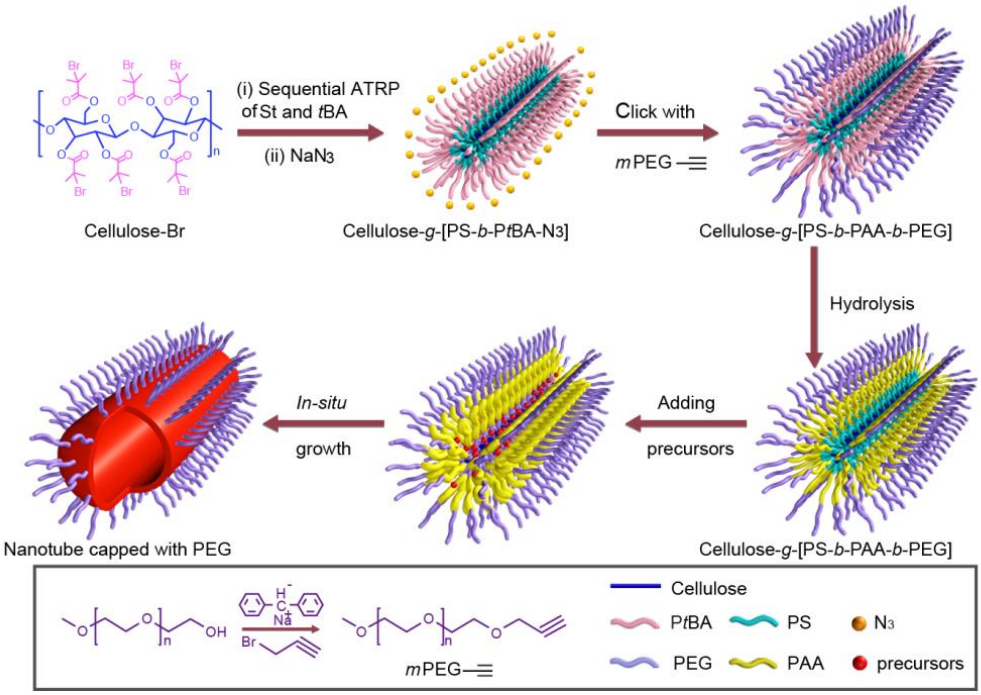

Figure S18. Schematic representation of synthesis of cellulose-*g*-[PS-*b*-PAA-*b*-PEG] BBCP and its use as cylindrical nanoreactor for the preparation of PEG-tethered (i.e., water-soluble) nanotubes.

Section IV

Detailed experimental conditions and procedures for the synthesis of a large variety of 1D nanocrystals with precisely controlled dimension, composition, surface chemistry and architecture by capitalizing on cylindrical bottlebrush-like block copolymers (BBCPs) as nanoreactors

1. Synthesis of plain nanorods and nanowires

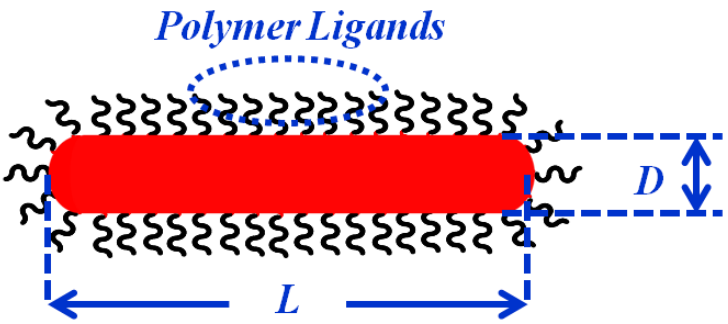

Figure S19. Schematic of a plain nanorod illustrating the dimension (i.e., diameter, *D*, and length, *L*). The length of nanorod is dictated by the molecular weight of cellulose-Br macroinitiator, and the diameter of nanorod is governed by the molecular weight of inner hydrophilic blocks (e.g., PAA blocks in amphiphilic cellulose-*g*-[PAA-*b*-PS] used as nanoreactor). The outer blocks (e.g., PS blocks; referred to as "polymer ligands" in the Schematic) impart the solubility of nanorods (e.g., organic solvent-soluble).

(1) Synthesis of plain nanorods and nanowires tethered with PS (i.e., organic solvent-soluble) by capitalizing on amphiphilic cylindrical cellulose-*g*-[PAA-*b*-PS] BBCP (i.e., samples in Table S2) as a nanoreactor (Figure 1a and Figure S7)

(a) Organic solvent-soluble <u>metallic nanorods</u>

(a1) Synthesis of organic solvent-soluble metallic Au nanorods with different diameters and lengths (Figure S20)

10 mg of cylindrical cellulose-*g*-[PAA-*b*-PS] template was dissolved in 10 mL of DMF at room temperature, followed by the addition of an appropriate amount of precursors ($HAuCl_4 \cdot 3H_2O$ with tert-butylamine-borane complex (TBAB) as reducer) that were selectively incorporated in the space occupied by inner PAA blocks. The molar ratio of acrylic acid (AA) units in PAA blocks to precursors was set at 1:10 in order to maximize the loading of precursors into the PAA compartment noted above. The mixture solution was stirred at room temperature under argon for 1h to ensure that all precursors were well dissolved in DMF. The reaction was then carried out at 60 ^{o}C for 2 h.

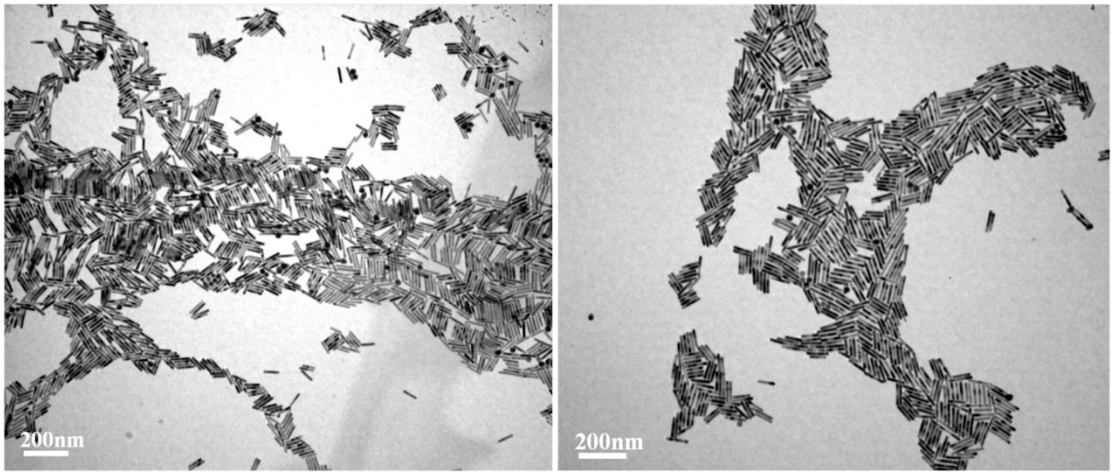

Figure S20. TEM images of Au nanorods (length, L = 98±8 nm; diameter, D = 10.4±0.6 nm) tethered with PS synthesized using cylindrical cellulose-*g*-[PAA-*b*-PS] (Samaple-2A in **Table S2**) as nanoreactor.

(a2) Synthesis of organic solvent-soluble metallic Pt nanorods with different lengths and diameters (Figure S21)

10 mg of cylindrical cellulose-*g*-[PAA-*b*-PS] template was dissolved in 10 mL of DMF at room temperature, followed by the addition of an appropriate amount of precursor $H_2PtCl_6.6H_2O$ that was selectively incorporated into the space occupied by inner PAA blocks. Ethylene glycol (EG) was used as reducer. The molar ratio of acrylic acid (AA) units in PAA blocks to precursors was set at 1:10 in order to maximize the loading of precursors into the PAA compartment noted above. The mixture solution was stirred at room temperature under argon for 1h to ensure that all

precursors were well dissolved in DMF. The reaction mixture was then heated and refluxed under argon for 2h.

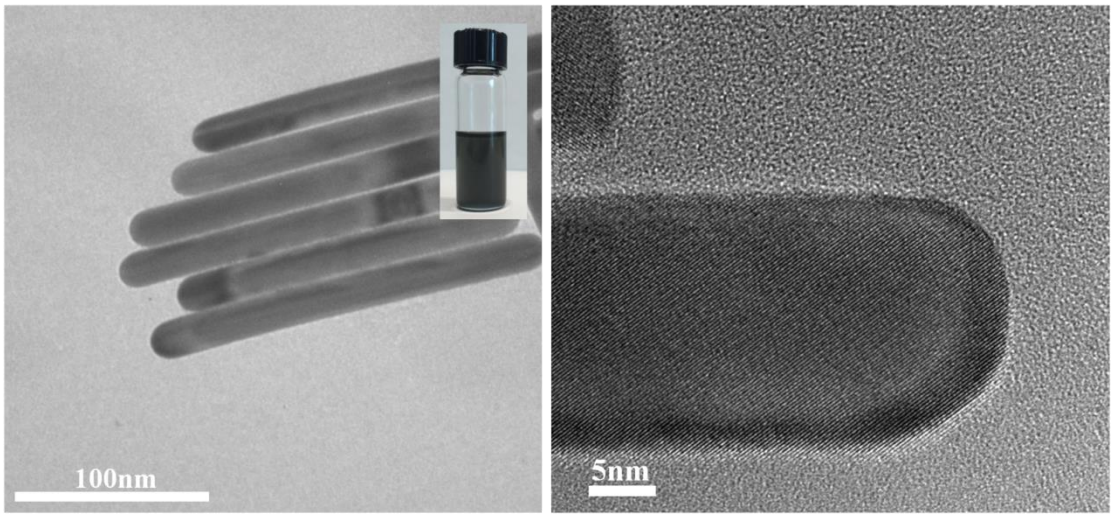

Figure S21. TEM and HRTEM images of Pt nanorods (L = 209±18 nm, D = 20.8±1.6 nm) tethered with PS synthesized using cylindrical cellulose-*g*-[PAA-*b*-PS] (Samaple-3B in **Table S2**) as a nanoreactor. Inset: digital image of Pt nanorods toluene solution (left).

(b) Organic solvent-soluble <u>upconversion nanorods</u>

(b1) Synthesis of rare-earth precursor (RE $(CF_3COO)_3$)[12, 13]

Rare-earth trifluoroacetates were prepared by reacting Y_2O_3, Yb_2O_3, Er_2O_3 and Tm_2O_3 with excess trifluoroacetic acid (TFA), respectively. RE_2O_3 (RE = Y, Yb, Er, and Tm) samples were added into a mixed solvent containing TFA and DI water (1:1, V/V). The mixture was then refluxed at 85 ^oC. After reaction for 1 h, the corresponding precursor solution became clear. The mixture was allowed to stay overnight. The impurity was filtered and the filtrate was dried under vacuum to completely remove solvent and the excess TFA. The purification process was carried out by recrystallization from DI water, and then completely dried in vacuum oven at 60 ^oC for 1 day.

(b2) Synthesis of organic solvent-soluble upconversion $NaYF_4$:Yb/Er (18%/2%) nanorods (Figures S22 and **S23)**

For the synthesis of plain upconversion $NaYF_4$:Yb/Er nanorods, 10 mg of cellulose-*g*-[PAA-*b*-PS] template was dissolved in 10 mL of DMF at room temperature, followed by the addition of an appropriate amount of precursors (i.e., $Na(CF_3COO)$, $Y(CF_3COO)_3$, $Yb(CF_3COO)_3$ and $Er(CF_3COO)_3$) that were selectively encapsulated within the space occupied by inner PAA blocks. The molar ratio of acrylic acid (AA) units in PAA blocks to precursors was set at 1:10 in order to maximize the loading of precursors into the PAA compartment noted above. The mixture solution was stirred for 1h under argon to ensure that all precursors were well dissolved in DMF. The reaction system was then slowly heated to the boiling point of DMF and refluxed for 2h. In order to synthesize a highly crystalline hexagonal phase of nanorod, the resulting solution and additional quantitative amount of CF_3COONa were then transferred to a 20 mL Teflon-lined autoclave, stirred and heated at 200^oC for 2h.

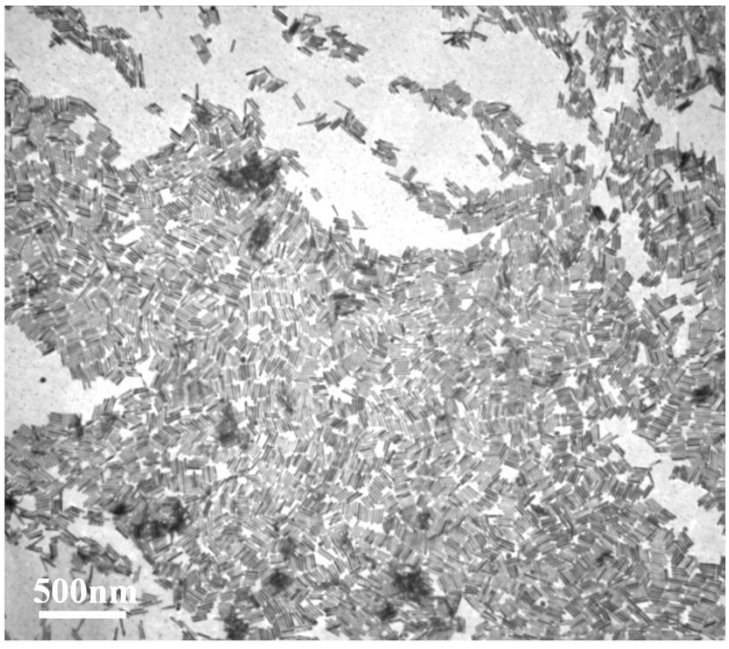

Figure S22. TEM image of upconversion $NaYF_4$:Yb/Er nanorods (L =97±9 nm, D = 9.8±0.5 nm) tethered with PS synthesized using cylindrical cellulose-*g*-[PAA-*b*-PS] (Samaple-2A in **Table S2**) as a nanoreactor.

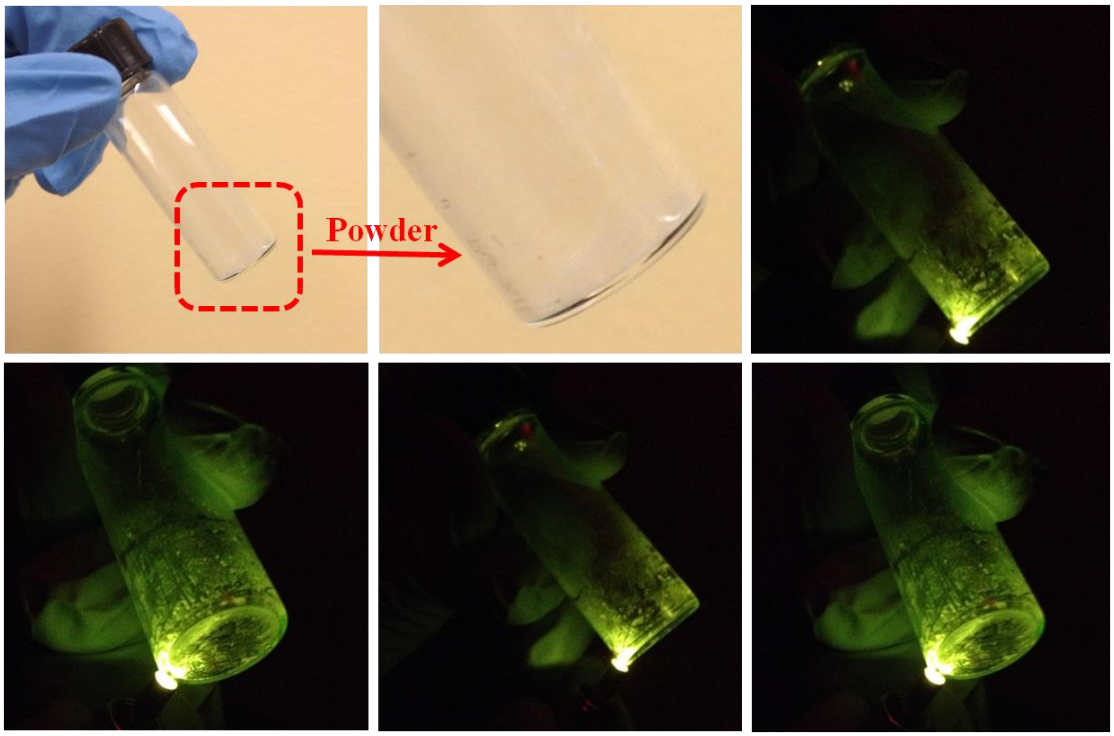

Figure S23. Digital images of upconversion $NaYF_4$:Yb/Er nanorods in dry state (i.e., power form) before (upper left and central panels) and after (upper right and all lower panels) exposure to a 2W 980-nm near-infrared laser, respectively.

(b3) Synthesis of organic solvent-soluble upconversion $NaYF_4$:Yb/Tm (30%/0.5%) nanorods (Figures S24 and **S25)**

For the synthesis of plain upconversion $NaYF_4$:Yb/Tm nanorods, 10 mg of cellulose-*g*-[PAA-*b*-PS] template was dissolved in 10 mL of DMF at room temperature, followed by the addition of an appropriate amount of precursors ($Na(CF_3COO)$, $Y(CF_3COO)_3$, $Yb(CF_3COO)_3$ and $Tm(CF_3COO)_3$) that were preferentially incorporated into the space occupied by inner PAA blocks. The molar ratio of acrylic acid (AA) units in PAA blocks to precursors was set at 1:10 in order to maximize the loading of precursors into the PAA compartment noted above. The mixture solution was stirred for 1h under argon to ensure that all precursors were well dissolved in DMF. The reaction system was then slowly heated to the boiling point of DMF and refluxed for 2h. In order to synthesize a highly crystalline hexagonal phase, the resulting solution and additional quantitative amount of CF_3COONa were then transferred to a 20 mL Teflon-lined autoclave, stirred and heated at 200^{o}C for 2h.

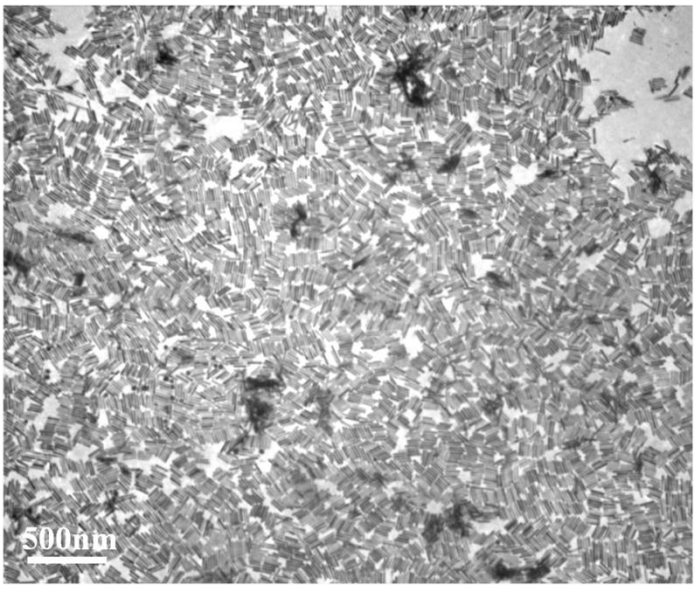

Figure S24. TEM image of upconversion $NaYF_4$:Yb/Tm nanorods (L = 103±7 nm, D =10.4±0.5 nm) tethered with PS synthesized using cylindrical cellulose-*g*-[PAA-*b*-PS] (Samaple-2A in **Table S2**) as nanoreactor.

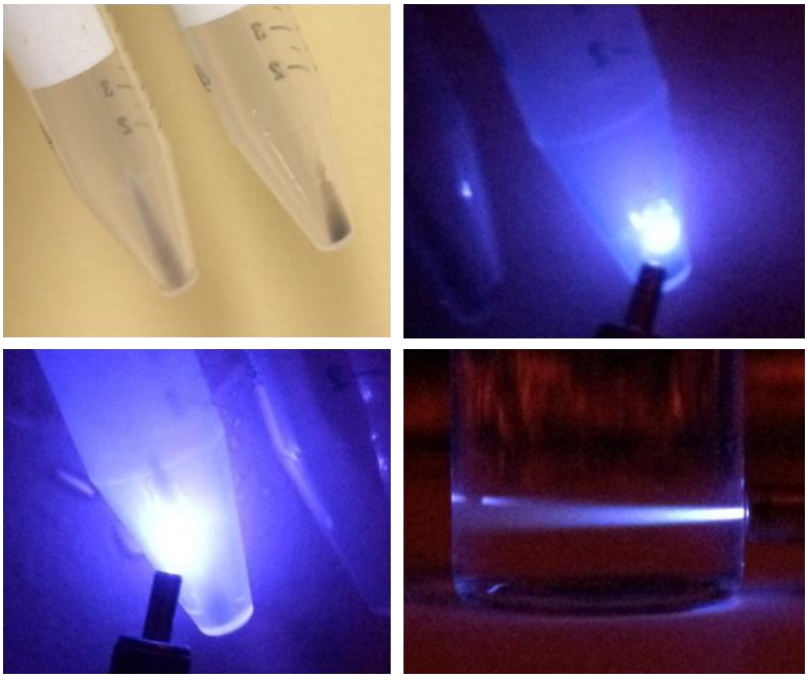

Figure S25. Digital images of upconversion $NaYF_4$:Yb/Tm nanorods in the dry state (upper two panels and lower left panel) and toluene solution (lower right panel) before (upper left panel) and after (upper right panel and lower two panels) exposure to a 2W 980-nm near-infrared laser, respectively.

(c) Organic solvent-soluble <u>ferroelectric $BaTiO_3$ nanorods</u> (Figure S26)

In a typical process, 10 mg of cellulose-*g*-[PAA-*b*-PS] template was dissolved in 10 mL of DMF at room temperature, followed by the addition of an appropriate amount of precursors ($BaCl_2 \cdot 2H_2O$ + $TiCl_4$ + NaOH) that selectively entered the space occupied by inner PAA blocks. The molar ratio of acrylic acid (AA) units in PAA blocks to precursors was set at 1:10 in order to maximize the loading of precursors into the PAA compartment noted above. The mixture was stirred for 1h under argon to ensure that all precursors were well dissolved in DMF. The reaction system was then slowly heated to the boiling point of DMF and refluxed for 2h. In order to synthesize highly crystalline $BaTiO_3$ nanorods, the resulting solution was transferred into a 20 mL Teflon-lined autoclave and heated at 200^{o}C for 2h.

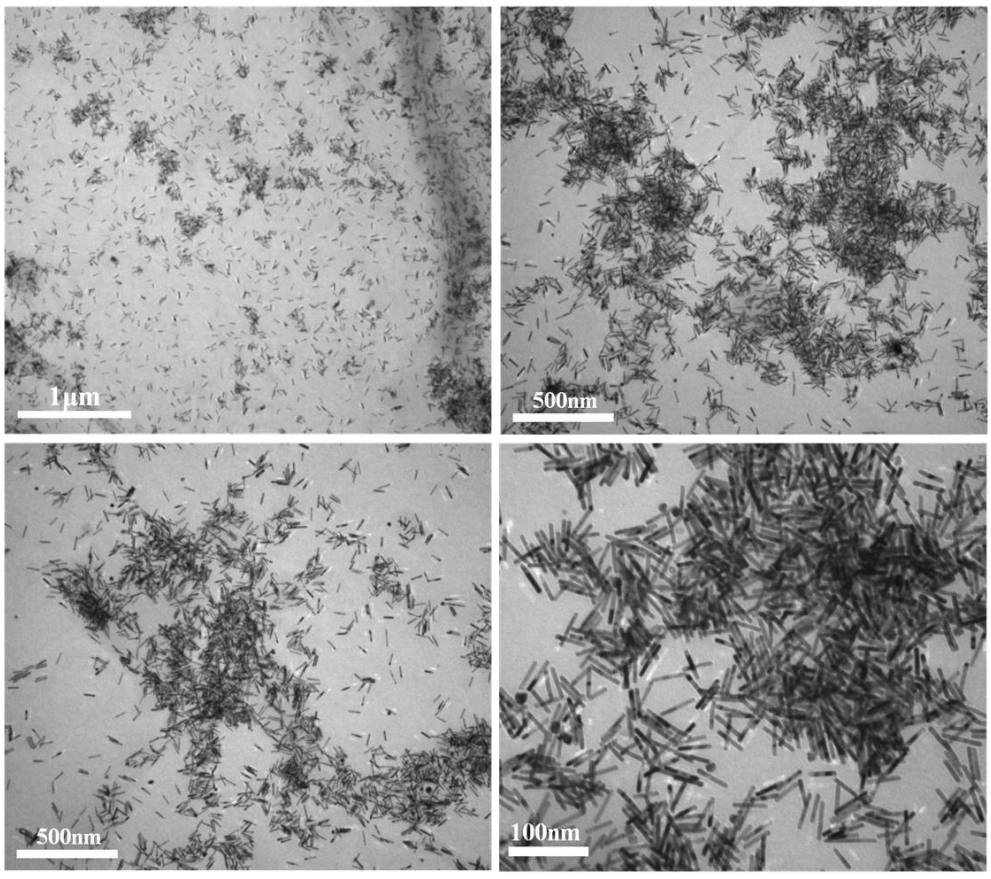

Figure S26. TEM images of ferroelectric $BaTiO_3$ nanorods (L = 51±6 nm, D = 10.8±0.7 nm) tethered with PS at different magnifications (i.e., scale bars). They were synthesized using cylindrical cellulose-*g*-[PAA-*b*-PS] (Samaple-1A in **Table S2**) as a

nanoreactor.

(d) Organic solvent-soluble semiconducting CdSe nanorods

(d1) Preparation of NaHSe[14, 15]

NaHSe was prepared by reacting sodium borohydride and selenium powder in DI water. In a typical process, 1 mmol of selenium powder was introduced into 50 mL of DI water in a three-neck flask. After that, 3 mmol of $NaBH_4$ was added into the reaction system under argon. The reaction was then carried out at room temperature for 8h under argon. After that, the solvent was removed by vacuum, and NaHSe was re-dispersed in dry DMF to yield the NaHSe DMF solution.

(d2) Synthesis of organic solvent-soluble CdSe nanorods (Figure S27)

In a typical process, 10 mg of cellulose-*g*-[PAA-*b*-PS] template was dissolved in 10 mL of DMF at room temperature, followed by the addition of an appropriate amount of precursor $Cd(acac)_2$ that was selectively incorporated in the space occupied by inner PAA blocks. The molar ratio of acrylic acid (AA) units in PAA blocks to precursors was set at 1:10 in order to maximize the loading of precursors into the PAA compartment noted above. Subsequently, an equimolar amount of freshly-prepared NaHSe DMF solution was added dropwise at room temperature, and The mixture was stirred for 1h under argon to ensure that all precursors were well dissolved in DMF. The reaction system was then slowly heated to the boiling point of DMF and refluxed for 2h.

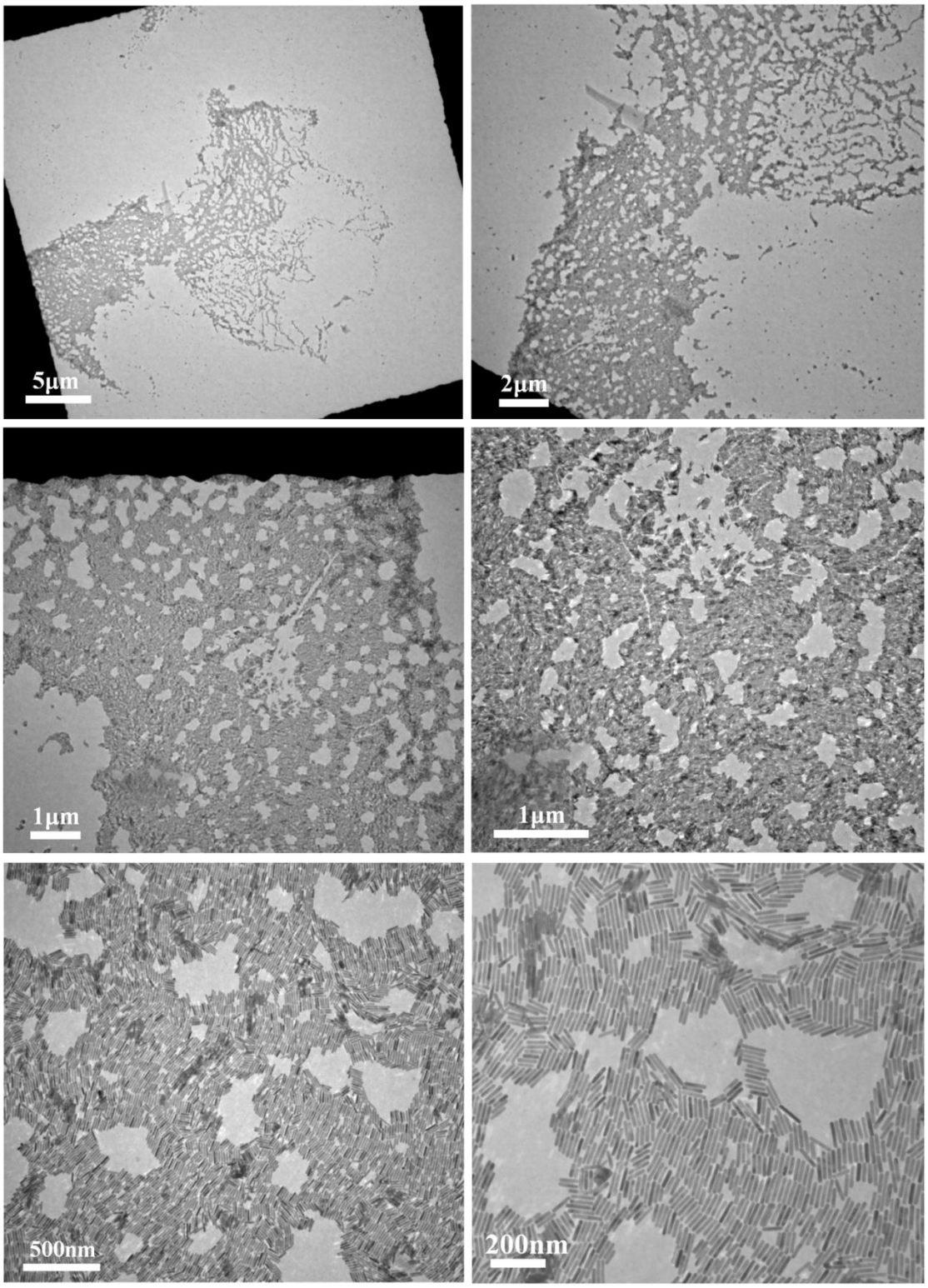

Figure S27. TEM images of semiconducting CdSe nanorods (L = 98±9 nm, D = 10.1±0.7 nm) tethered with PS at different magnifications (i.e., scale bars). They were synthesized using cylindrical cellulose-*g*-[PAA-*b*-PS] (Samaple-2A in **Table S2**) as nanoreactor.

(e) Organic solvent-soluble thermoelectric PbTe nanorods

(e1) Preparation of the precursor system

Prior to the synthesis of thermoelectric PbTe nanorods, their precursors were first prepared. In a typical synthetic process, tellurium powder was dispersed into DI water under argon, $NaBH_4$ (the molar ratio of $NaBH_4$ to Te powder was 3 : 1) was slowly introduced into the reaction solution at room temperature. The reaction solution was stirred to form NaHTe at room temperature under argon for 8 h. After that, an equimolar amount of $PbCO_3$ was added into the reaction solution. After stirring for 1 h, the resulting mixture was obtained by adding the excess cold methanol and centrifuging.

(**e2**) **Synthesis of organic solvent-soluble thermoelectric PbTe nanorods (Figure S28)**

For the synthesis of PbTe nanorods, 10 mg of cellulose-*g*-[PAA-*b*-PS] template was dissolved in 10 mL of DMF at room temperature, followed by the addition of an appropriate amount of precursors (NaHTe and $PbCO_3$) that were selectively encapsulated into the space occupied by inner PAA blocks. The molar ratio of acrylic acid (AA) units in PAA blocks to precursors was 1:10 in order to maximize the incorporating of precursors into the PAA compartment noted above. The mixture was stirred under argon for 1h to ensure that all precursors were well dissolved in DMF. The reaction system was then slowly heated to the boiling point of DMF and refluxed for 2h.

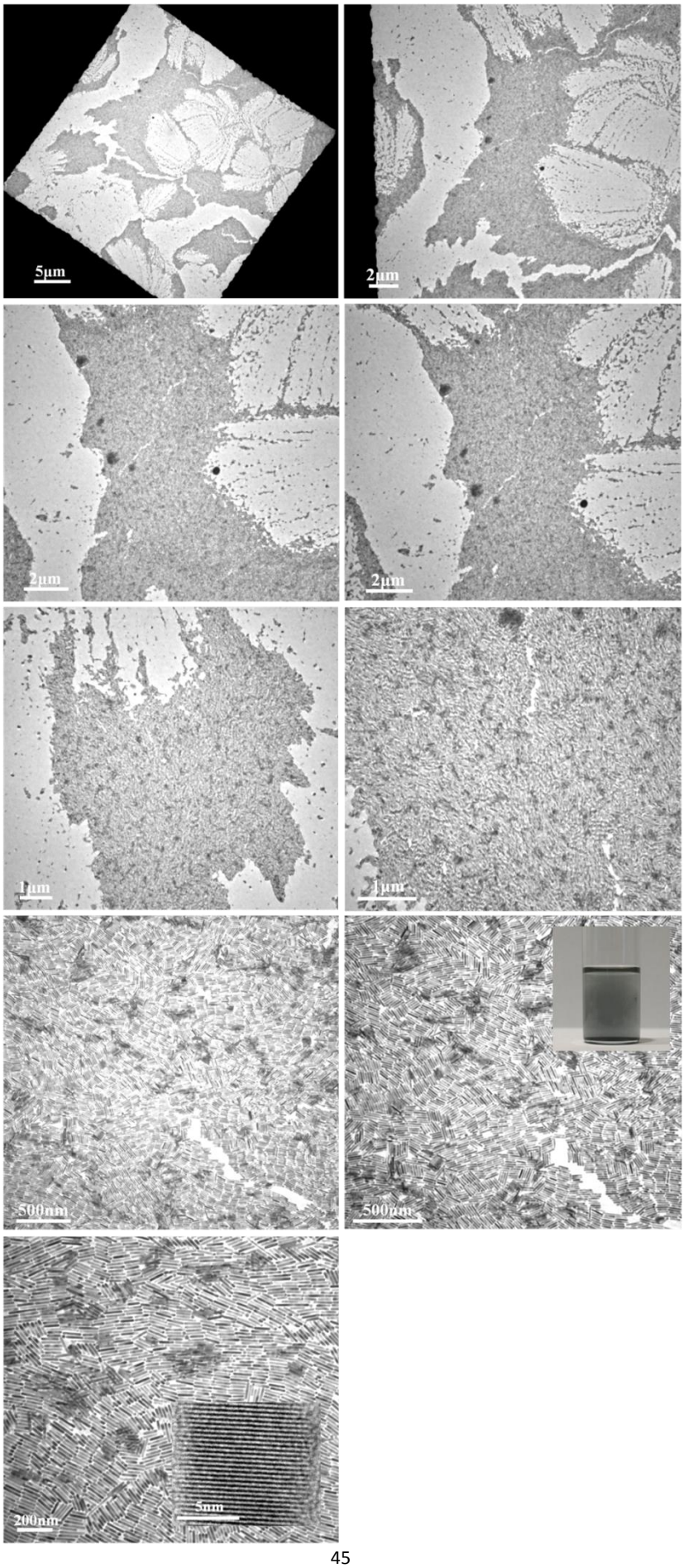
5μm
2μm
2μm
2μm
1μm
1μm
500nm
500nm
200nm
5nm

Figure S28. TEM images of thermoelectric PbTe nanorods tethered with PS (L = 102±10 nm, D = 9.9±0.6 nm) tethered with PS at different magnifications (i.e., scale bars). They were synthesized using cylindrical cellulose-*g*-[PAA-*b*-PS] (Samaple-2A in **Table S2**) as a nanoreactor. The digital image of PbTe nanorods toluene solution and HRTEM image illustrating the crystalline lattices of PbTe nanorod are shown as insets in right panels (fourth row) and left panels (fifth row), respectively.

(f) Organic solvent-soluble magnetic Fe_3O_4 nanorods and nanowires (Figure S29)

Synthesis of magnetic Fe_3O_4 nanorods and nanowires tethered with PS was described as follows. 10 mg of cellulose-*g*-[PAA-*b*-PS] template was dissolved in 10 mL of DMF at room temperature, followed by the addition of an appropriate amount of precursors ($FeCl_2 \cdot 4H_2O + FeCl_3 \cdot 6H_2O + NH_3.H_2O$ as the precursor system) that were preferentially incorporated in the space occupied by inner PAA blocks. The molar ratio of acrylic acid (AA) units in PAA blocks to precursors was set at 1:10 in order to maximize the loading of precursors into the PAA compartment noted above. The synthesis reaction was carried out at 50^{o}C for 30 min. The black mixture was then aged at 80°C for 1 h for improving the crystallization of the resulting nanorods and nanowires.

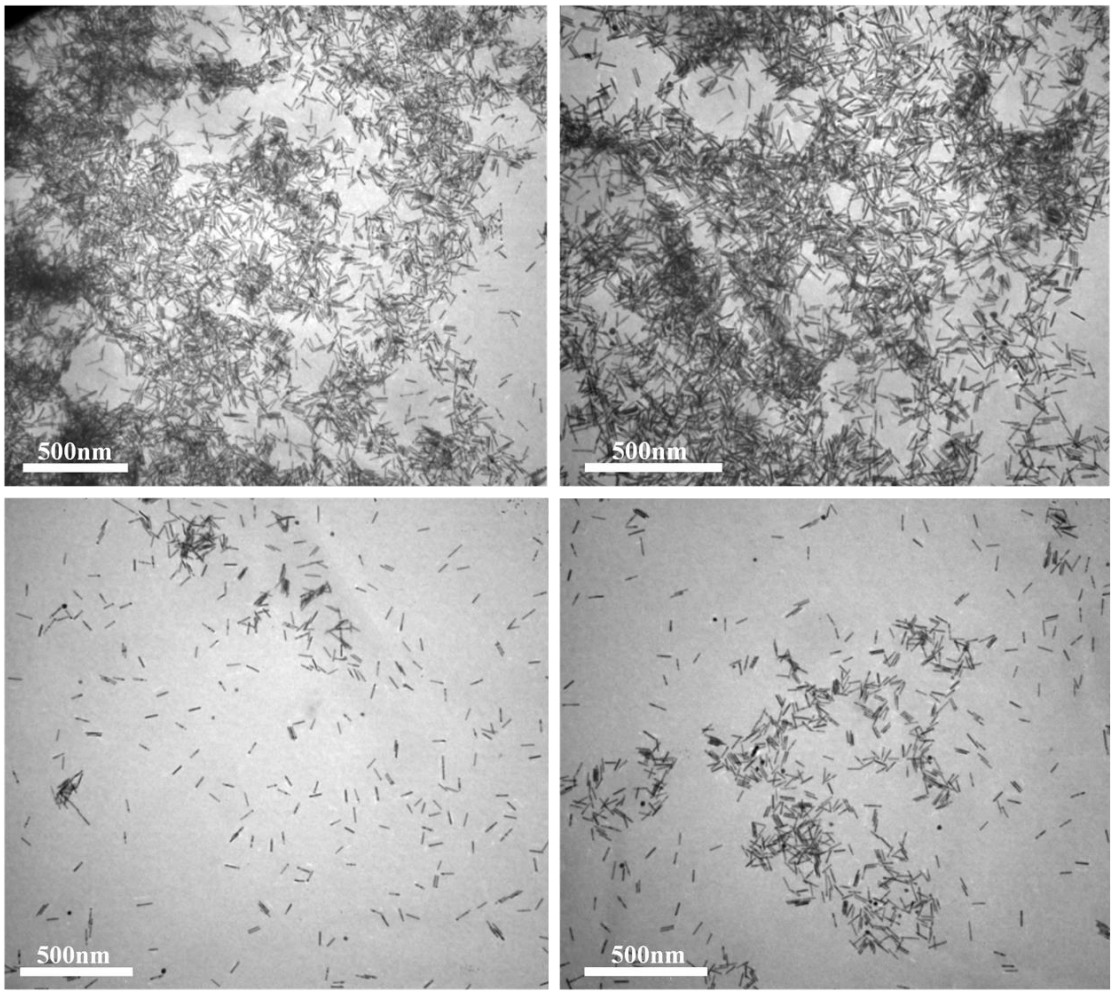

Figure S29. TEM images of magnetic Fe_3O_4 nanorods (L = 52±6 nm, D = 11.2±0.7 nm) tethered with PS synthesized using cylindrical cellulose-*g*-[PAA-*b*-PS] (Samaple-1A in **Table S2**) as nanoreactor.

We note that the aspect ratio of spherical nanoparticles is 1. According to the literature,[16] nanorods are defined as follows: a diameter of ~1-100 nm with the aspect ratio (the ratio of the length to diameter) larger than 1 but less than 20. For an aspect ratio larger than 20, it is referred to as nanowire. In the present work, we not only synthesized magnetic Fe_3O_4 nanorods (aspect ratio = ~5; **Figure S29**), but also produced magnetic Fe_3O_4 nanowires (aspect ratios = ~20 and ~90; **Figure 3**).

(2) Synthesis of plain nanorods and nanowires tethered with PEG (i.e., water-soluble) by capitalizing on double hydrophilic cylindrical

cellulose-*g*-[PAA-*b*-PEG] BBCP (i.e., samples in Table S3) as nanoreactor (Figure S14)

(a) Water-soluble <u>metallic Au nanorods</u> with different diameters and lengths (Figures S30 and **S31)**

10 mg of cellulose-*g*-[PAA-*b*-PEG] template was dissolved in 10 mL of DMF at room temperature, followed by the addition of an appropriate amount of precursors ($HAuCl_4 \cdot 3H_2O$ with tert-butylamine-borane complex (TBAB) as reducer) that were selectively incorporated into the space occupied by inner PAA blocks. The molar ratio of acrylic acid (AA) units in the PAA blocks was set at 1:10 in order to maximize the loading of precursors into the PAA compartment noted above. The mixture was stirred at room temperature under argon for 1h to ensure that all precursors were well dissolved in DMF. The reaction was carried out at 60 ^{o}C for 2 h.

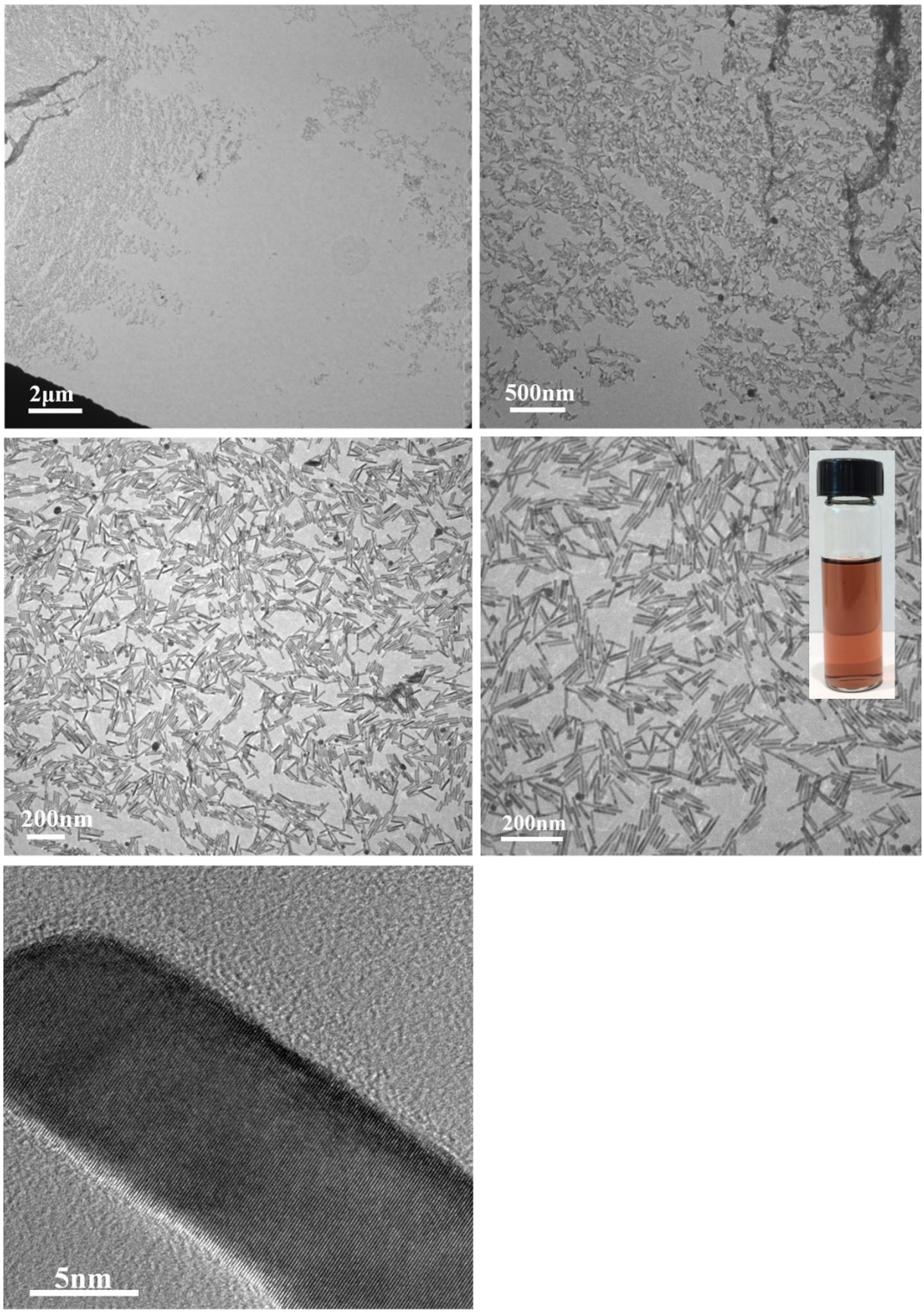

Figure S30. TEM (first and second rows) and HRTEM (third row) images of Au nanorods (L = 97±11 nm, D = 10.5±0.5nm) tethered with PEG at different magnifications (i.e., scale bars). They were synthesized using cylindrical cellulose-*g*-[PAA-*b*-PEG] (Samaple-2A in **Table S3**) as a nanoreactor. The digital image of Au nanorods water solution is shown as inset in right panels (second row).

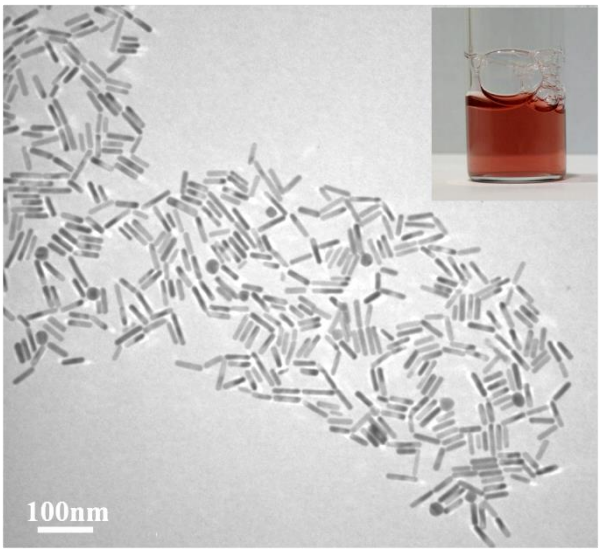

Figure S31. TEM image of Au nanorods (L = 49±5 nm, D = 9.5±0.7 nm) tethered with PEG synthesized using cylindrical cellulose-*g*-[PAA-*b*-PEG] (Samaple-1A in **Table S3**) as a nanoreactor. The digital image of Au nanorods water solution is shown as an inset.

(b) Water-soluble upconversion $NaYF_4$:Yb/Er (18%/2%) nanorods (Figure S32)

10 mg of cellulose-*g*-[PAA-*b*-PEG] template was dissolved in 10 mL of DMF at room temperature, followed by the addition of an appropriate amount of precursors ($Na(CF_3COO)$, $Y(CF_3COO)_3$, $Yb(CF_3COO)_3$ and $Er(CF_3COO)_3$) that were selectively incorporated in the space occupied by the inner PAA blocks. The molar ratio of acrylic acid (AA) units in PAA blocks to precursors was set at 1:10 in order to maximize the loading of precursors into the PAA compartment noted above. The mixture was stirred under argon for 1h to ensure that all precursors were well dissolved in DMF. The reaction system was then slowly heated to the boiling point of DMF and refluxed for 2h. In order to yield highly crystalline hexagonal of nanorods, the resulting solution and additional quantitative amount of CF_3COONa were then transferred to a 20 mL Teflon-lined autoclave, stirred and heated at 200^{o}C for 2h.

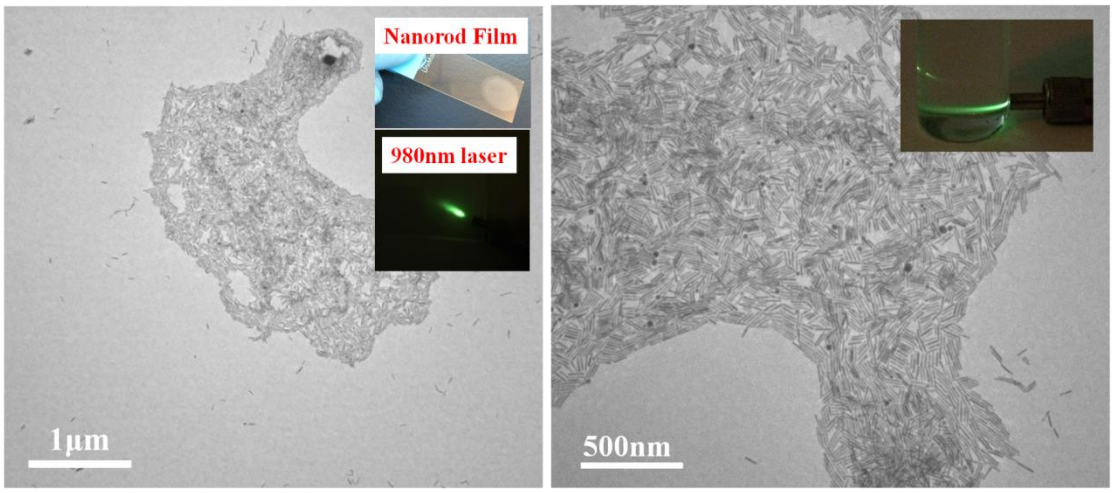

Figure S32. TEM images of upconversion $NaYF_4$:Yb/Er nanorods (L = 96±8 nm, D = 10.9±0.6 nm) tethered with PEG at different magnifications (i.e., scale bars). They were synthesized using cylindrical cellulose-*g*-[PAA-*b*-PEG] (Samaple-2A in **Table S3**) as a nanoreactor. Digital images of upconversion $NaYF_4$:Yb/Er nanorods in dry state (i.e., in a film form – deposited on glass substrate) before (upper panel) and after (lower panel) exposure to a 2W 980-nm near-infrared laser, respectively (left), and an upconversion $NaYF_4$:Yb/Er nanorods toluene solution after exposure to a 2W 980-nm near-infrared laser (right).

(c) Water-soluble magnetic Fe_3O_4 nanowires (Figure S33)

10 mg of cellulose-*g*-[PAA-*b*-PEG] template was dissolved in 10 mL of DMF at room temperature, followed by the addition of an appropriate amount of precursors ($FeCl_2 \cdot 4H_2O$+$FeCl_3 \cdot 6H_2O$+$NH_3.H_2O$ as the precursor system) that were selectively encapsulated in the space occupied by the inner PAA blocks. The molar ratio of acrylic acid (AA) units in PAA blocks to precursors was set at 1:10 in order to maximize the loading of precursors into the PAA compartment noted above. The reaction was carried out at 50^{o}C for 30 min. The black mixture was then aged at 80°C for 1 h to improve the crystallization of the resulting nanowires.

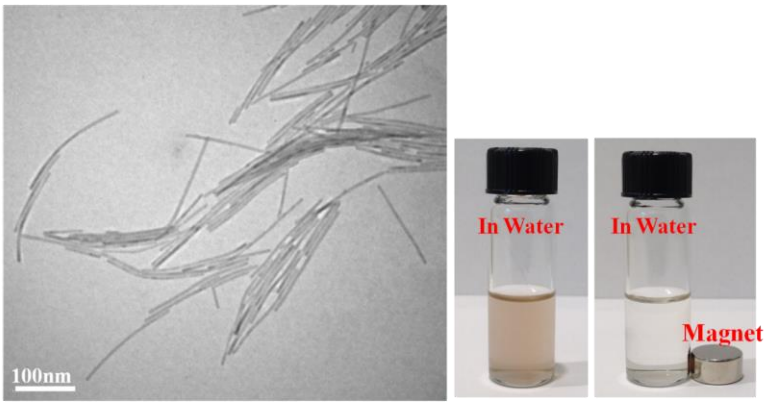

Figure S33. TEM image (left) of magnetic Fe_3O_4 nanowires (L = 209±17 nm, D = 10.5±0.6 nm) tethered with PEG synthesized using cylindrical cellulose-*g*-[PAA-*b*-PEG] (Samaple-3A in **Table S3**) as nanoreactor. Digital images (right) of Fe_3O_4 nanowires water solution demonstrating their magnetic properties. Fe_3O_4 nanowires were deposited on the wall of vials (right) in 30 min under the influence of magnet bar.

2. Synthesis of core/shell nanorods

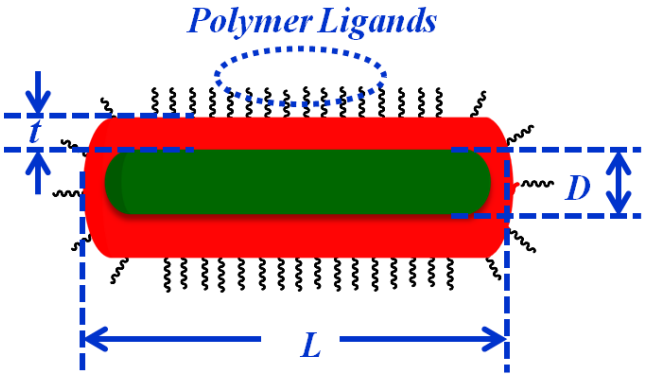

Figure S34. Schematic of a core/shell nanorod illustrating the dimension (i.e., core diameter, D; shell thickness, t; and length, L). The length of core/shell nanorod is dictated by the molecular weight of the cellulose-Br macroinitiator. The core diameter and shell thickness of core/shell nanorod are governed by the molecular weights of the inner and outer hydrophilic blocks (e.g., P4VP and P*t*BA blocks in amphiphilic cellulose-*g*-[P4VP-*b*-P*t*BA-*b*-PS] used as a nanoreactor, where the hydrolysis of P*t*BA yields PAA). The outer blocks (e.g., PS blocks; referred to as "polymer ligands" in the Schematic) enable the solubility of core/shell nanorods (e.g., organic solvent-soluble).

(1) Synthesis of core/shell nanorods tethered with PS (i.e., organic solvent-soluble) by employing amphiphilic cylindrical cellulose-*g*-[P4VP-*b*-P*t*BA-*b*-PS] BBCP (i.e., samples in Table S4) as a nanoreactor (Figure 1b and Figure S15)

(a) Organic solvent-soluble <u>metallic/magnetic Au/Fe_3O_4 core/shell nanorods</u>

For synthesis of PS-tethered Au/Fe_3O_4 core/shell nanorods, 10 mg of cellulose-*g*-[P4VP-*b*-P*t*BA-*b*-PS] template was dissolved in 10 mL of DMF at room temperature. The Au core nanorods were first produced by preferentially encapsulating its precursors ($HAuCl_4 \cdot 3H_2O$ with tert-butylamine-borane complex (TBAB) as reducer) in the space occupied by inner P4VP blocks and reacting at 60^oC for 2 h. The molar ratio of 4-vinylpyridine (4VP) units in P4VP blocks to precursors was set at 1:10. Subsequently, the P*t*BA blocks in P*t*BA-*b*-PS tethered on the surface of Au core nanorod were hydrolyzed into PAA blocks in trifluoroacetic acid (TFA). Similar to plain nanorods, the use of PAA blocks templated the formation of a Fe_3O_4 shell by incorporating its precursors (i.e., $FeCl_2 \cdot 4H_2O$+$FeCl_3 \cdot 6H_2O$+$NH_3 \cdot H_2O$), and reacting at 50^oC for 30 min in DMF. The black mixture was then aged at 80°C for 1 h for improving the crystallization of the resulting Au/Fe_3O_4 core/shell nanorods.

(b) Organic solvent-soluble <u>magnetic/metallic Fe_3O_4/Au core/shell nanorods</u> (Figure S35)

For the synthesis of PS-tethered Fe_3O_4/Au core/shell nanorods, 10 mg of cellulose-*g*-[P4VP-*b*-P*t*BA-*b*-PS] template was dissolved in 10 mL of DMF at room temperature, followed by the addition of an appropriate amount of precursors ($FeCl_2 \cdot 4H_2O$+$FeCl_3 \cdot 6H_2O$+$NH_3 \cdot H_2O$ as the precursor system) that were selectively incorporated into the space occupied by inner P4VP blocks. The molar ratio of 4VP units in P4VP blocks to precursors was set at 1:10 in order to maximize the loading of precursors into the P4VP compartment noted above. The synthesis reaction was carried out at 50^oC for 30 min. The black mixture was then aged at 80°C for 1 h to improve the crystallization of the resulting Fe_3O_4 core nanorods. Subsequently, the P*t*BA blocks in in P*t*BA-*b*-PS tethered on the surface of Fe_3O_4 core nanorod were hydrolyzed into PAA blocks by thermally annealing in phenyl ether at 200 ^oC for 2h. After that, the Au shell was prepared by adding an appropriate amount of precursors ($HAuCl_4 \cdot 3H_2O$ with tert-butylamine-borane complex (TBAB) as reducer) that were

preferentially encapsulated in the space occupied by PAA blocks. The molar ratio of acrylic acid (AA) units in PAA blocks to precursors was also set at 1:10 in order to maximize the loading of precursors into the PAA compartment noted above. The stirring was continued at room temperature under argon for 1h. The reaction was then carried out at 60 ^{o}C for 2 h.

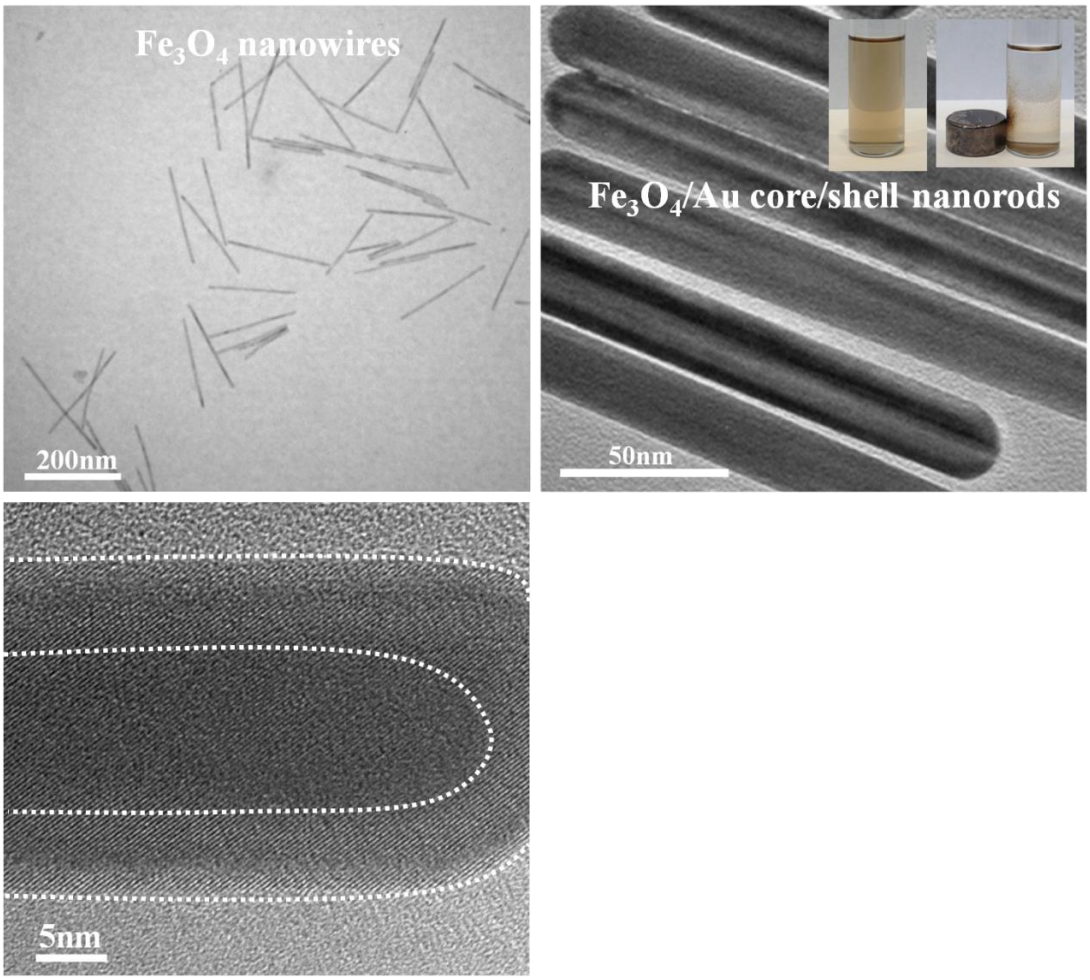

Figure S35. TEM (first row) and HRTEM (second row) images of Fe_3O_4 core nanowires (left) tethered with P*t*BA-*b*-PS and Fe_3O_4/Au core/shell nanowires (L = 198±18 nm, D = 9.6±0.8 nm, and t = 6.3±0.5 nm) tethered with PS synthesized using cylindrical cellulose-*g*-[P4VP-*b*-P*t*BA-*b*-PS] (Samaple-3A in **Table S4**) as a nanoreactor. Digital images (upper right insets) of Fe_3O_4/Au core/shell nanowires toluene solution that demonstrate their magnetic properties. Fe_3O_4/Au core/shell nanowires were deposited on the wall of vials (right) in 1 h under the influence of magnet bar.

(c) Organic solvent-soluble <u>metallic/semiconducting Au/TiO_2 core/shell nanorods</u> (Figures S36 and **S37)**

For the synthesis of PS-tethered Au/TiO_2 core/shell nanorods, 10 mg of cellulose-*g*-[P4VP-*b*-P*t*BA-*b*-PS] template was dissolved in 10 mL of DMF at room temperature. The Au core nanorods were first produced by encapsulating its precursors ($HAuCl_4 \cdot 3H_2O$ with tert-butylamine-borane complex (TBAB) as reducer) in the space occupied by the inner P4VP blocks and reacting at 60^{o}C for 2 h. The molar ratio of 4-vinylpyridine (4VP) units in P4VP blocks to precursors was set at 1:10. Subsequently, the P*t*BA blocks in P*t*BA-*b*-PS tethered on the surface of the Au core nanorod were hydrolyzed into PAA blocks in TFA. The semiconducting TiO_2 shell was prepared by the addition of an appropriate amount of titanium(IV) tetraisopropoxide (TTIP) precursor that was selectively incorporated into the space occupied by the PAA blocks. The molar ratio of acrylic acid (AA) units in PAA blocks to precursors was also set to 1:10 in order to maximize the loading of precursors into the PAA compartment noted above. The stirring was maintained under argon for 1h to ensure that all precursors were well dissolved in DMF. The reaction system was then slowly heated to the boiling point of DMF and refluxed for 2h. In order to yield highly crystalline Au/TiO_2 core/shell nanorods, the resulting solution was transferred into a 20 mL Teflon-lined autoclave, stirred and heated again at 200^{o}C for 2h.

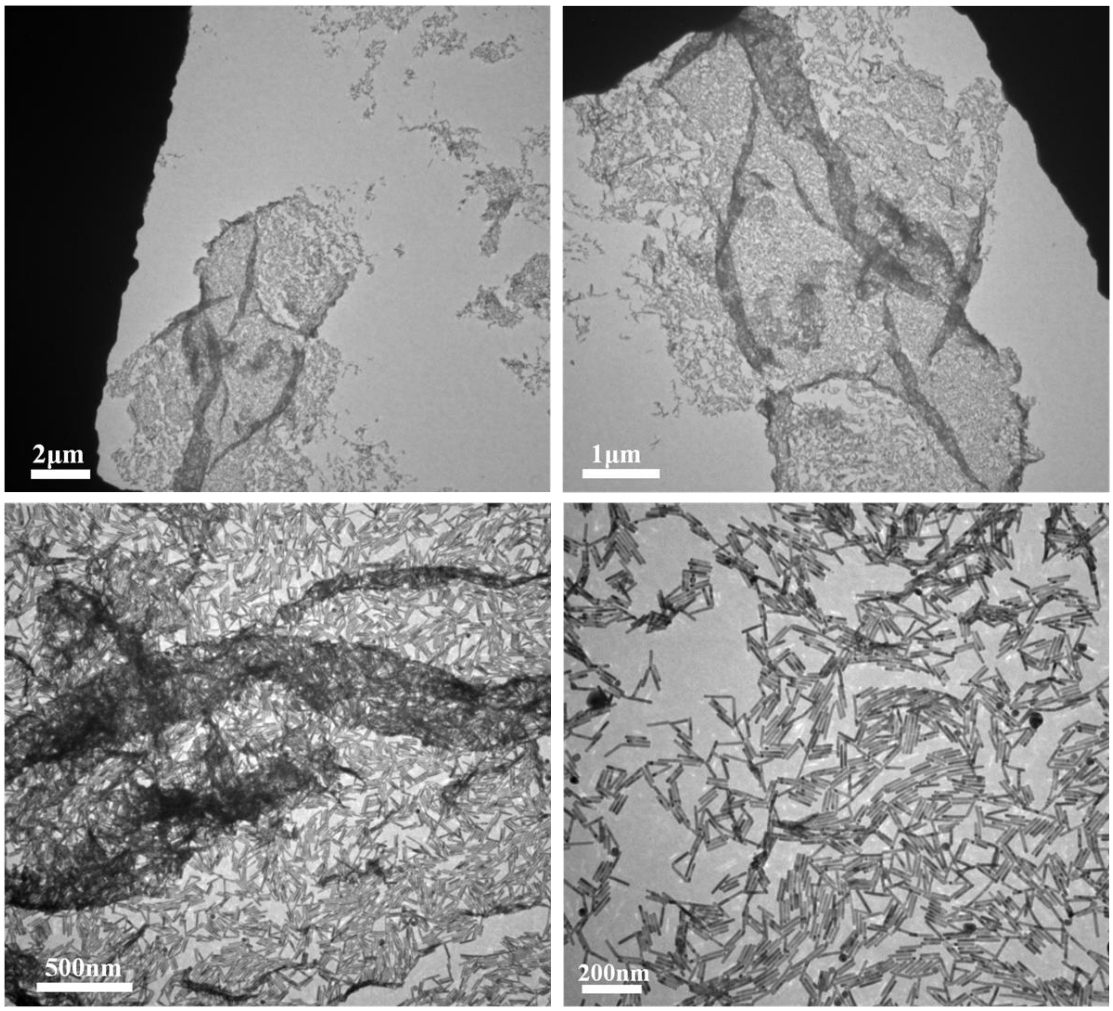

Figure S36. TEM images of Au core nanorods (L = 102±9 nm and D = 10.4±0.7 nm) tethered with P*t*BA-*b*-PS at different magnifications (i.e., scale bars). They were synthesized using cylindrical cellulose-*g*-[P4VP-*b*-P*t*BA-*b*-PS] (Samaple-2B in **Table S4**) as a nanoreactor.

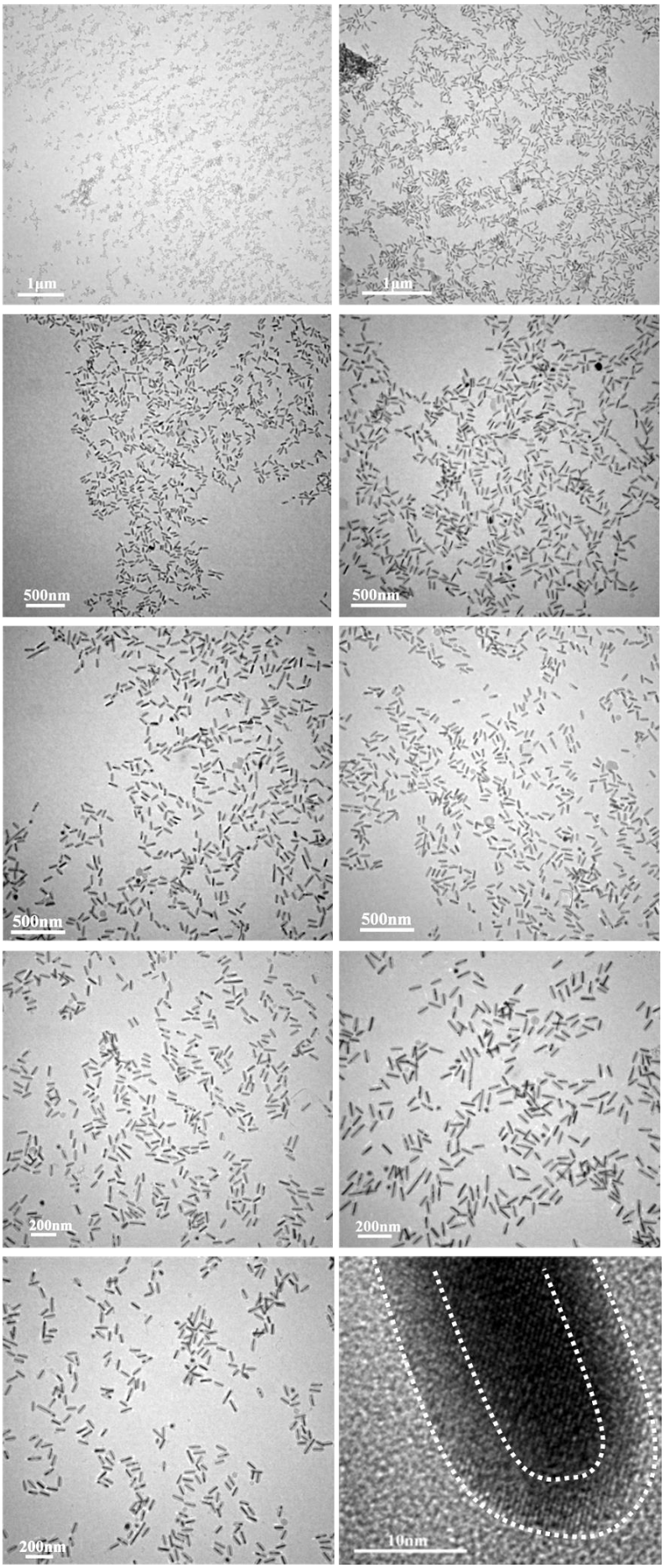
1μm
1μm
500nm
500nm
500nm
500nm
200nm
200nm
200nm
10nm

Figure S37. TEM and HRTEM (right panel; fifth row) images of Au/TiO_2 core/shell nanorods (L = 102±9 nm, D = 10.4±0.7 nm, and t = 5.2±0.5 nm) tethered with PS at different magnifications (i.e., scale bars). They were synthesized using cylindrical cellulose-*g*-[P4VP-*b*-P*t*BA-*b*-PS] (Samaple-2B in **Table S4**) as a nanoreactor.

(2) Synthesis of core/shell nanorods tethered with PEG (i.e., water-soluble) by employing amphiphilic cylindrical cellulose-*g*-[P4VP-*b*-P*t*BA-*b*-PEG] BBCP (i.e., samples in Table S5) as a nanoreactor (Figure 1b and Figure S16)

(a) Water-soluble <u>metallic/semiconducting Au/TiO_2 core/shell nanorods</u> (Figures S38 and **S39)**

For synthesis PEG-tethered Au/TiO_2 core/shell nanorods, 10 mg of cellulose-*g*-[P4VP-*b*-P*t*BA-*b*-PEG] template was dissolved in 10 mL of DMF at room temperature. The Au core nanorods were first synthesized by sequestering its precursors ($HAuCl_4 \cdot 3H_2O$ with tert-butylamine-borane complex (TBAB) as reducer) in the space occupied by the inner P4VP blocks and reacting at 60^{o}C for 2 h. Similarly, the molar ratio of 4-vinylpyridine (4VP) unit in P4VP blocks to precursors was 1:10. Subsequently, the P*t*BA blocks in P*t*BA-*b*-PS tethered on the surface of Au core nanorod were hydrolyzed into PAA blocks in TFA. The semiconducting TiO_2 shell was then prepared by the addition of an appropriate amount of precursors TTIP that were selectively encapsulated into the space occupied by the PAA blocks. The molar ratio of acrylic acid (AA) units in PAA blocks to precursors was also set at 1:10 in order to maximize the loading of precursors into the PAA compartment noted above. The stirring was continued under argon for 1h to ensure that all precursors were well dissolved in DMF. The reaction system was then slowly heated to the boiling point of DMF and refluxed for 2h. In order to synthesize highly crystalline Au/TiO_2 core/shell nanorods. The resulting solution was transferred into a 20 mL Teflon-lined autoclave, stirred and heated again at 200^{o}C for 2h.

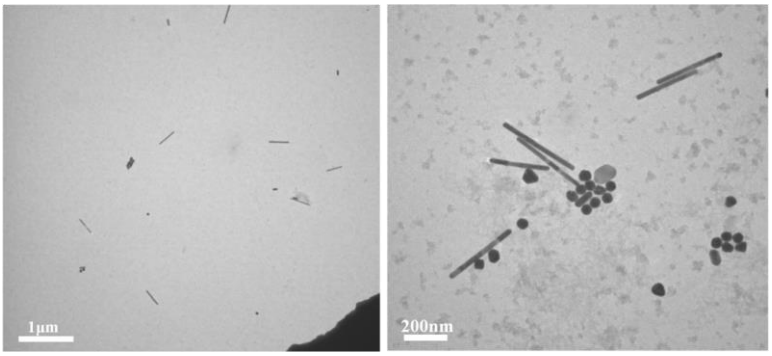

Figure S38. TEM images of Au core nanorods (L = 396±40 nm and D = 21.6±1.6 nm) caped with P*t*BA-*b*-PEG at different magnifications (i.e., scale bars). They were synthesized using cylindrical cellulose-*g*-[P4VP-*b*-P*t*BA-*b*-PEG] (Samaple-4A in **Table S5**) as a nanoreactor. The presence of irregular nanoparticles was resulted from the excess amount of Au precursors.

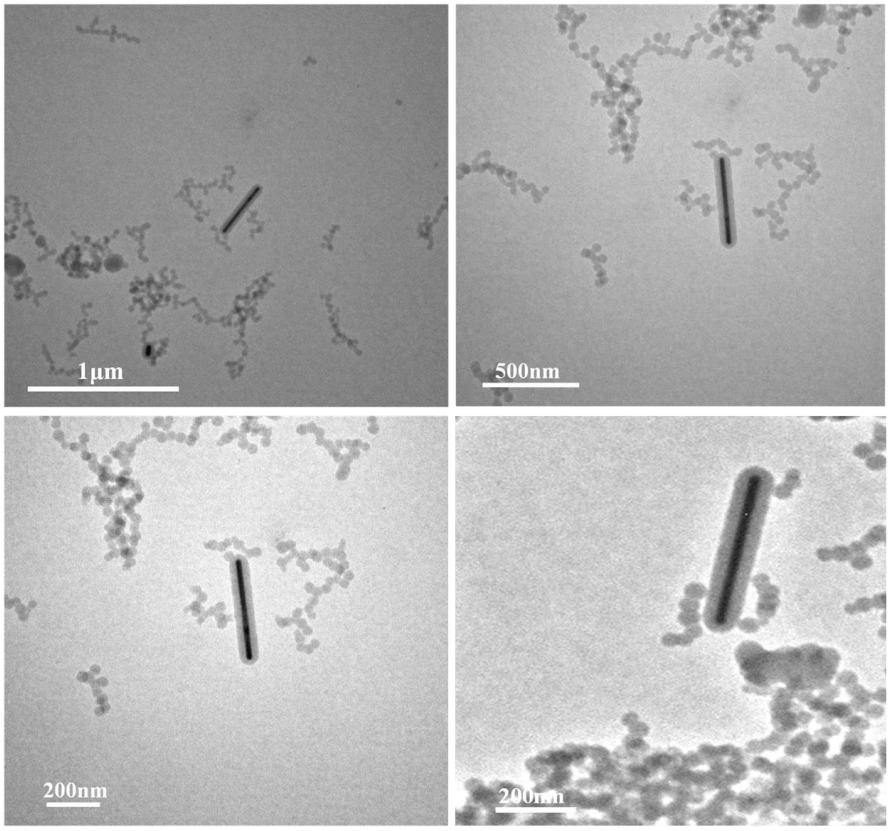

Figure S39. TEM images of Au/TiO_2 core/shell nanorods (L = 396±40 nm and D = 21.6±1.6 nm, and t = 22.8±1.8 nm) tethered with PEG at different magnifications (i.e., scale bars). They were synthesized using cylindrical cellulose-*g*-[P4VP-*b*-P*t*BA-*b*-PEG] (Samaple-2B in **Table S4**) as a nanoreactor.

(b) Water-soluble <u>metallic/upconversion Au/$NaYF_4$:Yb/Er core/shell nanorods</u> (Figure S40)

For the synthesis of PEG-tethered Au/$NaYF_4$:Yb/Er core/shell nanorods, 10 mg of cellulose-*g*-[P4VP-*b*-P*t*BA-*b*-PEG] template was dissolved in 10 mL DMF at room temperature. The Au core nanorods were first formed by encapsulating its precursors ($HAuCl_4 \cdot 3H_2O$ with tert-butylamine-borane complex (TBAB) as reducer) in the space occupied by the inner P4VP blocks and reacting at 60^{o}C for 2 h. Similarly, the molar ratio of 4-vinylpyridine (4VP) units in P4VP blocks to precursors was 1:10. Subsequently, the P*t*BA blocks in P*t*BA-*b*-PS tethered on the surface of Au core nanorods were hydrolyzed into PAA blocks in TFA. The upconversion $NaYF_4$:Yb/Er shell was then formed by the addition of an appropriate amount of precursors ($Na(CF_3COO)$, $Y(CF_3COO)_3$, $Yb(CF_3COO)_3$ and $Er(CF_3COO)_3$) that selectively entered into the space occupied by the PAA blocks. The molar ratio of acrylic acid (AA) units in PAA blocks to precursors was also set at 1:10 in order to maximize the loading of precursors into the PAA compartment noted above. The mixture was stirred under argon for 1h to ensure that all precursors were well dissolved in DMF. The reaction system was then slowly heated to the boiling point of DMF and refluxed for 2h. In order to yield highly crystalline hexagonal phase of upconversion $NaYF_4$:Yb/Er nanorods, the resulting solution and an additional quantitative amount of CF_3COONa were then transferred to a 20 mL Teflon-lined autoclave, stirred and heated at 200^{o}C for 2h.

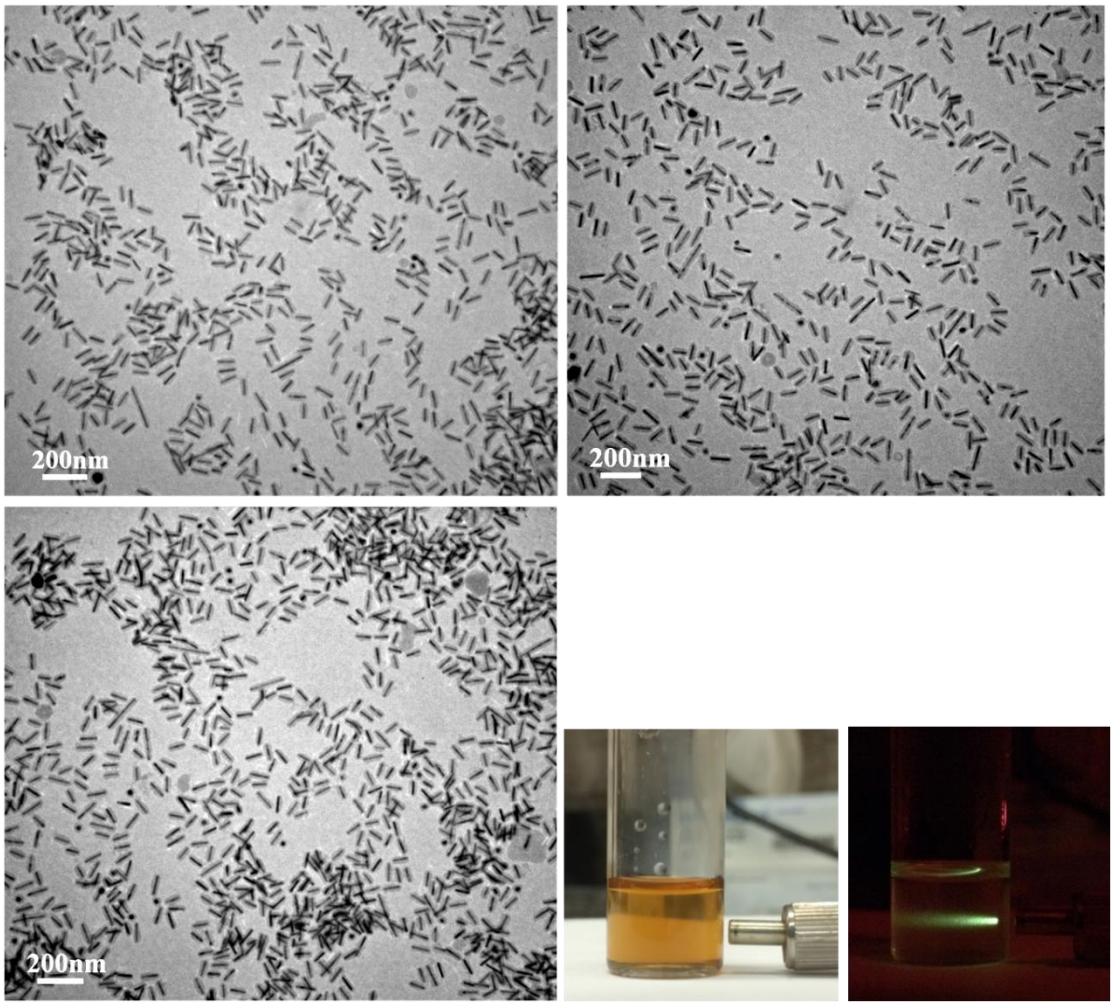

Figure S40. TEM images of Au/$NaYF_4$:Yb/Er core/shell nanorods (L = 102±9 nm, D = 10.4±0.7 nm, t = 5.4±0.6 nm) tethered with PEG at different magnifications (i.e., scale bars). They were synthesized using cylindrical cellulose-*g*-[P4VP-*b*-P*t*BA-*b*-PEG] (Samaple-2B in **Table S4**) as a nanoreactor. Digital images of Au/$NaYF_4$:Yb/Er core/shell nanorods water solution before (left) and after (right) exposure to a 2W 980-nm near-infrared laser, respectively.

3. Synthesis of nanotubes

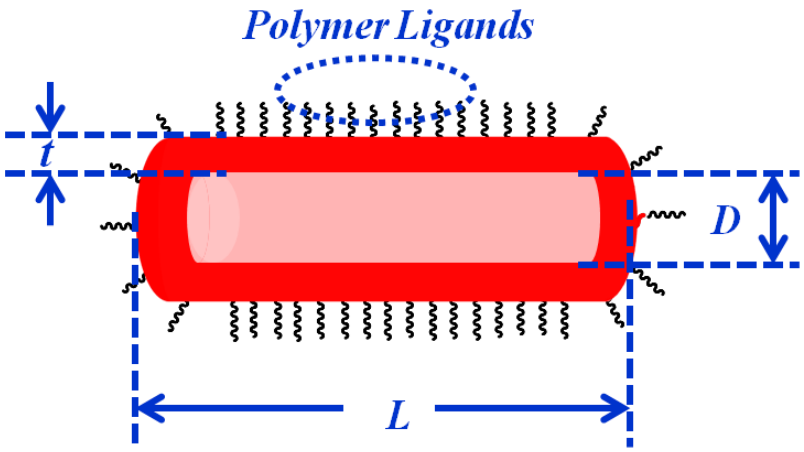

Figure S41. Schematic of a nanotube (i.e., hollow nanorod) illustrating the dimension (i.e., diameter of hollow interior, *D*; shell thickness, *t*; and length, *L*). The length of the nanotube is dictated by the molecular weight of cellulose-Br macroinitiator. The diameter of the hollow interior and the shell thickness are governed by the molecular weights of the inner hydrophobic and intermediate hydrophilic blocks (e.g., PS and PAA blocks in amphiphilic cellulose-*g*-[PS-*b*-PAA-*b*-PS] used as a nanoreactor (where the hydrolysis of P*t*BA yields PAA). The outer blocks (e.g., PS blocks; referred to as "polymer ligands" in the Schematic) enable the solubility of the nanotube (e.g., organic solvent-soluble).

(1) Synthesis of nanotubes tethered with PS (i.e., organic solvent-soluble) by utilizing amphiphilic cylindrical cellulose-*g*-[PS-*b*-PAA-*b*-PS] BBCP (i.e., samples in Table S6) as a nanoreactor (Figure 1c and Figure S17)

(a) Organic solvent-soluble <u>metallic Au nanotubes</u>

For the synthesis of PS-tethered Au nanotubes, 10 mg of cellulose-*g*-[PS-*b*-PAA-*b*-PS] template was dissolved in 10 mL of DMF at room temperature. Similarly, the precursor ($HAuCl_4 \cdot 3H_2O$ with TBAB used as reducer) was added into the template solution. The molar ratio of acrylic acid (AA) units in the intermediate PAA blocks to precursors was set at 1:10 in order to maximize the incorporation of precursors in the space occupied by PAA blocks. The mixture was

stirred under argon for 1h to ensure that all precursors were well dissolved in DMF. The reaction solution was then slowly heated to 60^{o}C for 2 h.

(b) Organic solvent-soluble <u>upconversion $NaYF_4$:Yb/Er (18%/2%) nanotubes</u> (Figures S42 and **S43)**

For the synthesis of PS-tethered upconversion $NaYF_4$:Yb/Er nanotubes, 10 mg of cellulose-*g*-[PS-*b*-PAA-*b*-PS] template was dissolved in 10 mL of DMF at room temperature, followed by the addition of an appropriate amount of precursors ($Na(CF_3COO)$, $Y(CF_3COO)_3$, $Yb(CF_3COO)_3$ and $Er(CF_3COO)_3$) that were selectively incorporated in the space occupied by the intermediate PAA blocks. The molar ratio of acrylic acid (AA) units in PAA blocks to precursors was 1:10 in order to maximize the loading of precursors into the PAA compartment noted above. The mixture was stirred under argon for 1h to ensure that all precursors were well dissolved in DMF. The reaction system was then slowly heated to the boiling point of DMF and refluxed for 2h. In order to produce highly crystalline hexagonal phase of upconversion $NaYF_4$:Yb/Er nanotubes, the resulting solution and an additional quantitative amount of CF_3COONa were then transferred to a 20 mL Teflon-lined autoclave, stirred and heated at 200^{o}C for 2h.

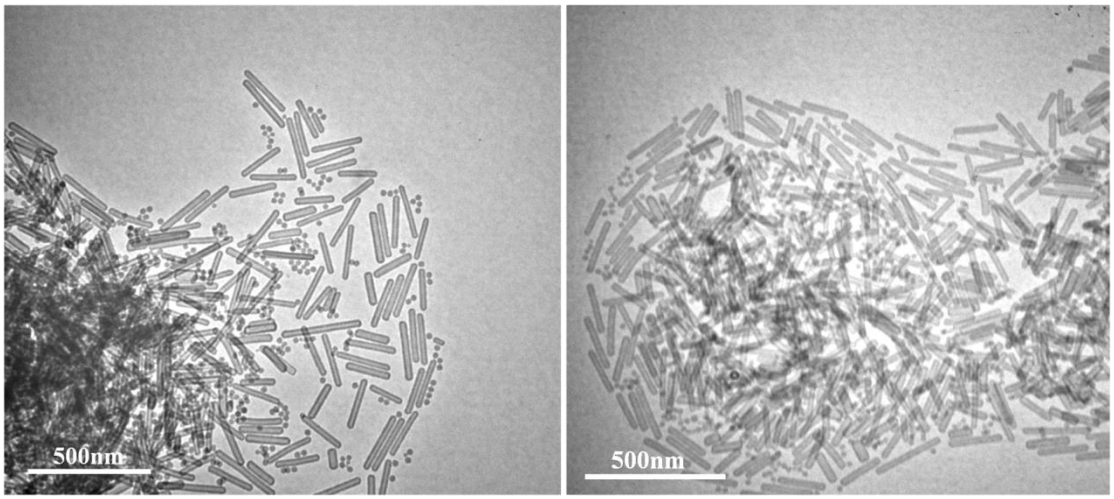

Figure S42. TEM images of upconversion $NaYF_4$:Yb/Er nanotubes (L = 208±22 nm, D of hollow interior = 10.5±0.8 nm, and t of shell thickness = 5.5±0.5 nm) tethered with PS synthesized using cylindrical cellulose-*g*-[PS-*b*-PAA-*b*-PS] (Samaple-3A in **Table S6**) as a nanoreactor.

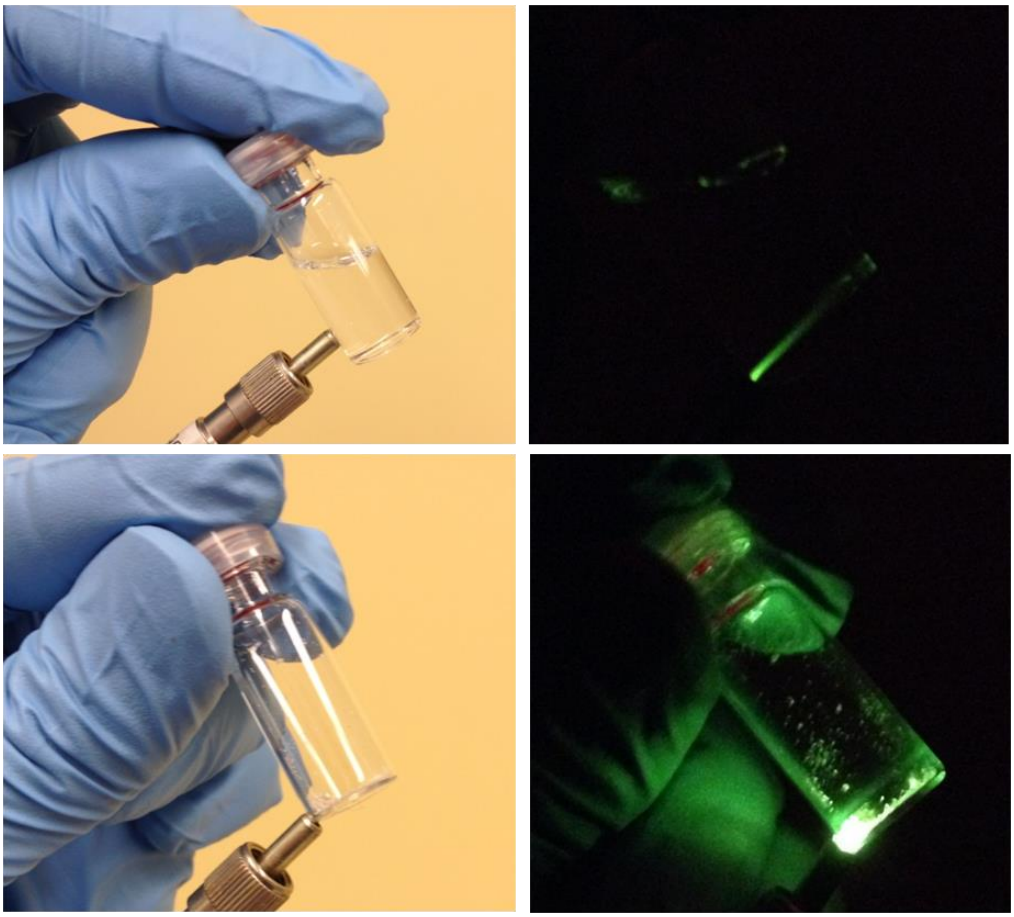

Figure S43. Digital images of upconversion $NaYF_4$:Yb/Er nanotubes tethered with PS synthesized using cylindrical cellulose-*g*-[PS-*b*-PAA-*b*-PS] (Samaple-3A in **Table S6**) as a nanoreactor (upper panels: toluene solution; lower panels: solid powder) before (left panels) and after (right panels) exposure to a 2W 980-nm near-infrared laser, respectively.

(c) Organic solvent-soluble <u>semiconducting TiO_2 nanotubes</u> (Figure S44)

For synthesis of PS-tethered semiconducting TiO_2 nanotubes, 10 mg of cellulose-*g*-[PS-*b*-PAA-*b*-PS] template was dissolved in 10 mL of DMF at room temperature, followed by the addition of an appropriate amount of TTIP precursor that was selectively incorporated into the space occupied by the intermediate PAA blocks. The molar ratio of acrylic acid (AA) units in PAA blocks to precursors was set at 1:10 in order to maximize the loading of precursors into the PAA compartment noted above. The mixture solution was stirred under argon for 1h to ensure that all

precursors were well dissolved in DMF. The reaction system was then slowly heated to the boiling point of DMF and refluxed for 2h. In order to produce highly crystalline TiO_2 nanotubes, the resulting solution was transferred into a 20 mL Teflon-lined autoclave, stirred and heated again at 200^{o}C for 2h.

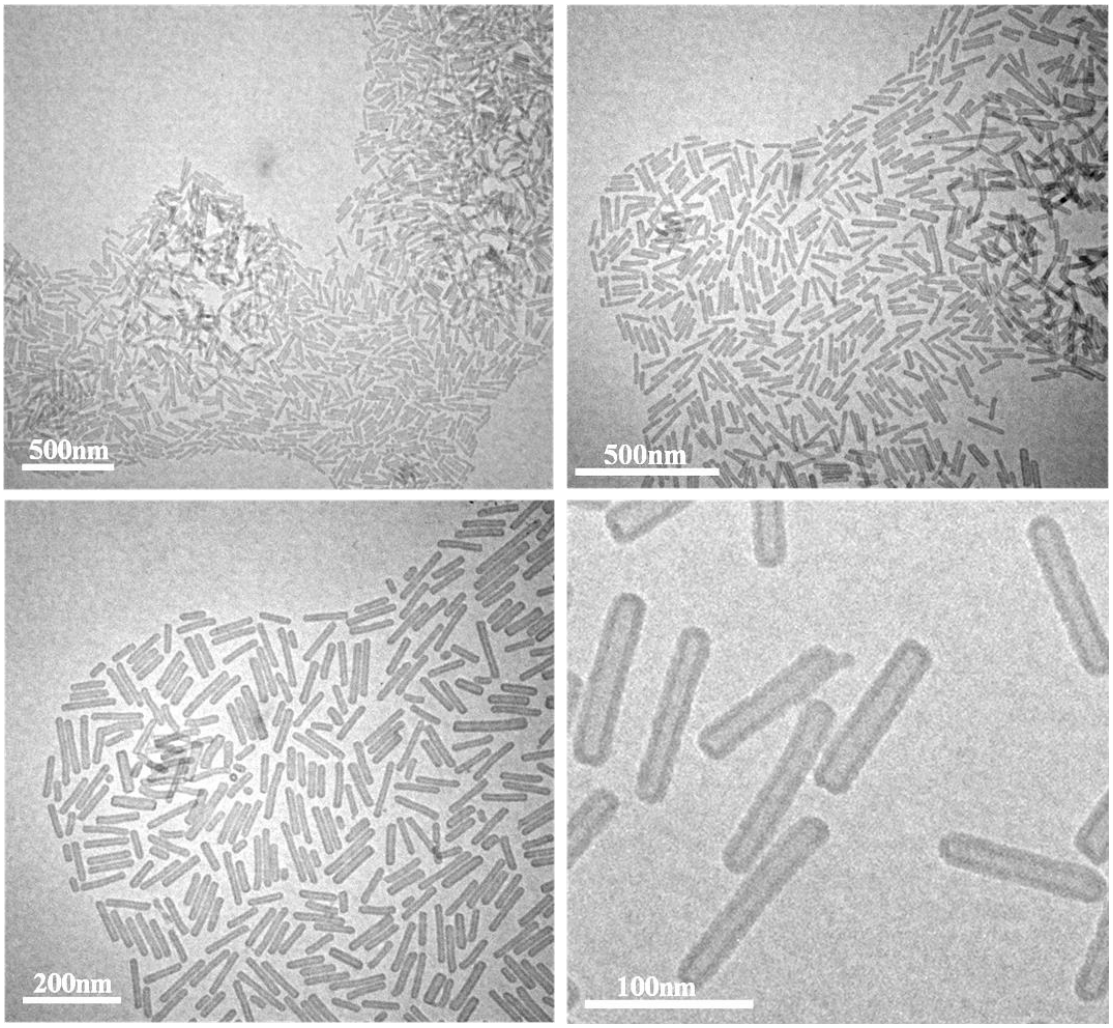

Figure S44. TEM images of TiO_2 nanotubes (L = 108±10 nm, D of hollow interior = 5.5±0.5 nm, and t of shell thickness = 5.6±0.6 nm) tethered with PS at different magnifications. They were synthesized using cylindrical cellulose-*g*-[PS-*b*-PAA-*b*-PS] (Samaple-2A in **Table S6**) as nanoreactor.

(2) Synthesis of nanotubes tethered with PEG (i.e., water-soluble) by utilizing amphiphilic cylindrical cellulose-*g*-[PS-*b*-PAA-*b*-PEG] BBCP (i.e., samples in Table S7) as a nanoreactor (Figure S18)

(a) Water-soluble <u>metallic Au nanotubes</u> (Figure S45)

For synthesis of PEG-tethered Au nanotubes, 10 mg of cellulose-*g*-[PS-*b*-PAA-*b*-PEG] template was dissolved in 10 mL of DMF at room temperature. Similarly, the precursor ($HAuCl_4 \cdot 3H_2O$ with TBAB used as a reducer) was added into the template solution. The molar ratio of acrylic acid (AA) units in the intermediate PAA template phase to precursors was 1:10 for maximizing the incorporating of precursors into PAA template domains. The stirring was maintained for 1h under argon to ensure that all the precursors were well dissolved in DMF solvent. The reaction solution was then slowly heated to 60^oC for 2 h.

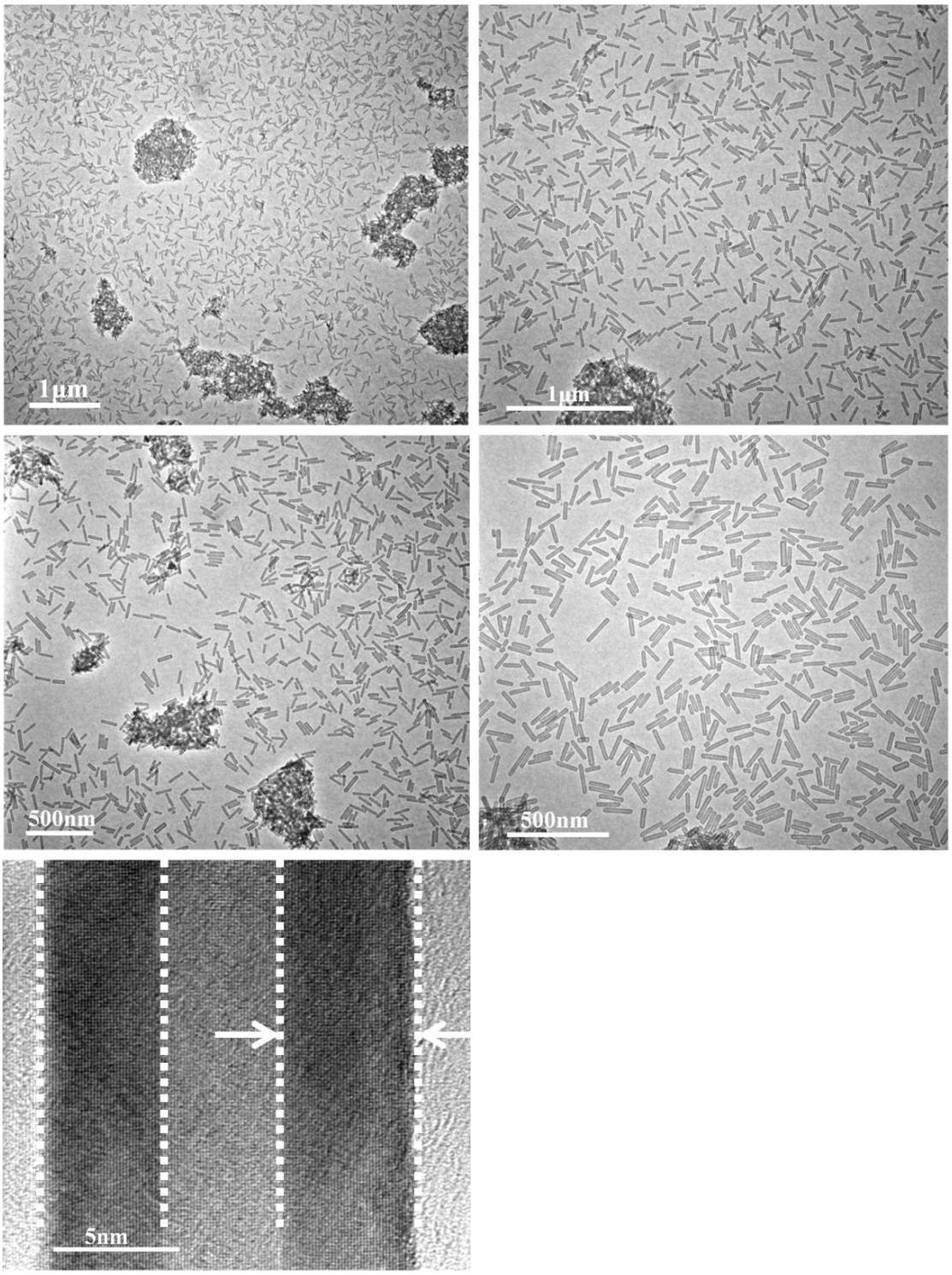

Figure S45. TEM (first and second rows) and HRTEM (third row) images of Au nanotubes (L = 106±11 nm, D of hollow interior = 5.1±0.6 nm, and t of shell thickness = 5.3±0.5 nm) tethered with PEG at different magnifications. They were synthesized using cylindrical cellulose-*g*-[PS-*b*-PAA-*b*-PEG] (Samaple-2A in **Table S7**) as a nanoreactor.

(b) Water-soluble semiconducting TiO_2 nanotubes (Figure S46)

For the synthesis of PEG-tethered semiconducting TiO_2 nanotubes, 10 mg of cellulose-*g*-[PS-*b*-PAA-*b*-PEG] template was dissolved in 10 mL of DMF at room temperature, followed by the addition of an appropriate amount of TTIP precursor that was selectively incorporated in the space occupied by the intermediate PAA blocks. The molar ratio of acrylic acid (AA) units in PAA blocks to precursors was set at 1:10 in order to maximize the loading of precursors into the PAA compartment noted above. The mixture was stirred under argon for 1h to ensure that all precursors were well dissolved in DMF. The reaction system was then slowly heated to the boiling point of DMF and refluxed for 2h. In order to yield highly crystalline TiO_2 nanotubes, the resulting solution was transferred into a 20 mL Teflon-lined autoclave, stirred and heated again at 200^{o}C for 2h.

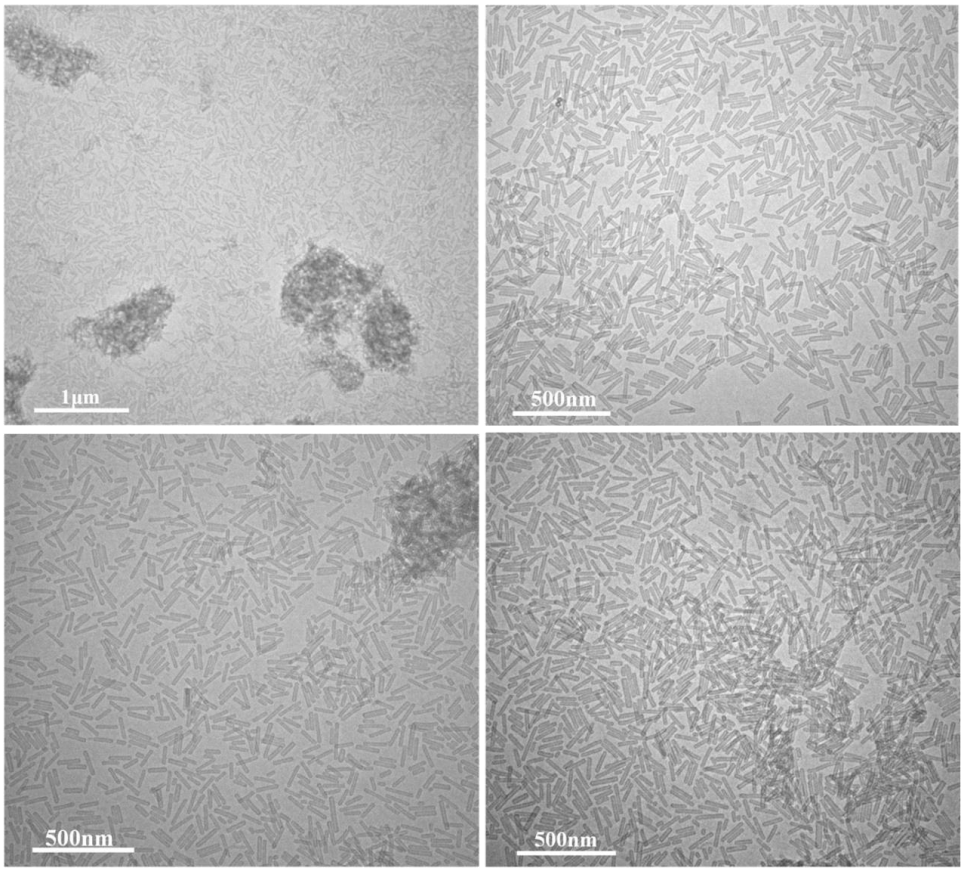

Figure S46. TEM images of TiO_2 nanotubes (L = 103±9 nm, D of hollow interior = 5.2±0.6 nm, and t of shell thickness = 5.5±0.5 nm) tethered with PEG at different magnifications. They were synthesized using cylindrical cellulose-*g*-[PS-*b*-PAA-*b*-PEG] (Samaple-2A in **Table S7**) as a nanoreactor.

(c) Water-soluble upconversion $NaYF_4$:Yb/Er (18%/2%) nanotubes (Figure S47)

For the synthesis of PEG-tethered upconversion $NaYF_4$:Yb/Er nanotubes, 10 mg of cellulose-*g*-[PS-*b*-PAA-*b*-PEG] template was dissolved in 10 mL of DMF at room temperature, followed by the addition of an appropriate amount of precursors ($Na(CF_3COO)$, $Y(CF_3COO)_3$, $Yb(CF_3COO)_3$ and $Er(CF_3COO)_3$) that were selectively incorporated into the space occupied by the intermediate PAA blocks. The molar ratio of acrylic acid (AA) units in PAA blocks to precursors was set at 1:10 in order to maximize the loading of precursors into the PAA compartment noted above. The reaction solution was stirred at room temperature under argon for 1h to ensure that all precursors were well dissolved in DMF. The reaction system was then slowly heated to the boiling point of DMF and refluxed for 2h. In order to achieve highly crystalline hexagonal phase of upconversion $NaYF_4$:Yb/Er nanotubes, the resulting solution and additional quantitative CF_3COONa were then transferred to a 20 mL Teflon-lined autoclave, stirred and heated at 200^oC for 2h.

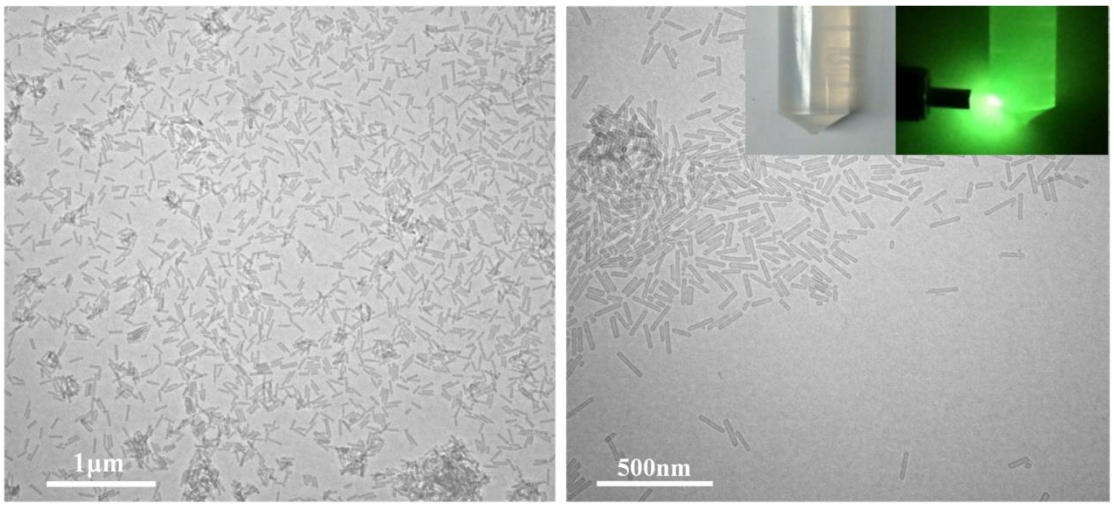

Figure S47. TEM images of upconversion $NaYF_4$:Yb/Er nanotubes (L = 105±11 nm, D of hollow interior = 5.4±0.5 nm, and t of shell thickness = 5.2±0.6 nm) tethered with PEG at different magnifications. They were synthesized using cylindrical cellulose-*g*-[PS-*b*-PAA-*b*-PEG] (Samaple-2A in **Table S7**) as a nanoreactor. Insets: digital images of upconversion $NaYF_4$:Yb/Er nanotubes water solution before (left) and after (right) exposure to a 2W 980-nm near-infrared laser, respectively.

Section V

Proposed growth mechanisms for 1D nanocrystals by selective incorporation of precursors in the space occupied by hydrophilic blocks (PAA and P4VP) of cylindrical BBCP nanoreactors and then growing into nanocrystals

The possible growth mechanisms of several 1D nanocrystals (plain nanorods and nanowires, core/shell nanorods, and nanotubes) are described as follows:

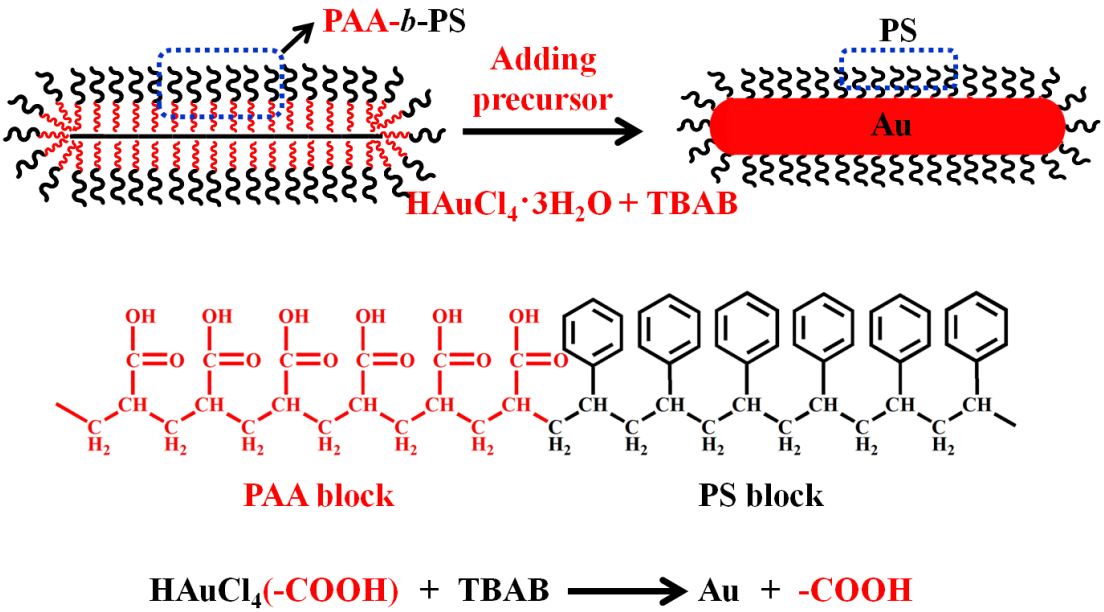

Figure S48. Formation of Au nanorods (or nanowires) using amphiphilic cylindrical cellulose-*g*-[PAA-*b*-PS] BBCP as a nanoreactor.

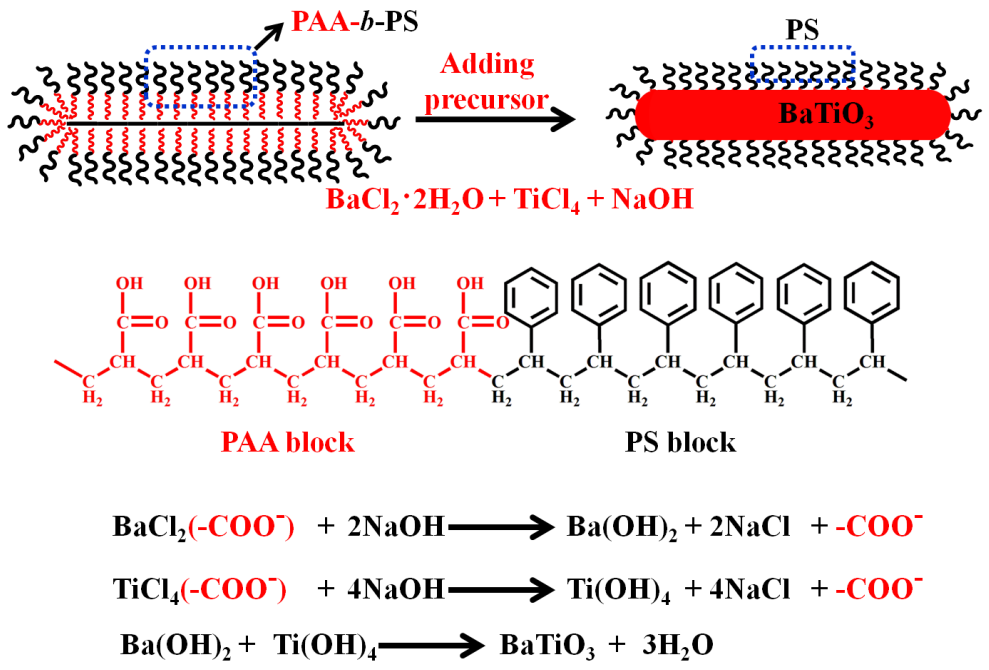

Figure S49. Formation of $BaTiO_3$ nanorods (or nanowires) using amphiphilic cylindrical cellulose-*g*-[PAA-*b*-PS] BBCP as a nanoreactor.

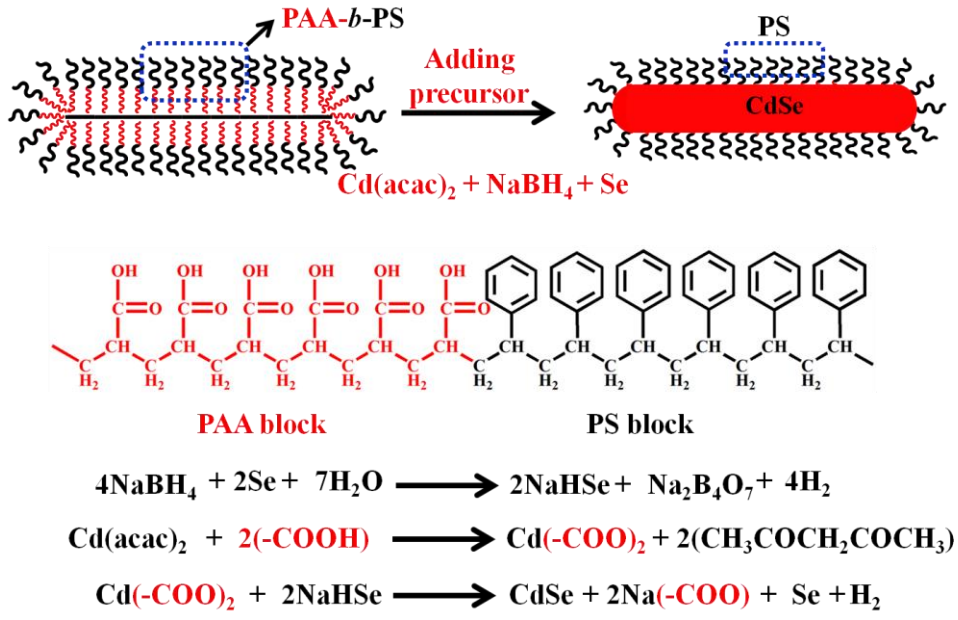

Figure S50. Formation of CdSe nanorods (or nanowires) using amphiphilic cylindrical cellulose-*g*-[PAA-*b*-PS] BBCP as a nanoreactor.

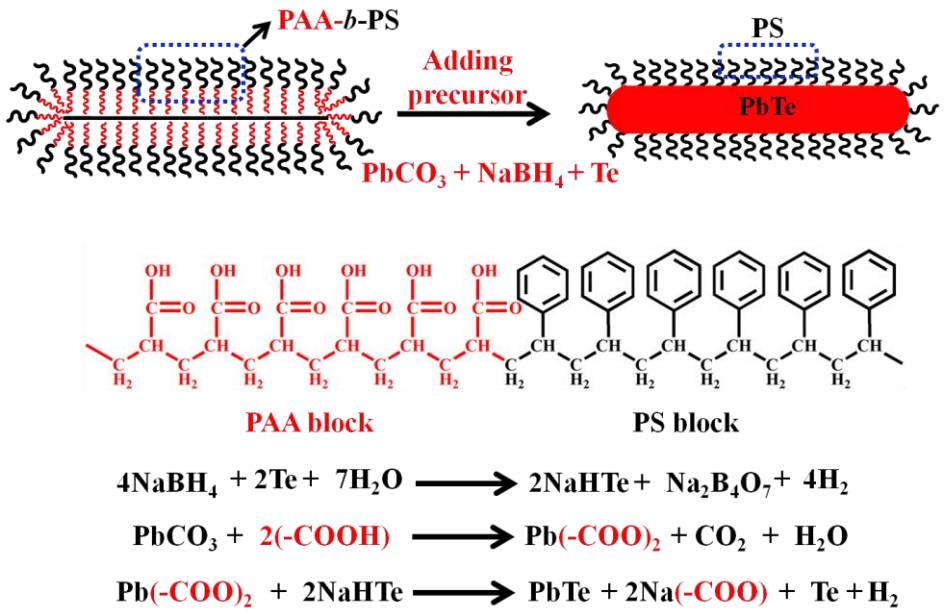

Figure S51. Formation of PbTe nanorods (or nanowires) using amphiphilic cylindrical cellulose-*g*-[PAA-*b*-PS] BBCP as a nanoreactor.

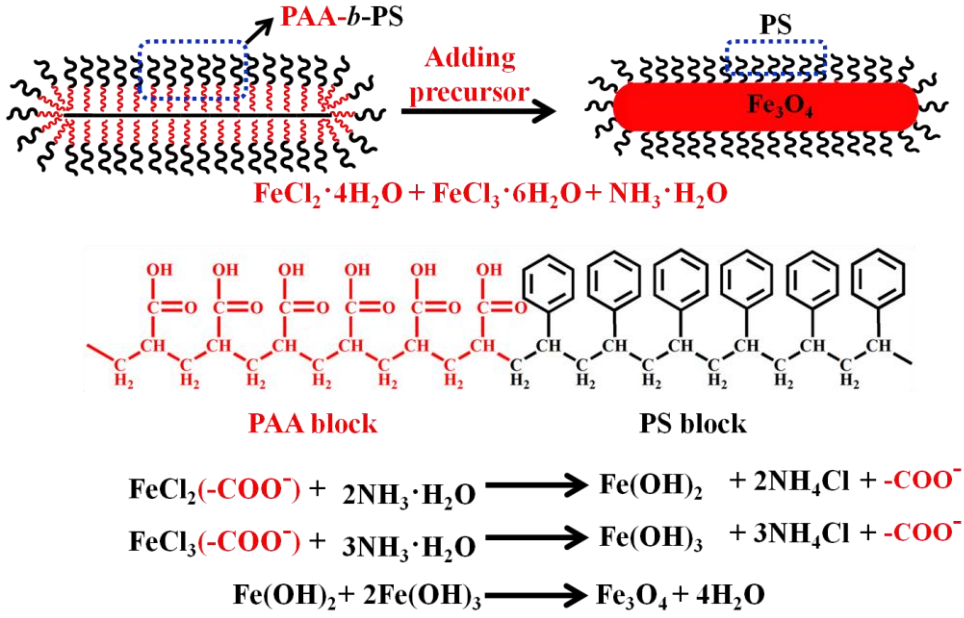

Figure S52. Formation of Fe_3O_4 nanorods (or nanowires) using amphiphilic cylindrical cellulose-*g*-[PAA-*b*-PS] BBCP as a nanoreactor.

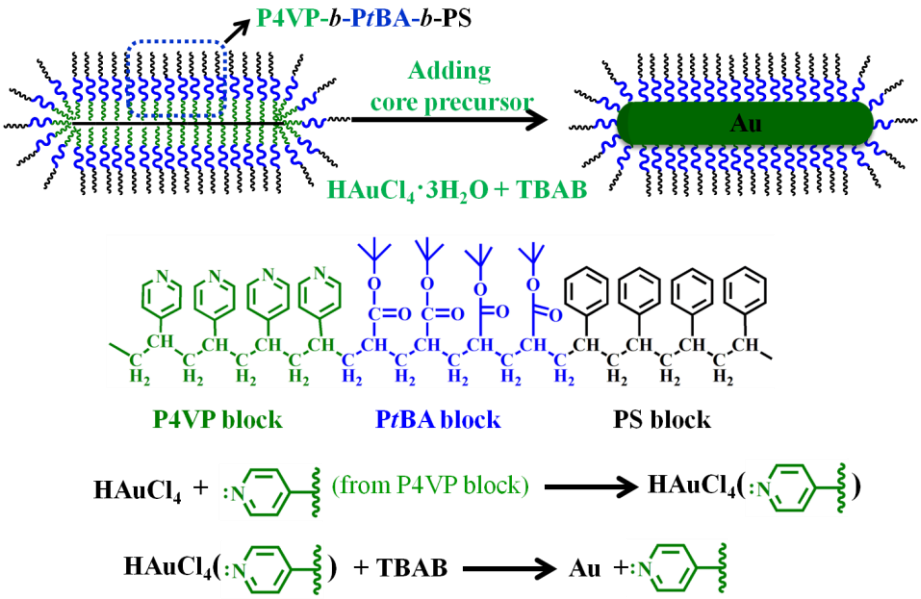

Figure S53. Formation of Au core nanorods using amphiphilic cylindrical cellulose-*g*-[P4VP-*b*-P*t*BA-*b*-PS] BBCP as a nanoreactor.

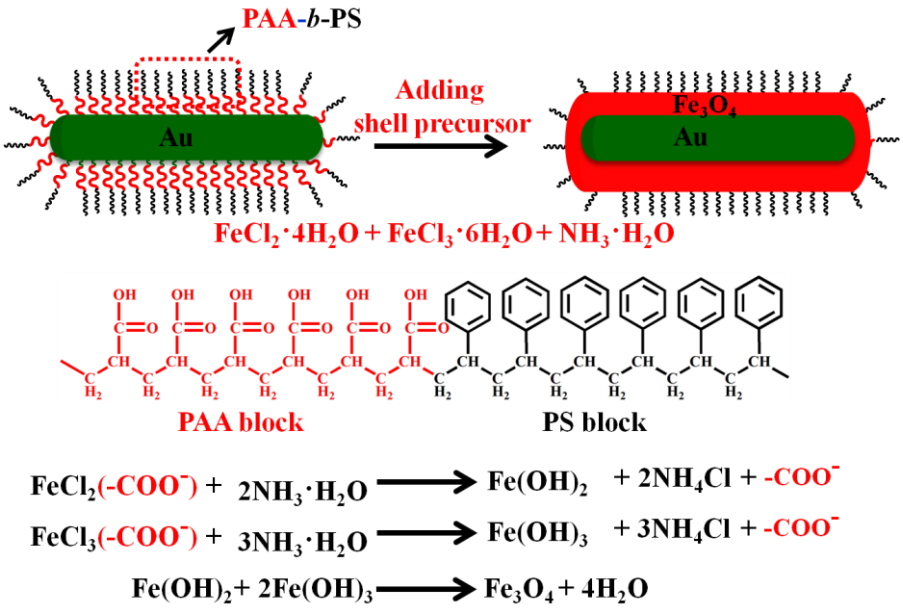

Figure S54. After the formation of Au core nanorods (see **Figure S53**), Au/Fe_3O_4 core/shell nanorods are created using amphiphilic cylindrical cellulose-*g*-[P4VP-*b*-PAA-*b*-PS] BBCP as a nanoreactor (more specifically, using cylindrical PAA-*b*-PS BBCP tethered on the surface of Au core nanorods as a nanoreactor)

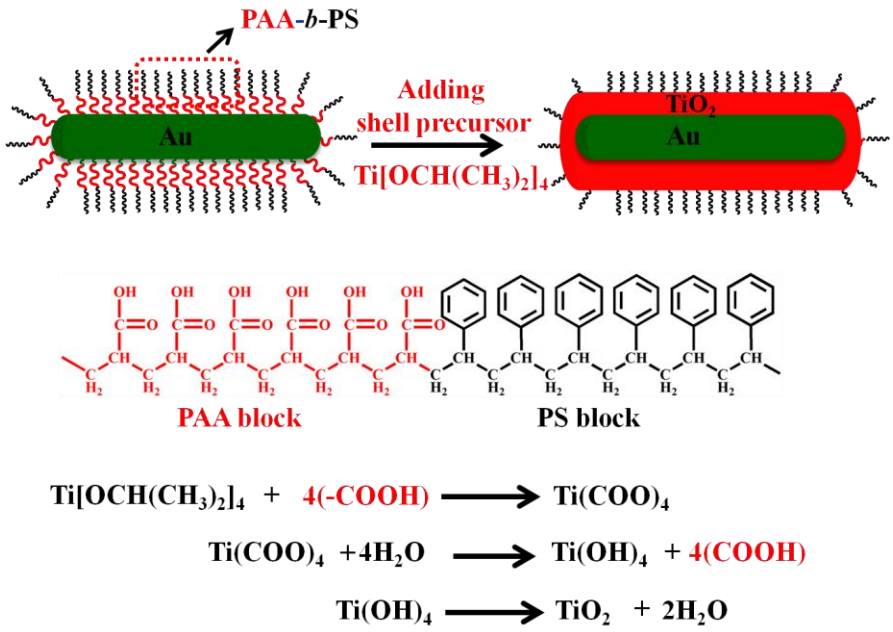

Figure S55. After the formation of Au core nanorods (see **Figure S53**), Au/TiO_2 core/shell nanorods are created using amphiphilic cylindrical cellulose-*g*-[P4VP-*b*-PAA-*b*-PS] BBCP as a nanoreactor (more specifically, using cylindrical PAA-*b*-PS BBCP tethered on the surface of Au nanorods as a nanoreactor)

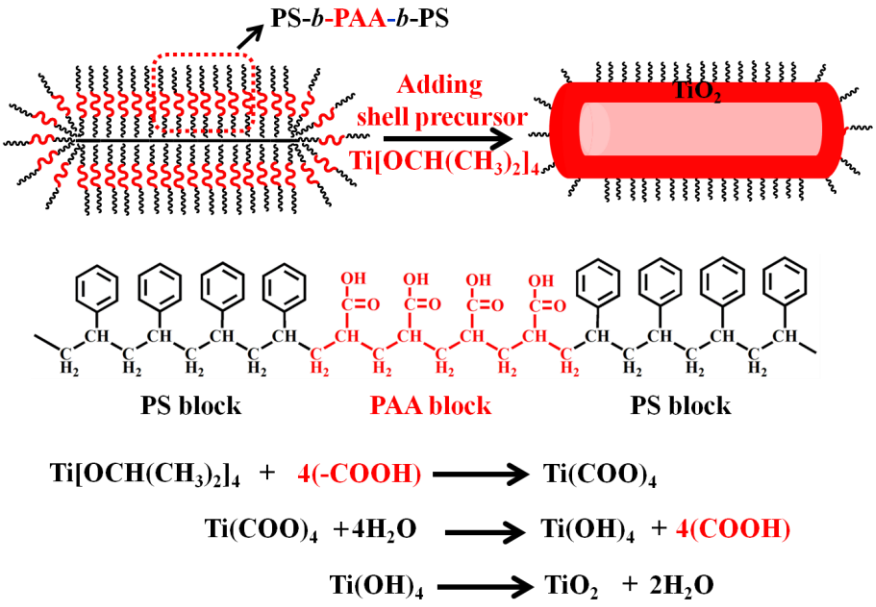

Figure S56. Formation of TiO_2 nanotubes using amphiphilic cylindrical cellulose-*g*-[PS-*b*-PAA-*b*-PS] BBCP as a nanoreactor.

Section VI

Characterization and determination of outer blocks (e.g., PS) that are tethered on the surface of 1D nanocrystals (e.g., PS-tethered upconversion $NaYF_4$:Yb/Er nanorods synthesized using cylindrical cellulose-*g*-[PAA-*b*-PS] BBCP as a nanoreactor)

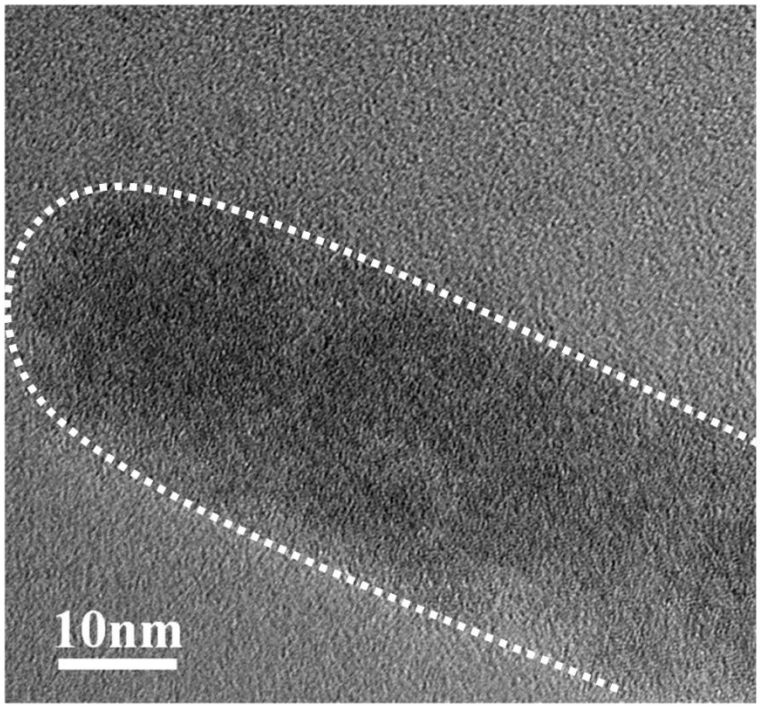

Figure S57. TEM image of cellulose-*g*-[PAA-*b*-PS] BBCP (i.e., Sample-2A in **Table S2**). Prior to TEM imaging, the cellulose-*g*-[PAA-*b*-PS] BBCP sample was completely stained with RuO_4 vapor. White dashed curve is for guidance.

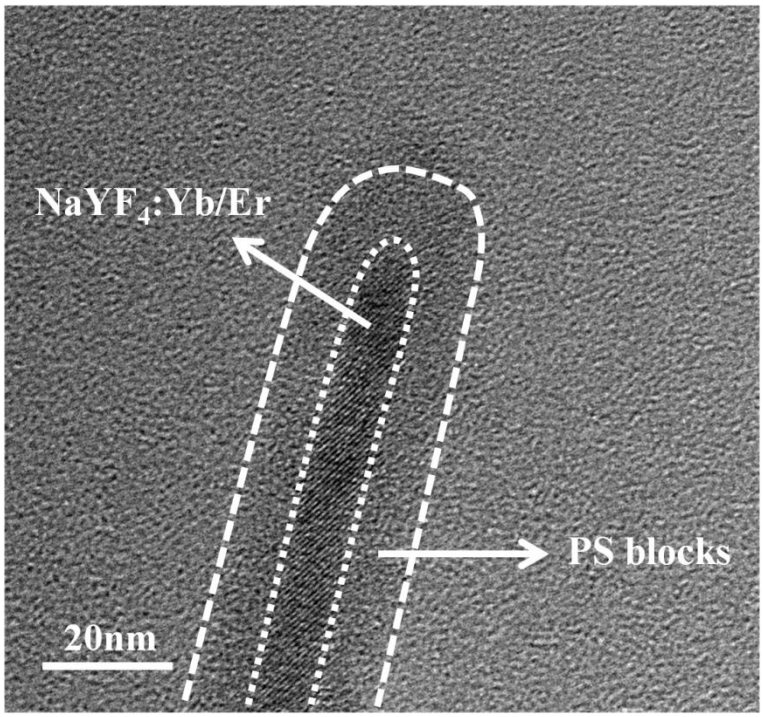

Figure S58. TEM image of upconversion $NaYF_4$:Yb/Er nanorods tethered with PS synthesized using cellulose-*g*-[PAA-*b*-PS] BBCP (i.e., Sample-2A in **Table S2**) as a nanoreactor. Prior to TEM imaging, the outer PS blocks in PS-tethered $NaYF_4$:Yb/Er nanorods were stained with RuO_4 vapor. White dashed curves are for guidance.

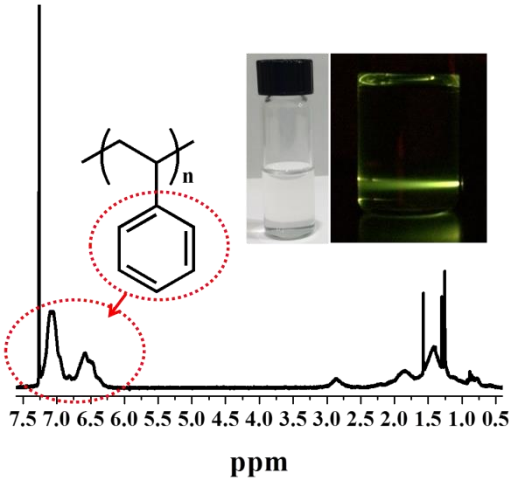

Figure S59. ^{1}H -NMR spectrum of upconversion $NaYF_4$:Yb/Er nanorods tethered with PS synthesized using cellulose-*g*-[PAA-*b*-PS] BBCP (i.e., Sample-2A in **Table S2**) as a nanoreactor (solvent: $CDCl_3$). Digital images of upconversion PS-tethered $NaYF_4$:Yb/Er nanorods $CDCl_3$ solution before (left) and after (right) exposure to a 2W 980-nm near-infrared laser are shown as insets.

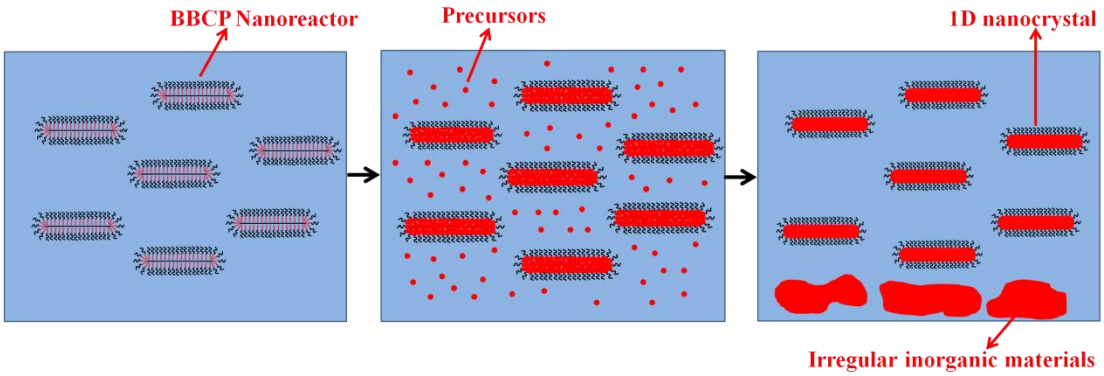

Figure S60. Purification process used in the BBCP nanoreactor strategy for the synthesis of 1D nanocrystals tethered with outer polymer chains (i.e., blocks; for example, PS as in the case of synthesis of plain nanorods using cellulose-*g*-[PAA-*b*-PS] BBCP as a nanoreactor) as ligands. As the surface of 1D nanocrystals is tethered with polymer chains, they can be well dissolved in certain solvents (e.g., PS for toluene, PEG for chloroform, etc.). In addition, the excess amount of precursors that are present outside the cylindrical BBCP nanoreactor can easily form irregular inorganic materials due to the lack of surface capping by polymer chains, and thus they readily precipitate from solution. Clearly, our nanoreactor strategy is very convenient and effective in producing relatively pure 1D nanocrystals.

Section VII

HRTEM images (showing clear crystalline lattices) and digital images of a large variety of plain nanorods synthesized by capitalizing on cylindrical cellulose-*g*-[PAA-*b*-PS] BBCP as a nanoreactor (Figure 1a and Figure S7)

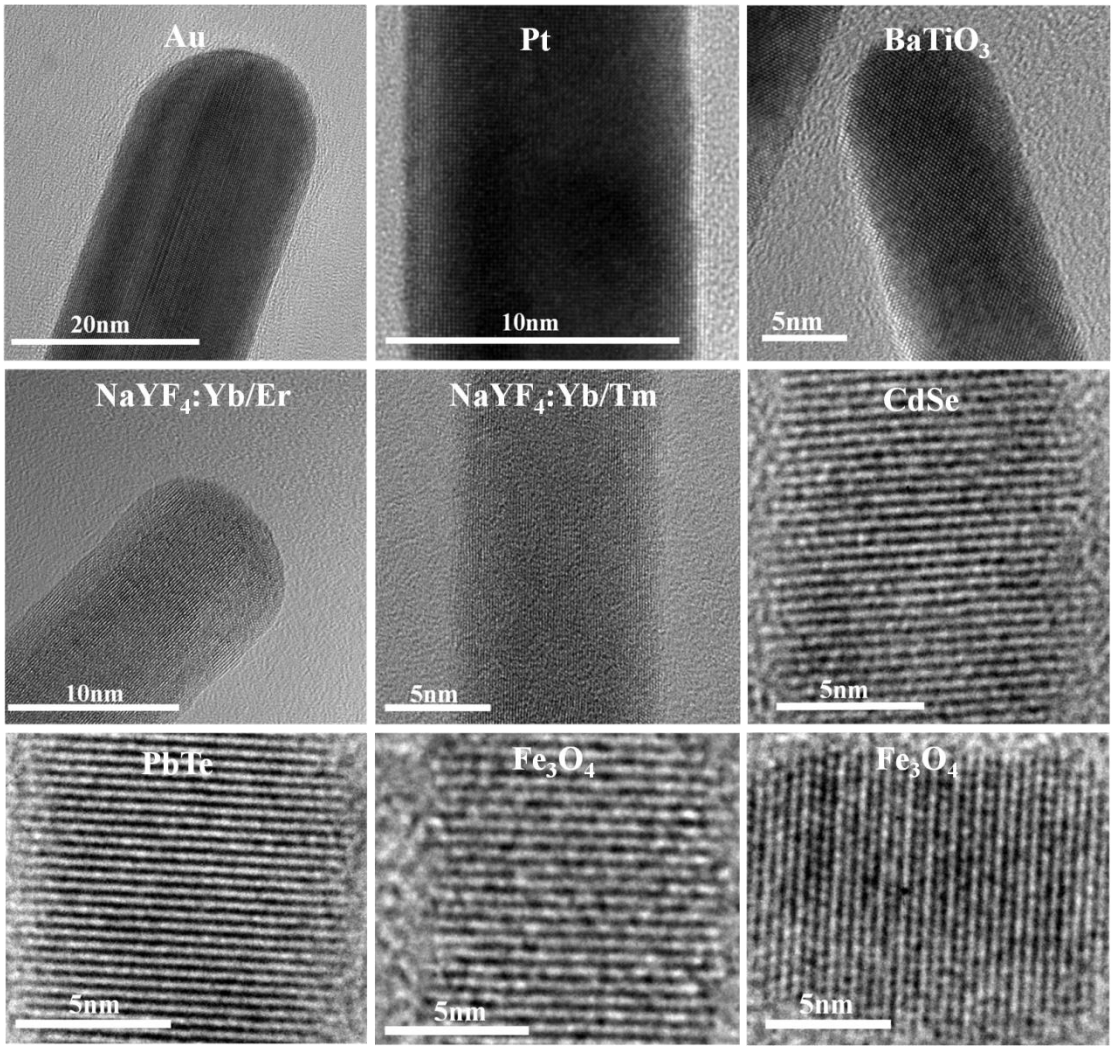

Figure S61. HRTEM images of a rich variety of plain nanorods and nanowires crafted by capitalizing on an amphiphilic cylindrical cellulose-*g*-[PAA-*b*-PS] BBCP nanoreactor (i.e., samples in **Table S2**).

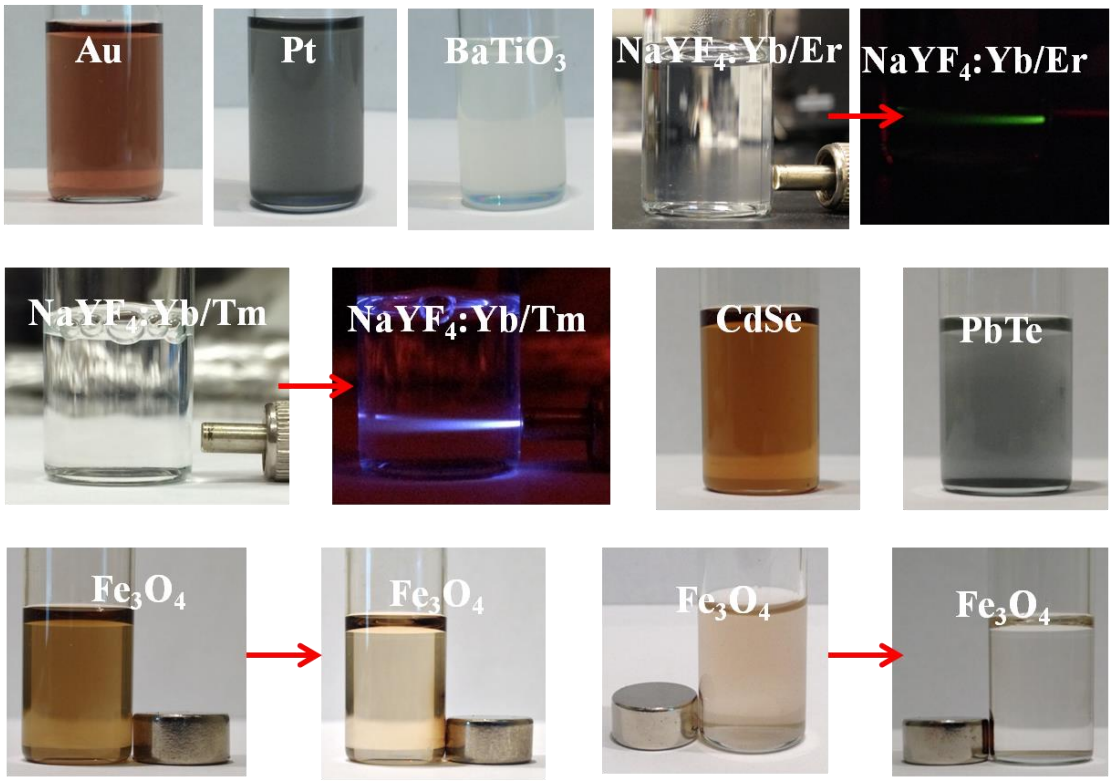

Figure S62. Digital images of a large variety of plain nanorods and nanowires dissolved in toluene. These plain nanorods and nanowires were synthesized using cylindrical cellulose-*g*-[PAA-*b*-PS] BBCP as a nanoreactor (i.e., samples in **Figure 3** and **Table S2**). Upconversion nanorods dissolved in toluene emitted green (for $NaYF_4$:Yb/Er nanorods) and blue ($NaYF_4$:Yb/Tm nanorods) fluorescence after (right) exposure to a 2W 980-nm near-infrared laser. Fe_3O_4 nanowires dissolved in toluene were deposited on the wall of vials (right) under the influence of a magnet placed next to the vial to demonstrate their magnetic properties.

Section VIII

Thermogravimetric analysis (TGA) measurements on 1D nanocrystals

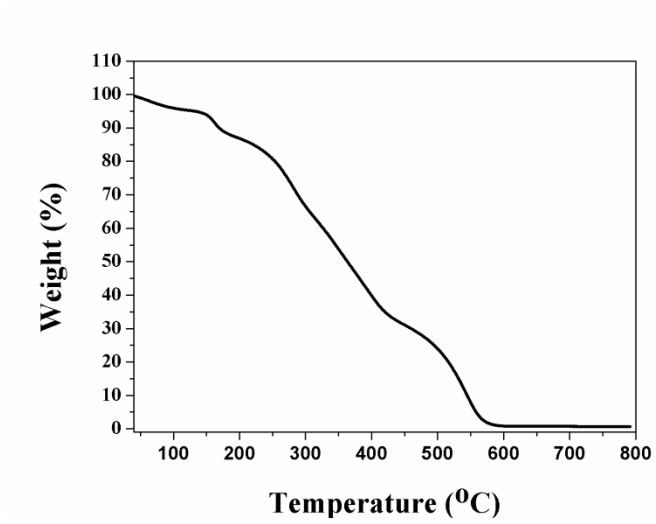

Figure S63. TGA curve of cellulose-*g*-[PAA-*b*-PS] BBCP nanoreactor in air (Sample-2A in **Table S2**).

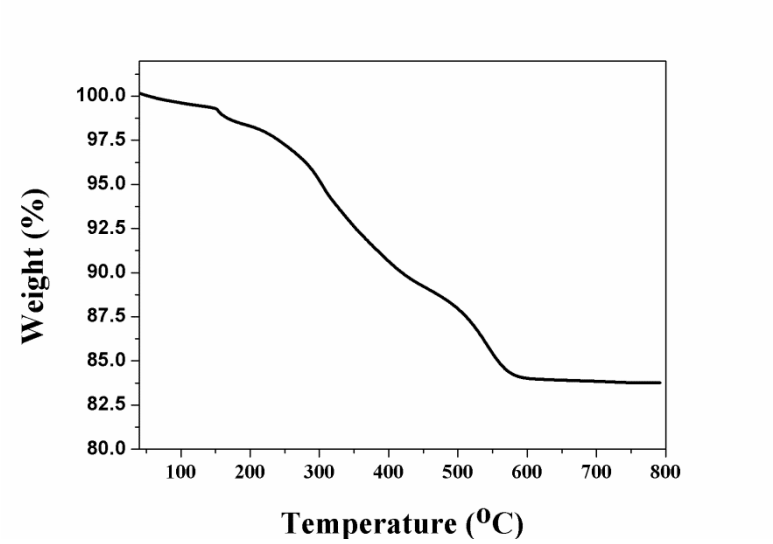

Figure S64. TGA curve of plain $NaYF_4$:Yb/Er nanorods in air. They were synthesized using cellulose-*g*-[PAA-*b*-PS] BBCP as a nanoreactor (Sample-2A in **Table S2**).

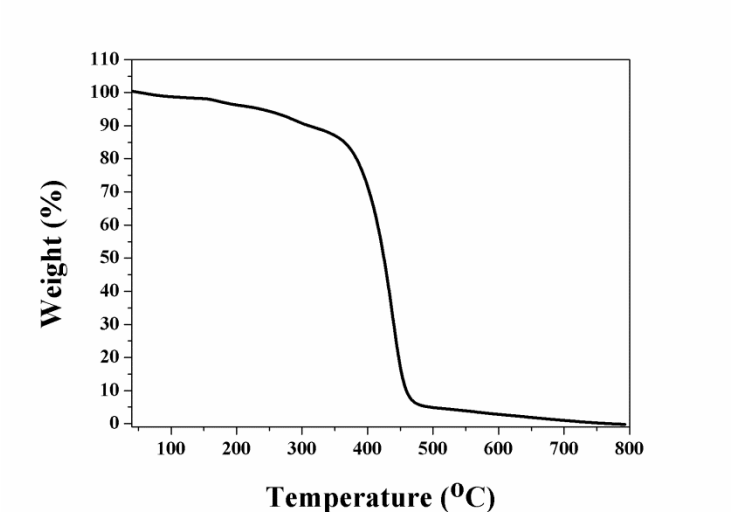

Figure S65. TGA curve of cellulose-*g*-[P4VP-*b*-P*t*BA-*b*-PS] BBCP nanoreactor in N_2 (Sample-3A in **Table S4**).

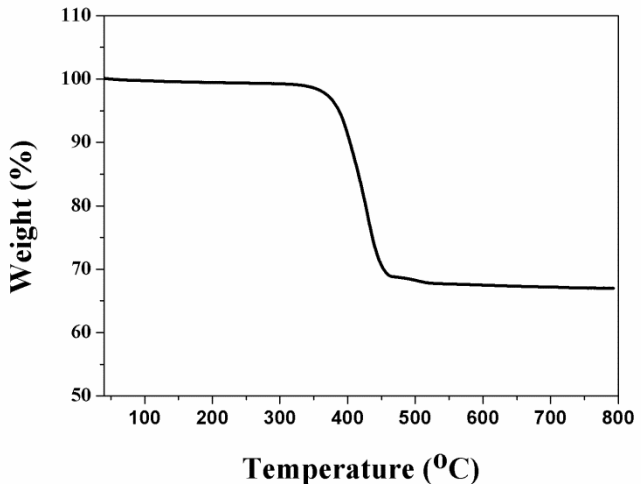

Figure S66. TGA curve of Fe_3O_4 core nanorods in N_2. They were synthesized using cellulose-*g*-[P4VP-*b*-P*t*BA-*b*-PS] BBCP as a nanoreactor (Sample-3A in **Table S4**).

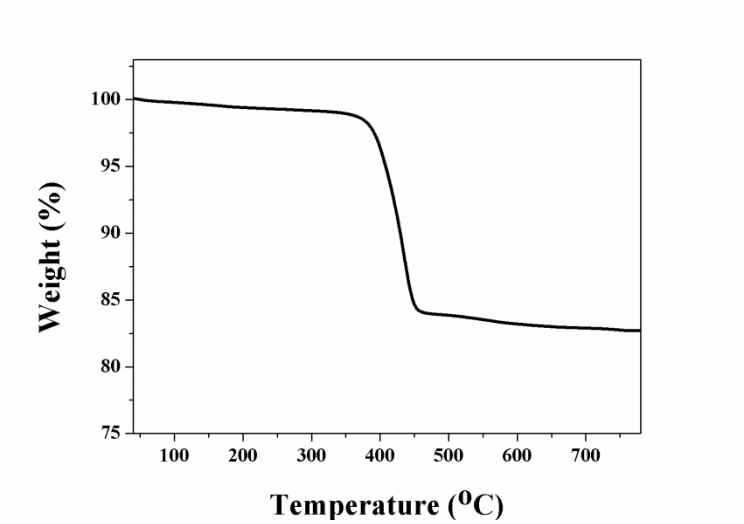

Figure S67. TGA curve of Fe_3O_4/Au core/shell nanorods in N_2. They were synthesized using cellulose-*g*-[P4VP-*b*-PAA-*b*-PS] BBCP as a nanoreactor (Sample-3A in **Table S4**). More specifically, they are produced by using cylindrical PAA-*b*-PS BBCP tethered on the surface of Fe_3O_4 core nanorods as a nanoreactor (**Figure S66**).

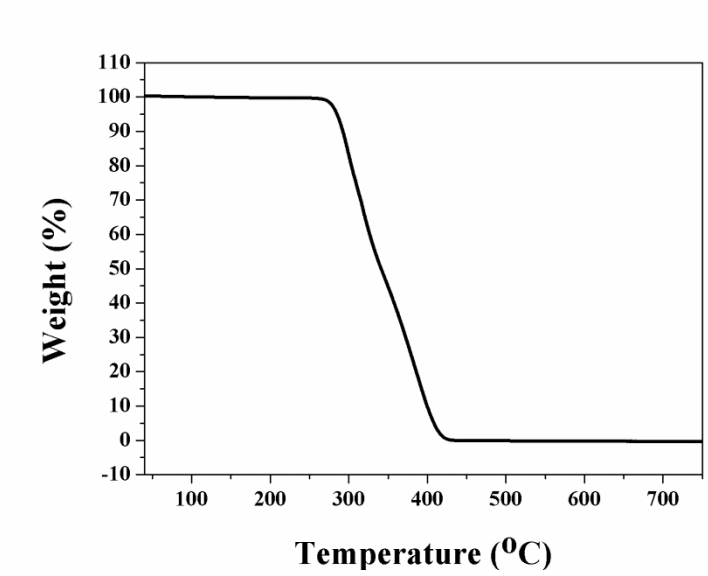

Figure S68. TGA curve of cellulose-*g*-[PS-*b*-PAA-*b*-PS] BBCP nanoreactor in air (Sample-3A in **Table S6**).

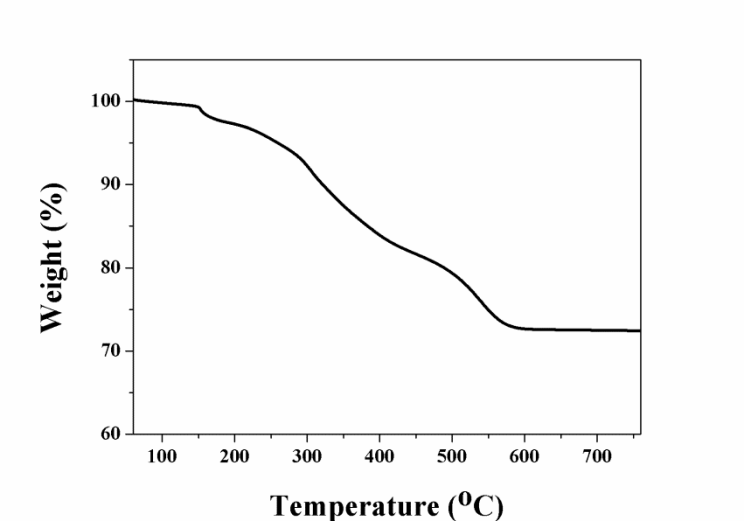

Figure S69. TGA curve of $NaYF_4$:Yb/Er nanotubes in air. They were synthesized using cellulose-*g*-[PS-*b*-PAA-*b*-PS] BBCP as a nanoreactor (Sample-3A in **Table S6**).

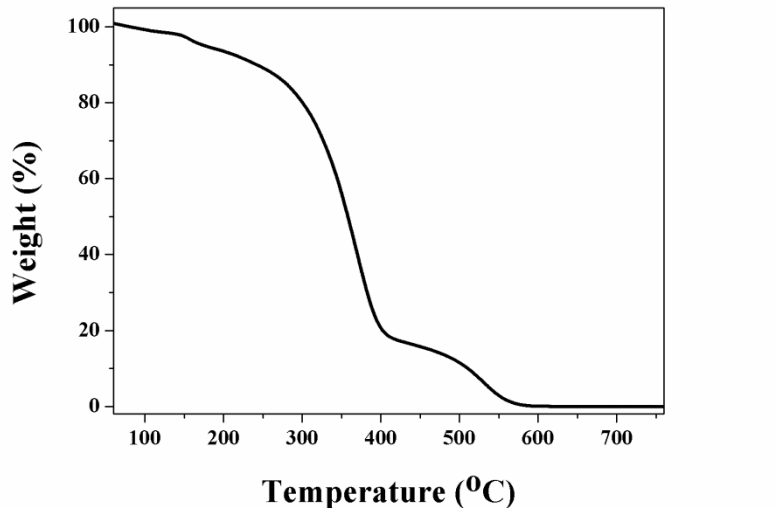

Figure S70. TGA curve of cellulose-*g*-[PAA-*b*-PEG] BBCP nanoreactor in air (Sample-2A in **Table S3**).

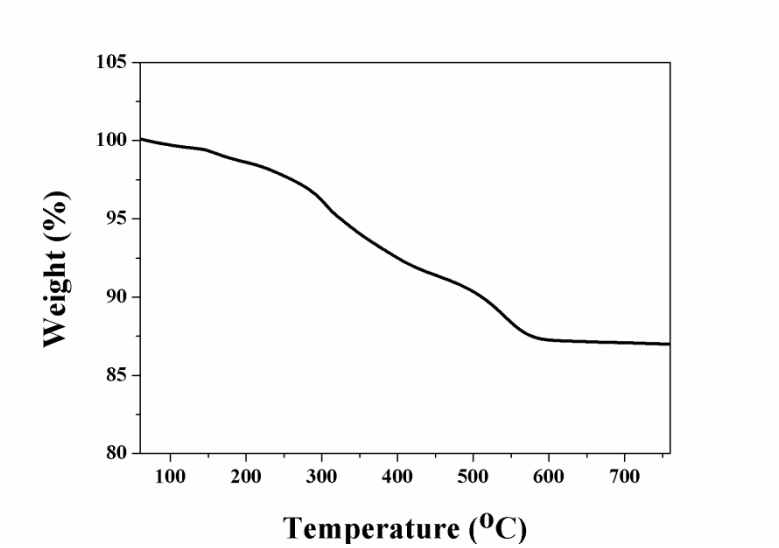

Figure S71. TGA curve of plain $NaYF_4$:Yb/Er nanorods in air. They were synthesized using cellulose-*g*-[PAA-*b*-PEG] BBCP as a nanoreactor (Sample-2A in **Table S3**).

Section IX

UV-vis absorption spectra of Au nanorods with different dimensions; UV-vis absorption and photoluminescence (PL) spectra of CdSe nanorods; Photoluminescence (PL) spectra of upconversion nanorods

1. UV-vis absorption spectra of Au nanorods with different dimensions

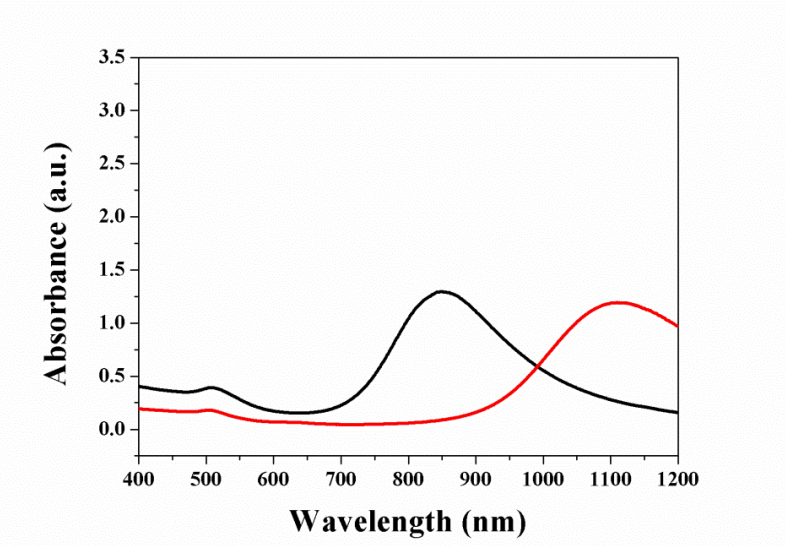

Figure S72. UV-vis absorption spectra of plain PS-tethered Au nanorods with different dimensions dissolved in toluene. They were synthesized using cellulose-*g*-[PAA-*b*-PS] BBCP as a nanoreactor (black: Sample-1A in **Table S2** (i.e., *D*=10.4±0.6 nm, *L*=51±4 nm); red: Sample-2A in **Table S2** (i.e., *D*=10.4±0.6nm, *L*= 98±8nm)). Clearly, they exhibited two absorption maxima: ~505 nm and ~854 nm (black), ~505 nm and ~1118 nm, corresponding to the transverse and longitudinal plasmonic modes, respectively.[17]

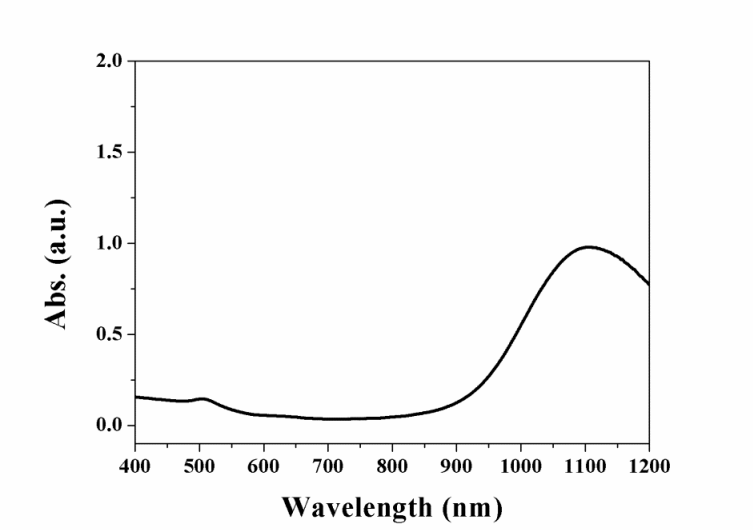

Figure S73. UV-vis absorption spectrum of PEG-tethered Au nanorods dissolved in water. They were synthesized using cellulose-*g*-[PAA-*b*-PEG] BBCP as a nanoreactor (Sample-2A in **Table S3** (*D*=10.5±0.5nm, *L*=97±11 nm)). The spectrum shows two absorption maxima at ~505 nm and ~1106 nm, corresponding to the transverse and longitudinal plasmonic modes, respectively.

2. **UV-vis absorption and photoluminescence (PL) spectra of CdSe nanorods.**

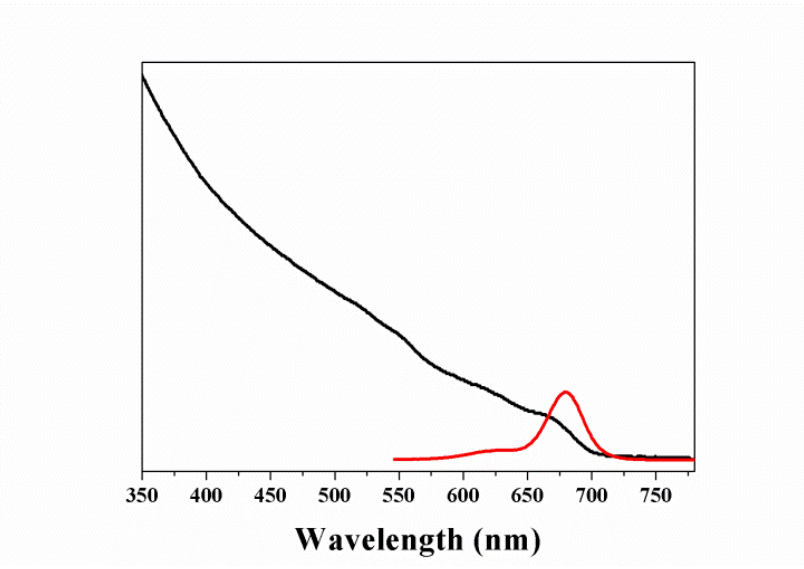

Figure S74. UV-vis absorption (black curve) and photoluminescence (PL; red curve) spectra of plain PS-tethered CdSe nanorods dissolved in toluene. They were synthesized using cellulose-*g*-[PAA-*b*-PS] BBCP as a nanoreactor (Sample-2A in **Table S2** (*D*=10.1±0.7 nm, *L*=98±9 nm)).

3. Photoluminescence (PL) spectra of upconversion nanorods.

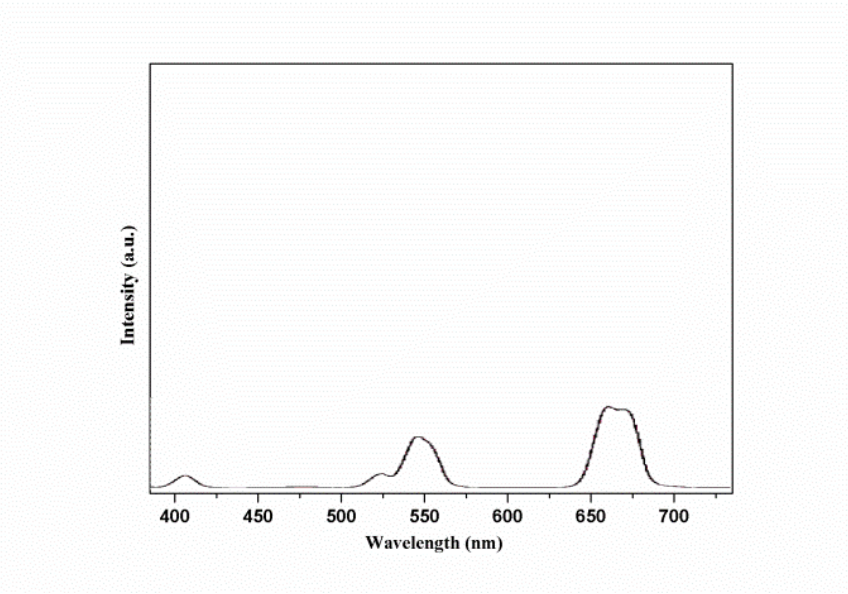

Figure S75. Emission spectrum of plain PS-capped upconversion $NaYF_4$:Yb/Er (18%/2%) nanorods dissolved in toluene. The solution was excited with a 2W 980-nm near-infrared laser. They were synthesized using cellulose-*g*-[PAA-*b*-PS] BBCP as a nanoreactor (Sample-2A in **Table S2** (*D*=9.6±0.4nm, *L*=99±10 nm)).

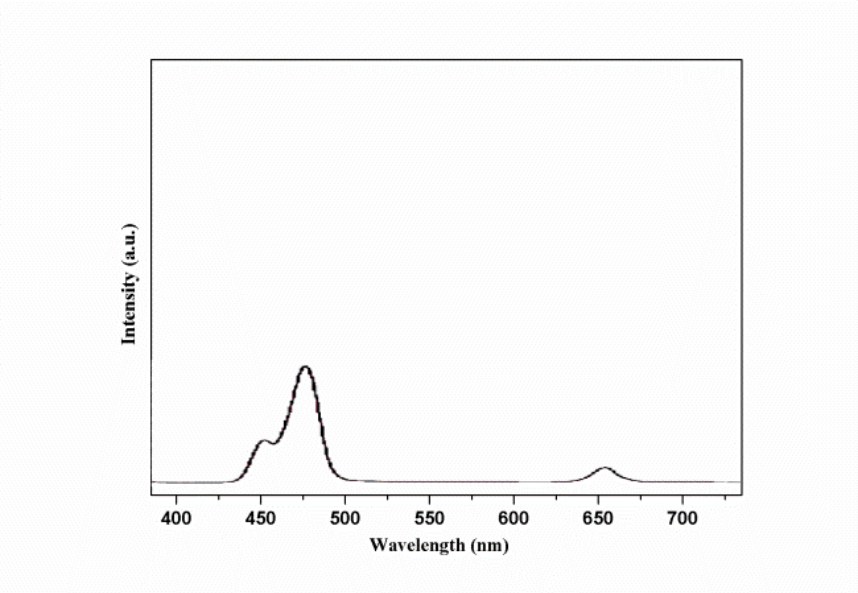

Figure S76. Emission spectrum of plain PS-capped upconversion $NaYF_4$:Yb/Tm (30%/0.5%) nanorods dissolved in toluene. The solution was excited with a 2W 980-nm near-infrared laser. They were synthesized using cellulose-*g*-[PAA-*b*-PS] BBCP as a nanoreactor (Sample-2A in **Table S2** (*D*=10.4±0.5 nm, *L*=103±7 nm)).

Section X

X-ray diffraction (XRD) and energy dispersive spectroscopy (EDS) characterizations of 1D nanocrystals produced using cylindrical BBCPs as nanoreactors

The EDS and XRD measurements further confirmed the compositions and crystal structures of 1D nanocrystals synthesized using the BBCP nanoreactor strategy. The standard spectra for these 1D nanocrystals are as follows: Au (JCPDS 04-0784), Pt (JCPDS 65-2868), hexagonal $NaYF_4$:Yb/Er and $NaYF_4$:Yb/Tm (JCPDS 16-0334), tetragonal BaTiO3 (JCPDS 74-1960), Wurtzite CdSe (JCPDS 77-2307), cubic PbTe (ICDD 08-0028), Fe3O4(JCPDS 76-1849), and anatase TiO2 (JCPDS 21-1272).

XRD measurements

1. Plain nanorods and nanowires

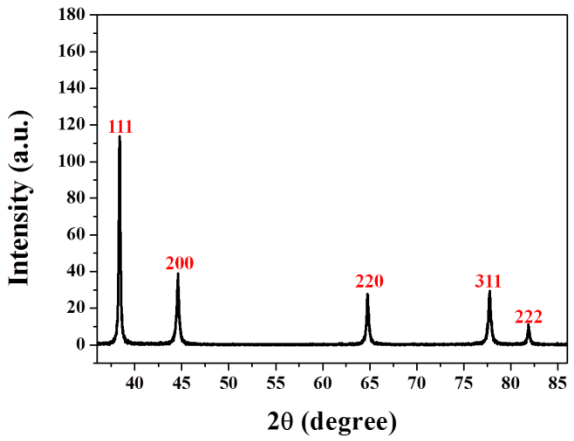

Figure S77. XRD pattern of plain Au nanorods tethered with PS synthesized using cellulose-*g*-[PAA-*b*-PS] BBCP as a nanoreactor (Sample-3B in **Table S2**).

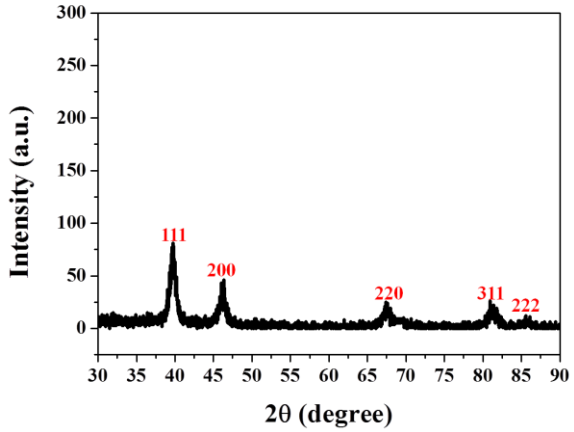

Figure S78. XRD pattern of plain Pt nanorods tethered with PS synthesized using cellulose-*g*-[PAA-*b*-PS] BBCP as a nanoreactor (Sample-1A in **Table S2**).

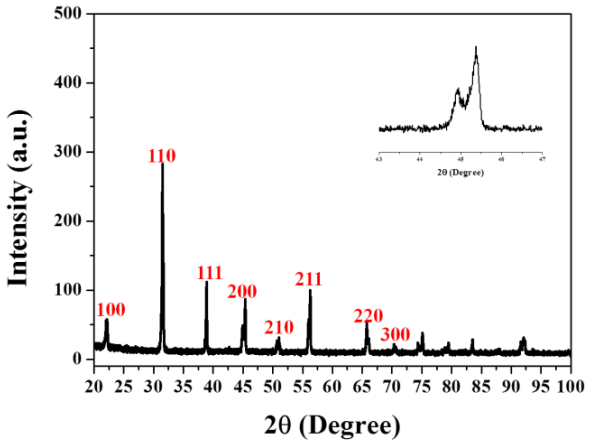

Figure S79. XRD pattern of plain $BaTiO_3$ nanorods tethered with PS synthesized using cellulose-*g*-[PAA-*b*-PS] BBCP as a nanoreactor (Sample-2A in **Table S2**).The (200) peak was split into two peaks, suggesting the formation of a tetragonal phase of $BaTiO_3$ nanorods.

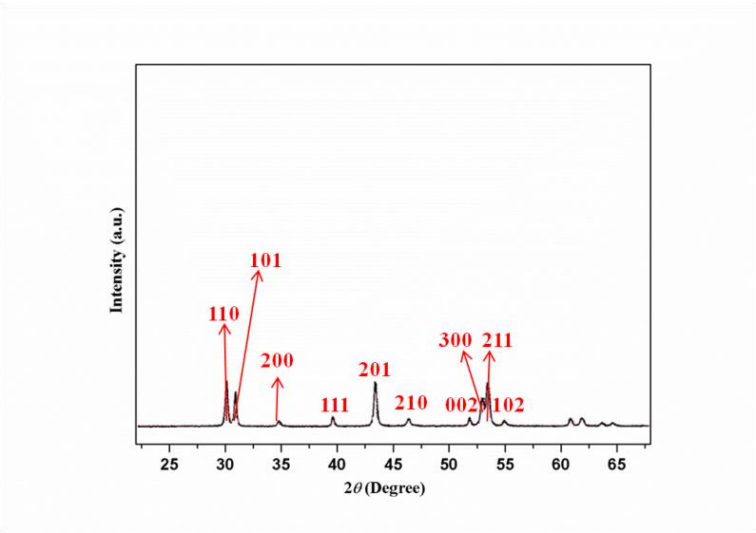

Figure S80. XRD pattern of plain $NaYF_4$:Yb/Er nanorods tethered with PS synthesized using cellulose-*g*-[PAA-*b*-PS] BBCP as a nanoreactor (Sample-2A in **Table S2**).

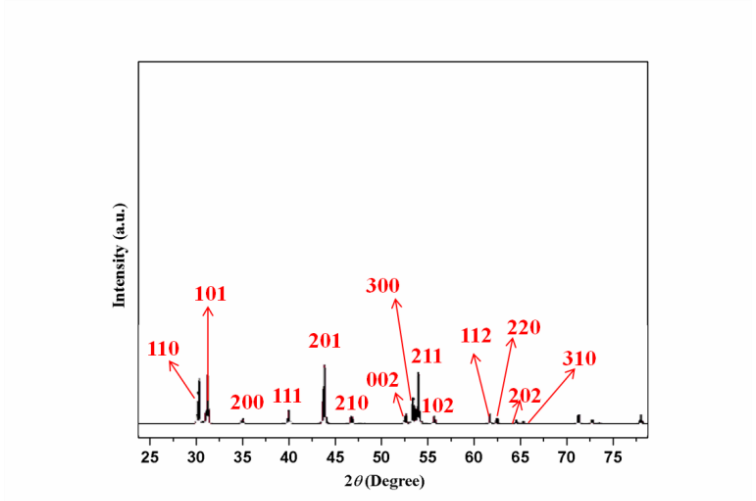

Figure S81. XRD pattern of plain $NaYF_4$:Yb/Tm nanorods tethered with PS synthesized using cellulose-*g*-[PAA-*b*-PS] BBCP as a nanoreactor (Sample-2A in **Table S2**).

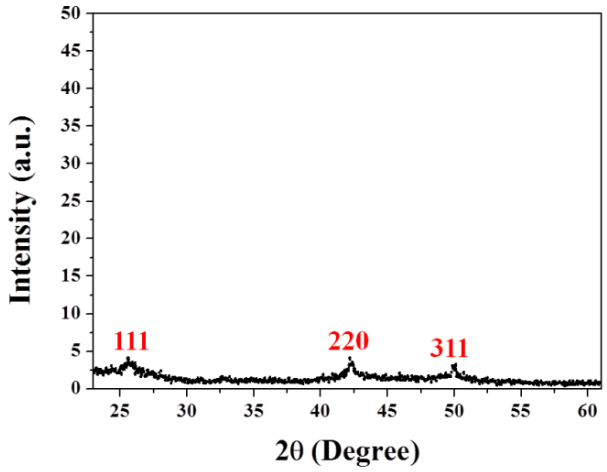

Figure S82. XRD pattern of plain CdSe nanorods tethered with PS synthesized using cellulose-*g*-[PAA-*b*-PS] BBCP as a nanoreactor (Sample-2A in **Table S2**).

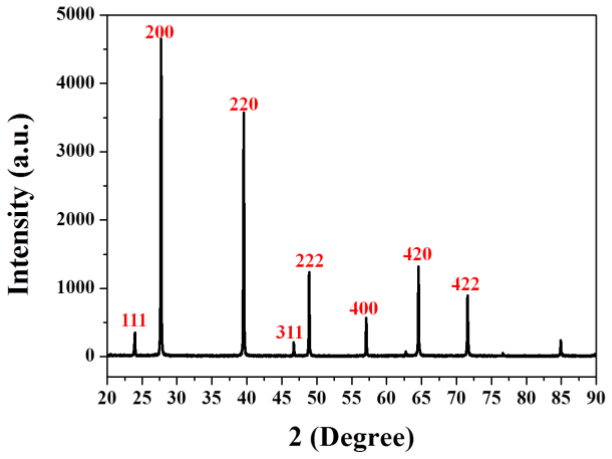

Figure S83. XRD pattern of plain PbTe nanorods tethered with PS synthesized using cellulose-*g*-[PAA-*b*-PS] BBCP as a nanoreactor (Sample-2A in **Table S2**).

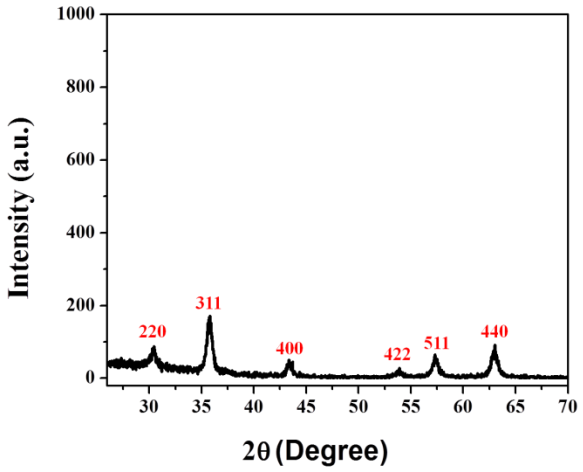

Figure S84. XRD pattern of plain Fe_3O_4 nanowires tethered with PS synthesized using cellulose-*g*-[PAA-*b*-PS] BBCP as a nanoreactor (Sample-3A in **Table S2**).

2. Core/shell nanorods

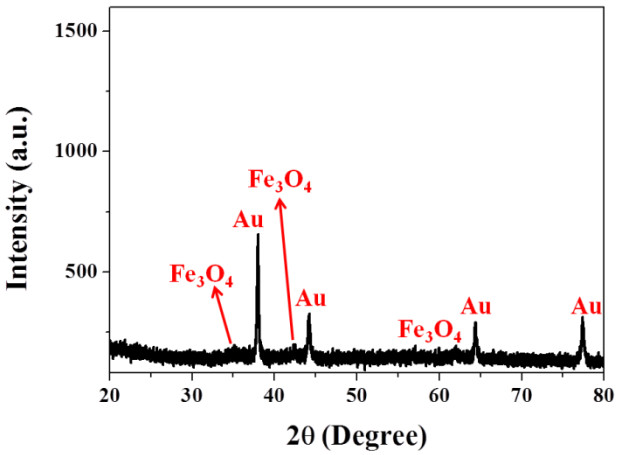

Figure S85. XRD pattern of Au/Fe_3O_4 core/shell nanorods tethered with PS synthesized using cellulose-*g*-[P4VP-*b*-P*t*BA-*b*-PS] BBCP as a nanoreactor (Sample-2B in **Table S4**).

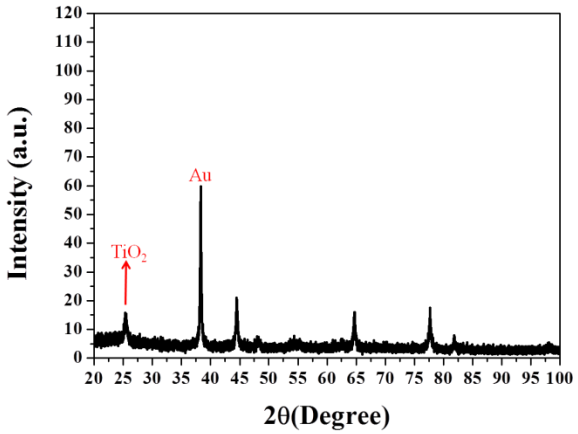

Figure S86. XRD pattern of Au/TiO_2 core/shell nanorods tethered with PS synthesized using cellulose-*g*-[P4VP-*b*-P*t*BA-*b*-PS] BBCP as a nanoreactor (Sample-2B in **Table S4**).

3. Nanotubes

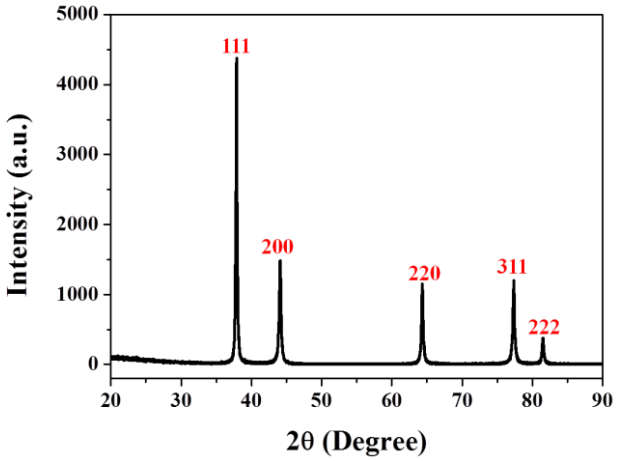

Figure S87. XRD pattern of Au nanotubes tethered with PS synthesized using cellulose-*g*-[PS-*b*-PAA-*b*-PS] BBCP as a nanoreactor (Sample-2A in **Table S6**).

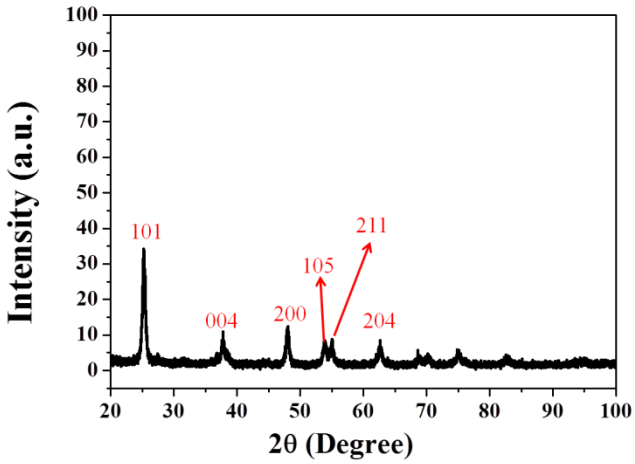

Figure S88. XRD pattern of TiO_2 nanotubes tethered with PS synthesized using cellulose-*g*-[PS-*b*-PAA-*b*-PS] BBCP as a nanoreactor (Sample-2A in **Table S6**).

EDS measurements

1. Plain nanorods and nanowires

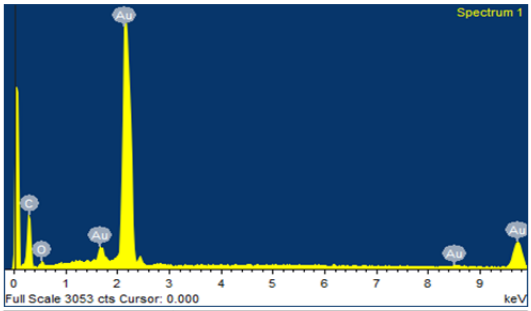

Element	Weight%	Atomic%
C K	30.52	83.90
O K	2.35	4.85
Au M	67.14	11.26
Totals	100.00	

Figure S89. EDS spectrum of plain Au nanorods tethered with PS synthesized using cellulose-*g*-[PAA-*b*-PS] BBCP as a nanoreactor (Sample-3B in **Table S2**).

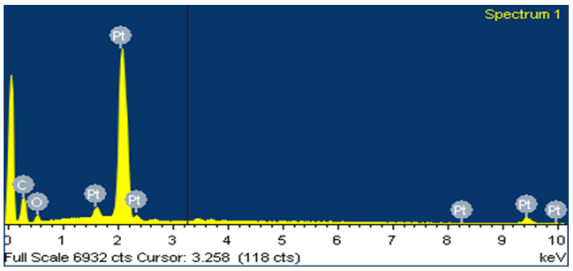

Element	Weight%	Atomic%
C K	19.29	71.28
O K	4.07	11.29
Pt M	76.63	17.43
Totals	100.00	

Figure S90. EDS spectrum of plain Pt nanorods tethered with PS synthesized using cellulose-*g*-[PAA-*b*-PS] BBCP as a nanoreactor (Sample-1A in **Table S2**).

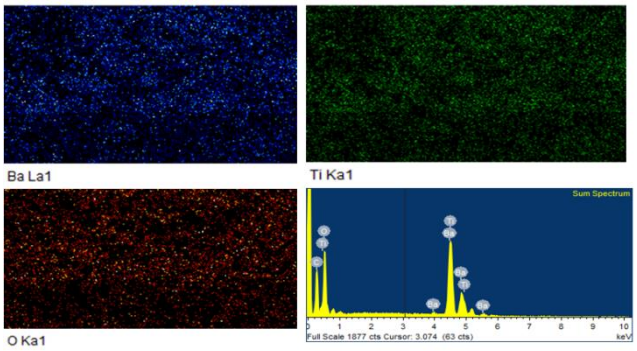

Element	Weight%	Atomic%
C K	16.17	36.29
O K	23.87	42.43
Ti K	17.76	10.54
Ba L	42.20	10.74
Totals	100.00	

Figure S91. EDS spectrum of plain $BaTiO_3$ nanorods tethered with PS synthesized using cellulose-*g*-[PAA-*b*-PS] BBCP as a nanoreactor (Sample-2A in **Table S2**).

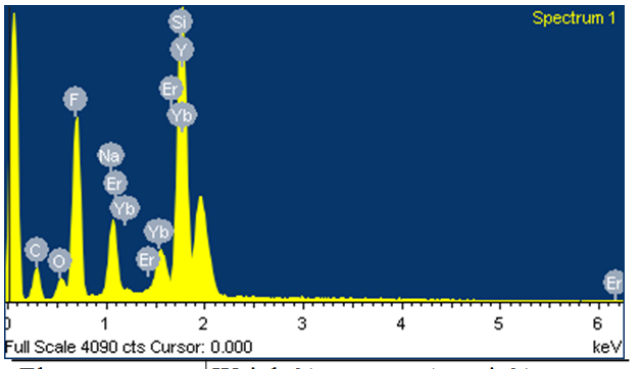

Element	Weight%	Atomic%
C K	16.75	32.05
O K	4.11	5.90
F K	**31.01**	**37.52**
Na K	**5.00**	**5.00**
Si K	16.90	13.83
Y L	**17.62**	**4.56**
Er L	**0.75**	**0.10**
Yb L	**7.87**	**1.04**
Totals	100.00	

Figure S92. EDS spectrum of plain $NaYF_4$:Yb/Er nanorods tethered with PS synthesized using cellulose-*g*-[PAA-*b*-PS] BBCP as a nanoreactor (Sample-2A in **Table S2**).

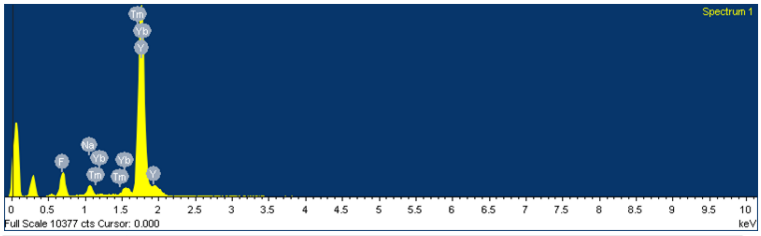

Element	App Conc.	Intensity Corrn.	Weight%	Weight% Sigma	Atomic%
F K	32.87	0.7499	50.70	1.55	76.46
Na K	10.67	1.0765	11.46	0.49	14.28
Y L	11.68	0.7068	19.11	1.27	6.16
Tm L	0.42	0.8059	0.61	1.50	0.10
Yb L	12.45	0.7952	18.11	1.69	3.00
Totals			100.00		

Figure S93. EDS spectrum of plain $NaYF_4$:Yb/Tm nanorods tethered with PS synthesized using cellulose-*g*-[PAA-*b*-PS] BBCP as a nanoreactor (Sample-2A in **Table S2**).

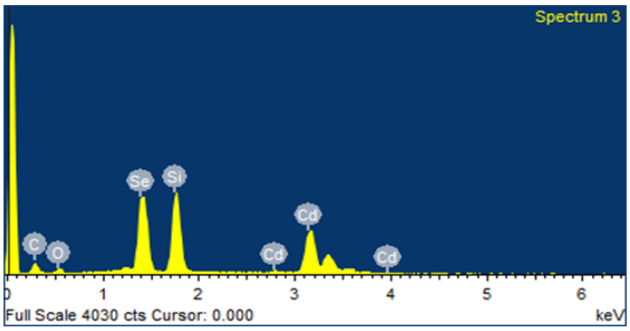

Element	Weight%	Atomic%
C K	13.76	41.07
O K	5.66	12.68
Si K	17.87	22.80
Se L	25.59	11.62
Cd L	37.11	11.83
Totals	100.00	

Figure S94. EDS spectrum of plain CdSe nanorods tethered with PS synthesized using cellulose-*g*-[PAA-*b*-PS] BBCP as a nanoreactor (Sample-2A in **Table S2**).

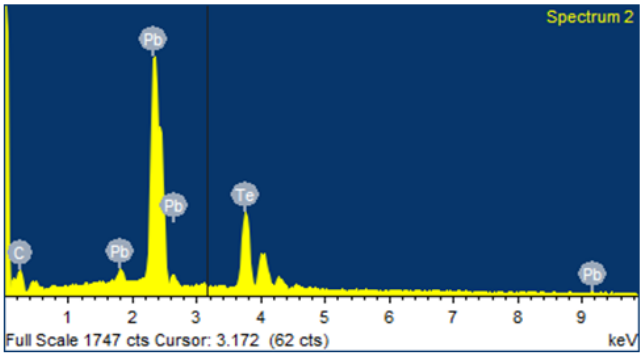

Element	Weight%	Atomic%
C K	5.22	43.35
Te L	**36.69**	**28.68**
Pb M	**58.09**	**27.96**
Totals	100.00	

Figure S95. EDS spectrum of plain PbTe nanorods tethered with PS synthesized using cellulose-*g*-[PAA-*b*-PS] BBCP as a nanoreactor (Sample-2A in **Table S2**).

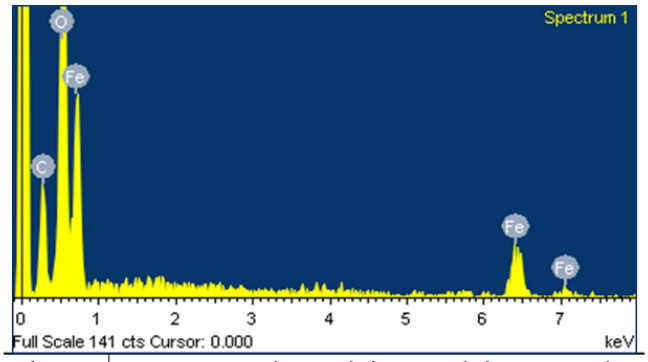

Element	App Conc.	Intensity Corrn.	Weight %	Weight % Sigma	Atomic %
C K	14.55	1.0015	11.35	1.43	25.13
O K	74.88	2.1239	27.55	2.27	45.78
Fe K	68.28	0.8730	61.10	3.05	29.09
Totals			100.00		

Figure S96. EDS spectrum of plain Fe_3O_4 nanorods tethered with PS synthesized using cellulose-*g*-[PAA-*b*-PS] BBCP as a nanoreactor (Sample-3A in **Table S2**).

2. Core/shell nanorods

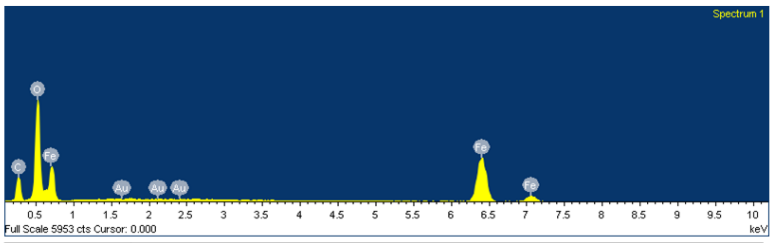

Element	App Conc.	Intensity Corrn.	Weight%	Weight% Sigma	Atomic%
C K	0.75	0.7043	16.02	0.47	32.05
O K	2.92	1.4745	29.70	0.55	44.63
Fe L	1.95	0.5392	54.15	0.78	13.31
Au M	0.01	0.7056	0.13	0.25	10.02
Totals			100.00		

Figure S97. EDS spectrum of Au/Fe_3O_4 core/shell nanorods tethered with PS synthesized using cellulose-*g*-[P4VP-*b*-P*t*BA-*b*-PS] BBCP as a nanoreactor (Sample-2B in **Table S4**).

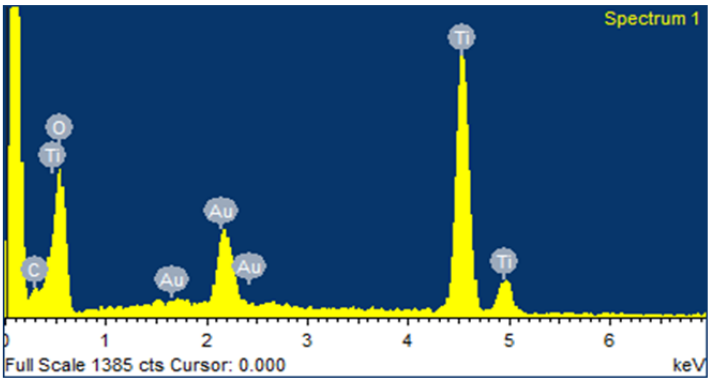

Element	App Conc.	Intensity Corrn.	Weight%	Weight% Sigma	Atomic %
C K	32.11	2.0110	4.92	0.99	18.15
O K	172.38	2.5681	20.70	0.92	57.28
Ti K	45.54	1.2508	11.23	0.42	10.38
Au M	160.75	0.7850	63.15	1.44	14.19
Totals			100.00		

Figure S98. EDS spectrum of Au/TiO_2 core/shell nanorods tethered with PS synthesized using cellulose-*g*-[P4VP-*b*-P*t*BA-*b*-PS] BBCP as nanoreactor (Sample-2B in **Table S4**).

3. Nanotubes

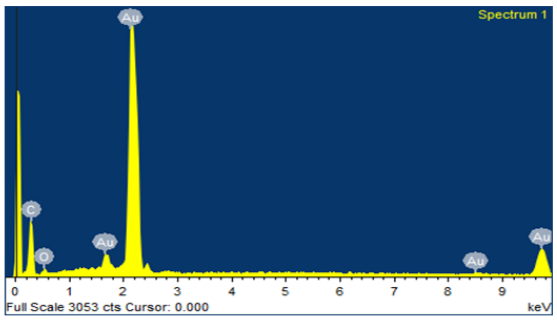

Element	Weight%	Atomic%
C K	30.52	83.90
O K	2.35	4.85
Au M	67.14	11.26
Totals	100.00	

Figure S99. EDS spectrum of Au nanotubes tethered with PS synthesized using cellulose-*g*-[PS-*b*-PAA-*b*-PS] BBCP as a nanoreactor (Sample-2A in **Table S6**).

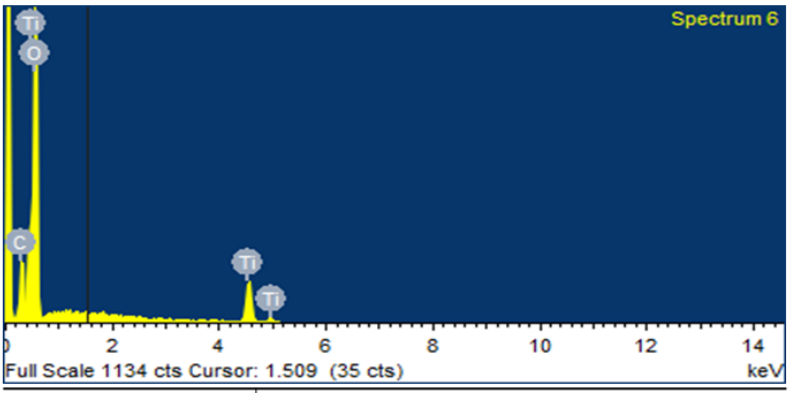

Element	Weight%	Atomic%
C K	8.24	12.86
O K	65.61	76.90
Ti K	26.15	10.24
Totals	100.00	

Figure S100. EDS spectrum of TiO_2 nanotubes tethered with PS synthesized using cellulose-*g*-[PS-*b*-PAA-*b*-PS] BBCP as a nanoreactor (Sample-2A in **Table S6**).

Section XI

Comparison of cylindrical BBCPs and the corresponding linear block copolymers employed as nanoreactors for synthesis of 1D nanostructures

To compare the use of cylindrical BBCPs and the corresponding linear block copolymers as nanoreactors for synthesis of 1D nanocrystals, linear block copolymers, PAA-*b*-PS, P4VP-*b*-P*t*BA-*b*-PS and PS-*b*-PAA-*b*-PS, with similar molecular weights and ratios of different blocks to those of cylindrical BBCPs composed of identical block copolymers as side chains (i.e., arms; they are PAA-*b*-PS, P4VP-*b*-P*t*BA-*b*-PS and PS-*b*-PAA-*b*-PS) were also synthesized by sequential ATRP. Similarly, these linear block copolymers were employed as nanoreactors to synthesize nanocrystals under the same experimental conditions as cylindrical BBCP templates. Au and PbTe materials were taken as examples using linear PAA-*b*-PS as a nanoreactor, Au material was taken as an example utilizing linear P4VP*b*-P*t*BA-*b*-PS as a nanoreactor, and Au material was taken as an example employing linear PS-*b*-PAA-*b*-PS as a nanoreactor, respectively.

1. Synthesis of linear PAA-*b*-PS diblock copolymer for preparation of Au and PbTe materials

Table S8. Summary of linear PAA-*b*-PS diblock copolymer

Sample	$M_{n,\ PAA}$ (g/mol)	$M_{n,PS}$ (g/mol)	PDI
Sample-A	5.6K	6.3K	1.14

Number-average molecular weight, M_n, of each block in linear PAA-*b*-PS diblock copolymer was calculated based on ^{1}H-NMR data. PDI was determined by GPC. This linear PAA-*b*-PS diblock copolymer possessed similar molecular weights and ratios of PAA to PS to those of PAA-*b*-PS arms in cellulose-*g*-[PAA-*b*-PS] BBCP (Sample-2A in **Table S2**) prepared by sequential ATRP.

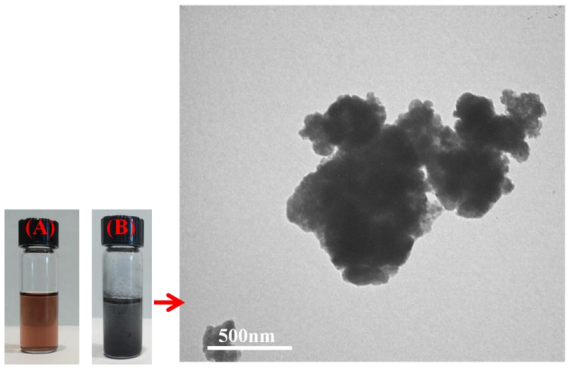

Figure S101. Comparison of cylindrical cellulose-*g*-[PAA-*b*-PS] BBCP and the corresponding linear PAA-*b*-PS diblock copolymer used as nanoreactors, respectively, for synthesis of Au materials. (A) Digital image of original solution of plain Au nanorods synthesized using cellulose-*g*-[PAA-*b*-PS] BBCP as nanoreactor. (B) Digital image of original solution of Au materials prepared by employing linear PAA-*b*-PS diblock copolymer as template; right: TEM image of Au materials synthesized by utilizing linear PAA-*b*-PS diblock copolymer as template.

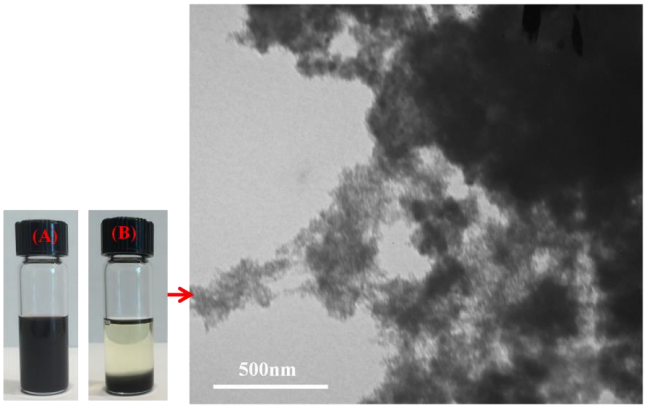

Figure S102. Comparison of cylindrical cellulose-*g*-[PAA-*b*-PS] BBCP and the corresponding linear PAA-*b*-PS diblock copolymer used as nanoreactors, respectively, for synthesis of PbTe materials. (A) Digital image of original solution of plain PbTe nanorods synthesized using cellulose-*g*-[PAA-*b*-PS] BBCP as a nanoreactor. (B) Digital image of original solution of PbTe materials prepared by employing linear PAA-*b*-PS diblock copolymer as template; right: TEM image of PbTe materials synthesized by utilizing linear PAA-*b*-PS diblock copolymer as a template.

We note that when cylindrical cellulose-*g*-[PAA-*b*-PS] BBCP was exploited as a nanoreactor, the original solutions of plain Au and PbTe nanorods were homogeneous and stable. In sharp contrast, when the corresponding linear PAA-*b*-PS diblock copolymer was employed as a template, the precipitates quickly appeared. Based on TEM images of these precipitates, only large irregular structures were obtained, and no uniform plain nanorods were produced.

2. Synthesis of linear P4VP-*b*-P*t*BA-*b*-PS triblock copolymer for preparation of Au materials

Table S9. Summary of linear P4VP-*b*-P*t*BA-*b*-PS triblock copolymer

Sample	$M_{n,\ P4VP}$ (g/mole)	$M_{n,\ PtBA}$ (g/mol)	$M_{n,\ PS}$ (g/mol)	PDI
Sample-A	7.5K	11.3K	13.8K	1.15

The number-average molecular weight, M_n, of each block in the linear P4VP-*b*-P*t*BA-*b*-PS triblock copolymer was calculated based on ^{1}H-NMR data. PDI was determined by GPC. This linear P4VP-*b*-P*t*BA-*b*-PS triblock copolymer possessed similar molecular weights and ratios of different blocks (P4VP, P*t*BA and PS) to those of the P4VP-*b*-P*t*BA-*b*-PS arms in cellulose-*g*-[P4VP-*b*-P*t*BA-*b*-PS] BBCP (Sample-2B in **Table S4**) prepared by sequential ATRP.

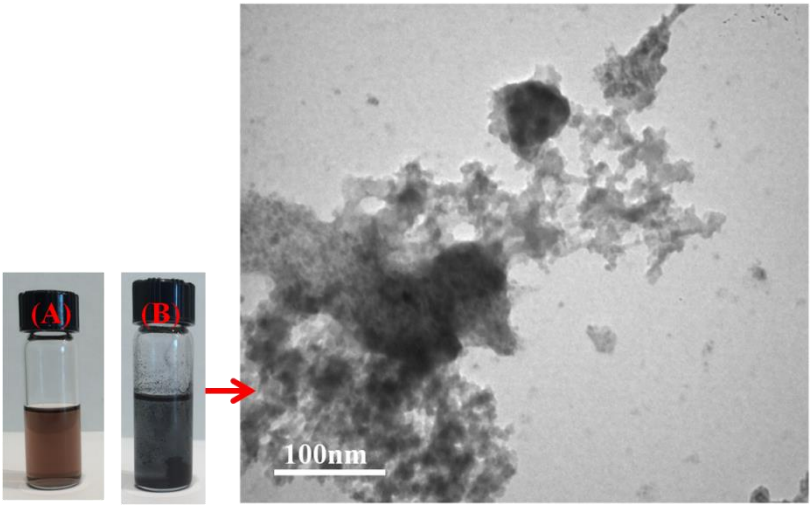

Figure S103. Comparison of cylindrical cellulose-*g*-[P4VP-*b*-P*t*BA-*b*-PS] BBCP and the corresponding linear P4VP-*b*-P*t*BA-*b*-PS triblock copolymer used as nanoreactors, respectively, for synthesis of Au materials. (A) Digital image of original solution of plain Au core nanorods synthesized using cellulose-*g*-[P4VP-*b*-P*t*BA-*b*-PS] BBCP as a nanoreactor. (B) Digital image of original solution of Au materials prepared by employing linear P4VP-*b*-P*t*BA-*b*-PS triblock copolymer as a template; right: TEM image of Au materials synthesized by utilizing linear P4VP-*b*-P*t*BA-*b*-PS triblock copolymer as a template.

Similarly, when cylindrical cellulose-*g*-[P4VP-*b*-P*t*BA-*b*-PS] BBCP was used as a nanoreactor, the original solutions of Au core nanorods were homogeneous and stable. In stark contrast, when the corresponding linear P4VP-*b*-P*t*BA-*b*-PS triblock copolymer was employed as a template, precipitates appeared. On the basis of TEM images, only large irregular structures were achieved, and no uniform nanorods were produced.

3. Synthesis of linear PS-*b*-PAA-*b*-PS triblock copolymer for preparation of Au materials

Table S10. Summary of linear PS-*b*-PAA-*b*-PS triblock copolymer

Sample	$M_{n,\ PS}$ (g/mole)	$M_{n,\ PAA}$ (g/mole)	$M_{n,\ PS}$ (g/mole)	PDI
Sample-A	4.5K	6.3K	8.5K	1.18

The number-average molecular weight, M_n, of each block in linear PS-*b*-PAA-*b*-PS triblock copolymer was calculated based on ^{1}H-NMR data. PDI was determined by GPC. This linear PS-*b*-PAA-*b*-PS triblock copolymer possessed similar molecular weights and ratios of different blocks (PS, PAA and PS) to those of PS-*b*-PAA-*b*-PS brushes in cellulose-*g*-[PS-*b*-PAA-*b*-PS] BBCP (Sample-2A in **Table S6**) prepared by sequential ATRP.

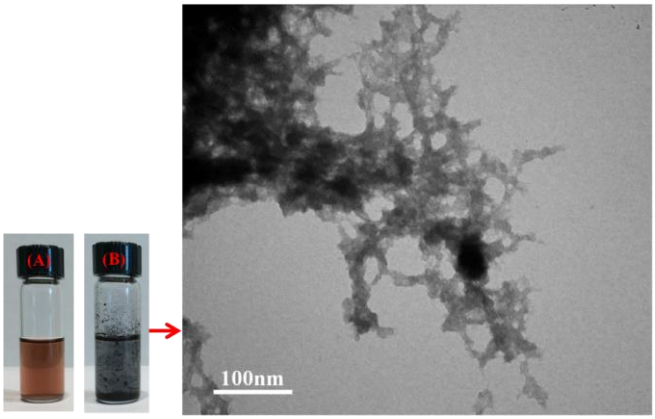

Figure S104. Comparison of cylindrical cellulose-*g*-[PS-*b*-PAA-*b*-PS] BBCP and the corresponding linear PS-*b*-PAA-*b*-PS triblock copolymer used as nanoreactors, respectively, for the synthesis of Au materials. (A) Digital image of original solution of Au nanotubes synthesized capitalizing on cellulose-*g*-[PS-*b*-PAA-*b*-PS] BBCP as nanoreactor. (B) Digital image of original solution of Au materials prepared by using linear PS-*b*-PAA-*b*-PS triblock copolymer as a template; right: TEM image of Au materials synthesized by utilizing linear PS-*b*-PAA-*b*-PS triblock copolymer as a template.

It is not surprising that same as described above for cylindrical cellulose-*g*-[P4VP-*b*-P*t*BA-*b*-PS] and cellulose-*g*-[PAA-*b*-PS] BBCPs, when cylindrical cellulose-*g*-[PS-*b*-PAA-*b*-PS] BBCP was capitalized on as nanoreactor, the original solutions of Au nanotubes were homogeneous and stable. However, when the corresponding linear PS-*b*-PAA-*b*-PS triblock copolymer was used as a template, precipitates appeared. Only large irregular structures were obtained based on the TEM images and no uniform nanotubes were produced.

4. Comparison of the formation mechanisms of nanocrystals by utilizing cylindrical BBCP nanoreactors and their corresponding linear block copolymers

It is clear that when the linear block copolymers were chosen for the synthesis of inorganic materials, as DMF is a good solvent for all blocks in linear block copolymers (i.e., PS, P*t*BA, PAA and P4VP), instead of forming micelles, these linear block copolymers are fully dissolved individually. As a result, upon the addition of precursors of inorganic materials into the DMF solution of linear block copolymers, the precursors simply react themselves as there is no compartment composed of hydrophilic blocks for them to coordinate within. This leads to the formation of irregular precipitates (**Figure S105**).

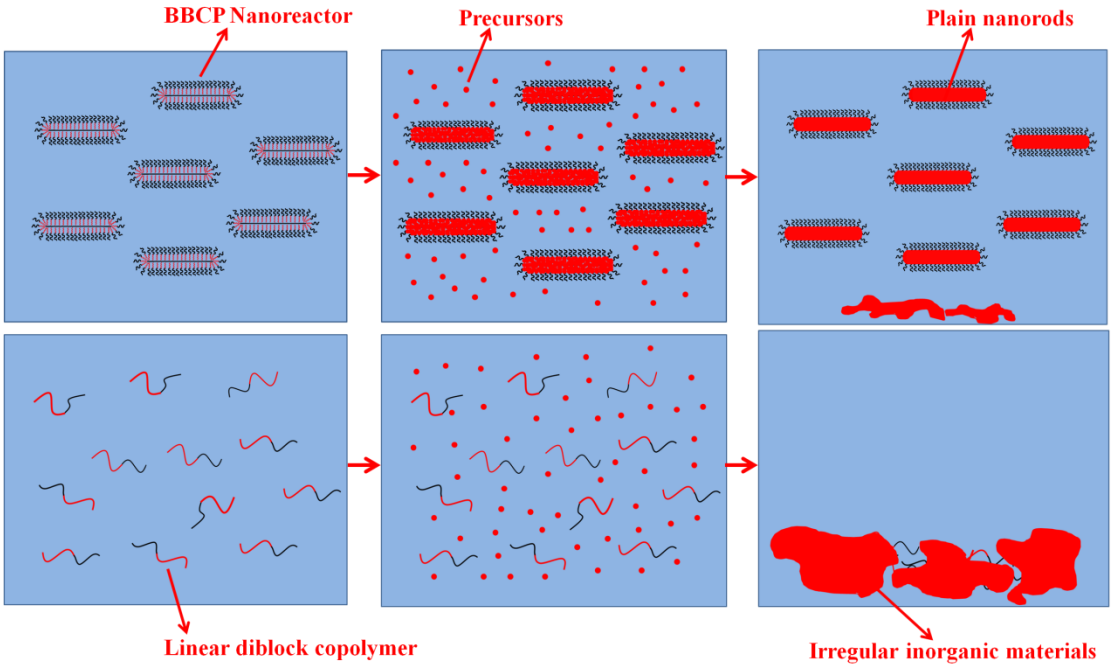

Figure S105. Comparison of the formation mechanisms of nanocomposites by utilizing cylindrical BBCP nanoreactors (upper panels) and their corresponding linear block copolymers (lower panels).

References

1. Li, Z., Li, P. & Huang, J. Synthesis of amphiphilic copolymer brushes: Poly(ethylene oxide)-graft-polystyrene. *J. Polym. Sci. Part A: Polym. Chem.* **44**, 4361-4371 (2006).
2. Mora-Pale, M., Meli, L., Doherty, T.V., Linhardt, R.J. & Dordick, J.S. Room temperature ionic liquids as emerging solvents for the pretreatment of lignocellulosic biomass. *Biotechnol. Bioeng.* **108**, 1229-1245 (2011).
3. Fort, D.A. et al. Can ionic liquids dissolve wood? Processing and analysis of lignocellulosic materials with 1-n-butyl-3-methylimidazolium chloride. *Green Chem.* **9**, 63-69 (2007).
4. Dibble, D.C. et al. A facile method for the recovery of ionic liquid and lignin from biomass pretreatment. *Green Chem.* **13**, 3255-3264 (2011).
5. Stark, A. Ionic liquids in the biorefinery: a critical assessment of their potential. *Energ. Environ. Sci.* **4**, 19-32 (2011).
6. Turner, M.B., Spear, S.K., Holbrey, J.D. & Rogers, R.D. Production of Bioactive Cellulose Films Reconstituted from Ionic Liquids. *Biomacromolecules* **5**, 1379-1384 (2004).
7. Zhang, H., Wu, J., Zhang, J. & He, J. 1-Allyl-3-methylimidazolium Chloride Room Temperature Ionic Liquid: A New and Powerful Nonderivatizing Solvent for Cellulose. *Macromolecules* **38**, 8272-8277 (2005).
8. Matyjaszewski, K. & Tsarevsky, N.V. Macromolecular Engineering by Atom Transfer Radical Polymerization. *J. Am. Chem. Soc.* **136**, 6513-6533 (2014).
9. Matyjaszewski, K. & Xia, J. Atom Transfer Radical Polymerization. *Chem. Rev.* **101**, 2921-2990 (2001).
10. Kolb, H.C., Finn, M.G. & Sharpless, K.B. Click Chemistry: Diverse Chemical Function from a Few Good Reactions. *Angew. Chem. Int. Ed.* **40**, 2004-2021 (2001).
11. Binder, W.H. & Sachsenhofer, R. 'Click' Chemistry in Polymer and Material Science: An Update. *Macromol. Rapid Comm.* **29**, 952-981 (2008).
12. Yi, G.S. & Chow, G.M. Synthesis of Hexagonal-Phase NaYF4:Yb,Er and

NaYF4:Yb,Tm Nanocrystals with Efficient Up-Conversion Fluorescence. *Adv. Funct. Mater.* **16**, 2324-2329 (2006).

13. Roberts, J.E. Lanthanum and Neodymium Salts of Trifluoroacetic Acid. *J. Am. Chem. Soc.* **83**, 1087-1088 (1961).
14. Pan, D., Wang, Q., Jiang, S., Ji, X. & An, L. Low-Temperature Synthesis of Oil-Soluble CdSe, CdS, and CdSe/CdS Core−Shell Nanocrystals by Using Various Water-Soluble Anion Precursors. *J. Phys. Chem. C* **111**, 5661-5666 (2007).
15. Ziqubu, N., Ramasamy, K., Rajasekhar, P.V.S.R., Revaprasadu, N. & O'Brien, P. Simple Route to Dots and Rods of PbTe Nanocrystals. *Chem. Mater.* **22**, 3817-3819 (2010).
16. Murphy, C.J. & Jana, N.R. Controlling the Aspect Ratio of Inorganic Nanorods and Nanowires. *Adv. Mater.* **14**, 80-82 (2002).
17. Link, S., Mohamed, M.B. & El-Sayed, M.A. Simulation of the Optical Absorption Spectra of Gold Nanorods as a Function of Their Aspect Ratio and the Effect of the Medium Dielectric Constant. *J. Phys. Chem. B* **103**, 3073-3077 (1999).

1.

1. Report Type

Final Report

Primary Contact E-mail
Contact email if there is a problem with the report.

zhiqun.lin@mse.gatech.edu

Primary Contact Phone Number
Contact phone number if there is a problem with the report

404-385-4404

Organization / Institution name

Georgia Institute of technology

Grant/Contract Title
The full title of the funded effort.

General and Robust Strategies for Multifunctional Organic-Inorganic Nanocomposites via Direct Growth of Monodisperse Nanocrystals Intimately and Permanently Connected with Polymers

Grant/Contract Number
AFOSR assigned control number. It must begin with "FA9550" or "F49620" or "FA2386".

FA9550-13-1-0101

Principal Investigator Name
The full name of the principal investigator on the grant or contract.

Zhiqun Lin

Program Manager
The AFOSR Program Manager currently assigned to the award

Charles Lee

Reporting Period Start Date

03/01/2013

Reporting Period End Date

05/31/2016

Abstract

The objectives of this proposal are to: (1) Synthesize a series of novel amphiphilic block copolymers with well-defined molecular architectures (i.e., star-like block copolymers, bottlebrush-like block copolymers, and Janus star-like block copolymers) and block ratios based on β-cyclodextrin (β-CD) by living polymerization techniques; (2) Craft a large variety of monodisperse plain and core/shell NPs and NRs as well as Janus NPs of different dimension, chemistry, and properties, which are intimately and permanently capped by polymers on their surface (i.e., forming organic-inorganic nanocomposites), by capitalizing on amphiphilic star-like, bottlebrush-like, and Janus star-like block copolymers as nanoreactors; and (3) Characterize and explore these multifunctional organic-inorganic nanocomposites by measuring their physical properties (e.g., dielectric, magnetic, magnetoelectric, and optical properties) for potential use in spintronic devices, capacitors, actuators, transducers, sensors, photocatalysis, and photonic devices that are anticipated to fill a critical need in future military.

Distribution Statement
This is block 12 on the SF298 form.

Distribution A - Approved for Public Release

Explanation for Distribution Statement

If this is not approved for public release, please provide a short explanation. E.g., contains proprietary information.

SF298 Form

Please attach your SF298 form. A blank SF298 can be found here. Please do not password protect or secure the PDF The maximum file size for an SF298 is 50MB.

AFD-070820-035.pdf

Upload the Report Document. File must be a PDF. Please do not password protect or secure the PDF . The maximum file size for the Report Document is 50MB.

Final report for FA 9550-13-1-0101.pdf

Upload a Report Document, if any. The maximum file size for the Report Document is 50MB.

Archival Publications (published) during reporting period:

Publications from 2013 to 2016 on this AFOSR project (FA 9550-13-1-0101):

13. X. Pang, Y, He, J. Jung, and Z. Lin*, "An Enticing and General Strategy for Crafting One-Dimensional Nanocrystals with Unprecedented Control over Dimension, Composition and Architecture", Science (revision submitted).
12. M. He, X. Pang, X. Liu, B. Jiang, Y. He, H. Snaith, and Z. Lin*, "Monodisperse Dual-Functional Upconversion Nanoparticles-Enabled Near-Infrared Organolead Halide Perovskite Solar Cells", Angewandte Chemie International Edition, 55, 4280 (2016). (featured on the Cover of Angewandte Chemie International Edition)
11. H. Xu, Y. Xu, X. Pang, Y. He, J. Jung, H. Xia, and Z. Lin*, "A general route to nanocrystal kebabs periodically assembled on stretched flexible polymer shish", Science Advances. 1, e1500025 (2015). (Highlighted by: [Science]; [Georgia Institute of Technology]; [PhysOrg]; [ScienceDaily]; [Nanowerk]; [World of Chemicals]; [Nanotechnology Now]; [Pinterest]; [Fnews]; [Nano Daily]; [TrendsSoul]; and [more])

10. B. Jiang, X. Pang, B. Li, and Z. Lin*, "Organic-inorganic nanocomposites via placing monodisperse ferroelectric nanocrystals in direct and permanent connect with ferroelectric polymers", Journal of the American Chemical Society, 137, 11760 (2015).

9. D. Yang, X. Pang, Y. He, Y. Wang, G. Chen, W. Wang, and Z. Lin*, "Precisely Size-Tunable Magnetic/Plasmonic Core/Shell Nanoparticles with Controlled Optical Properties", Angewandte Chemie International Edition, 127, 12259 (2015).

8. D. Zheng, X. Pang, M. Wang, Y. He, C. Lin, and Z. Lin*, "Unconventional Route to Hairy Plasmonic/Semiconductor Core/Shell Nanoparticles with Precisely Controlled Dimensions and Their Use in Solar Energy Conversion", Chemistry of Materials, 27, 5271 (2015).

7. H. Xu, X. Pang, Y. He, M. He, J. Jung, H. Xia, and Z. Lin*, "An Unconventional Route to Monodisperse and Intimate Semiconducting Organic-Inorganic Nanocomposites", Angewandte Chemie International Edition, 54, 4636 (2015). (featured on the Cover of Angewandte Chemie International Edition).

6. Y. Xu, C. Wang, S. Zhong, W. Li, and Z. Lin*, "Self-assembly of Miktoarm Star-Like ABn Block Copolymers: From Wet to Dry Brushes", Langmuir, 31, 2905 (2015).

5. X. Pang, C. Wan, M. Wang, and Z. Lin*, "Strictly biphasic soft and hard Janus structures: synthesis, properties and applications", Angewandte Chemie International Edition, 53, 5524 (2014).

4. M. He, M. Wang, C. Lin, and Z. Lin*, "Optimization of molecular organization and nanoscale morphology for high performance low bandgap polymer solar cells", Nanoscale, 6, 3984 (2014). (featured on Inside Front Cover of Nanoscale).

3. M. He, D. Zheng, M. Wang, C. Lin, and Z. Lin*, "High efficiency perovskite solar cells: from complex nanostructure to planar heterojunction", Journal of Materials Chemistry A, 2, 5994 (2014). (featured on Cover of Journal of Materials Chemistry A).

2. X. Pang, C. Feng, H. Xu, W. Han, X. Xin, H. Xia, and Z. Lin*, "Unimolecular micelles composed of inner coil-like blocks and outer rod-like blocks crafted by combination of living polymerization with click chemistry", Polymer Chemistry, 5, 2747 (2014).

1. C. Feng, X. Pang, Y. He, B. Li, and Z. Lin*, "Robust Route to Unimolecular Core–Shell and Hollow Polymer Nanoparticles", Chemistry of Materials, 26, 6058 (2014). (Highlighted by ACS Noteworthy Chemistry.

Changes in research objectives (if any):

Change in AFOSR Program Manager, if any:

Extensions granted or milestones slipped, if any:

AFOSR LRIR Number

LRIR Title

Reporting Period

Laboratory Task Manager

Program Officer

Research Objectives

Technical Summary

Funding Summary by Cost Category (by FY, $K)

	Starting FY	FY+1	FY+2
Salary			
Equipment/Facilities			
Supplies			
Total			

Report Document

Report Document - Text Analysis

Report Document - Text Analysis

Appendix Documents

2. Thank You

E-mail user

Apr 17, 2016 11:38:28 Success: Email Sent to: zhiqun.lin@mse.gatech.edu